SOIL-STRUCTURE INTERACTION OF DEEPLY EMBEDDED STRUCTURES

SOIL-STRUCTURE INTERACTION OF DEEPLY EMBEDDED STRUCTURES

By

Mahmoud Mohammed Madany Mohammed

B.A.Sc., M.A.Sc.

A Thesis Submitted to the School of Graduate Studies in Partial Fulfillment of the Requirements for the Degree Doctor of Philosophy

Doctor of Philosophy (2021) McMaster University

(Civil Engineering) Hamilton, Ontario

TITLE: SOIL-STRUCTURE INTERACTION OF DEEPLY EMBEDDED STRUCTURES

AUTHOR: Mahmoud Madany
B.A.Sc., M.A.Sc. (Cairo University)

SUPERVISOR: Prof. Peijun Guo

NUMBER OF PAGES: xxiii, 173

Dedications

To

My Father & Mother,

Shaima

LAY ABSTRACT

Small Modular Reactors (SMRs) are the cornerstone of recent developments in the nuclear industry. However, the SMRs technology faces several safety-related challenges, which includes the earthquake hazards related to the large embedment depth of the enclosing structure. In particular, the major concerns are about the risks related to seismic surface waves as well as the seismic interaction between nearby structural and non-structural elements (e.g., pipelines). The thesis addressed these major concerns by developing analytical and numerical methods to complement the analysis for the integrity of SMRs with sufficient seismic resistance. The solutions are verified and benchmarked using data in the literature. Future researches are suggested to further improve seismic analysis of SMRs.

ABSTRACT

In recent years, the desperate need for reliable clean and relatively small power demand has emerged for edge-of-grid or off-grid regions to keep pace with development demands. A salient technology that has gained much attention for this purpose is the Small Modular Reactors, i.e., SMRs. SMRs differ from conventional Nuclear Power Plants (NPPs) in many aspects, specifically the enclosing structure of the reactor. The burial depth of the SMR structure is expected to reach great depths. For example, the substructure depth reaches 30 m in the SMR design proposed by NuScale (NuScale Power, 2020). Consequently, seismic analysis of deeply embedded structures with a relatively small footprint has been identified as one of the challenges to the safe implementation of SMR technology (DIS-16-04, 2016). Such structures are expected to be more sensitive to surface wave propagation and the seismic interaction with nearby substructures and nonstructural elements such as pipelines.

This dissertation develops analytical and numerical methods to analyze the seismic earth pressure exerted on the SMR substructure by considering the effects of seismic surface waves, structure-soil-structure interaction (SSSI), and the interaction with nearby pipelines. The three-dimensional wave propagation theory is employed in the analysis. Solutions for the earth pressure induced by Rayleigh waves are obtained for substructures deeply embedded into homogeneous or multilayered soil profiles. In addition, the effect of thin soil layer (stiff or soft) soils in a soil profile is investigated in the presence of Rayleigh waves. Furthermore, additional earth pressure due to SSSI is examined, and a simplified procedure is proposed based on the three-dimensional wave propagation theory and a guided flow chart to track seismic wave interference. The SSSI analysis yields solutions for the optimal distance between substructures corresponding to the minimum SSSI in new designs. The interaction between substructures and nearby pipelines is explored numerically using the Spectral Element Method. SPECFEM2D software is adopted to perform the analysis, where the three-dimensional wave propagation

is successfully implemented. Based on the analysis for pipelines with different configurations, general conclusions are drawn regarding the additional earth pressure on substructures and pipelines based on a comprehensive parametric study of various parameters. In addition, this research also provides an approach to determine the backfill configuration and the selection of backfill materials, which could minimize the seismic amplitudes transmitted to substructures.

ACKNOWLEDGMENTS

Firstly, I would like to express my sincere gratitude and immeasurable appreciation to my advisor Professor Peijun Guo for his guidance and patience throughout the research. I was fortunate to work under his supervision and really appreciate our valuable discussions, which at some stages served as a compass that changed my course in the right direction and opened new horizons. I deeply appreciate the guidance and constructive feedback that I had always been receiving from the committee members Drs. Ayman Saudy, John Luxat, and Wael El-Dakhakhni.

I would also like to thank the Canadian Nuclear Energy Infrastructure Resilience under Systemic Risk (CaNRisk) – Collaborative Research and Training Experience (CREATE) program of the Natural Science and Engineering Research Council (NSERC) of Canada for the financial support of the research. Profound gratitude should also be directed to Bruce Power for giving the opportunity to explore the different structures, components and systems of Nuclear Power Plants and gain tremendous knowledge and insights into the challenges currently facing the nuclear industry that have influenced this research.

Deep gratitude goes to my two brothers and lifelong friends Mohamad Gamal and Yassien Yassien, who have always been supportive and have been among the reasons I am here today. My special gratitude extends to my colleagues Ahmed Yassien, Ahmed Yosri, Ahmed Elsayed, Maysara Gaith, Mohamad Elseify, Mohamad Elganzory, Mouna Reda, and everyone who helped me in this journey.

Last but not least, words cannot describe how thankful I am to my family, the source of every achievement in my life. Thank you for your continued support and encouragement throughout my life. Your advice shaped my character and taught me not to stop until I reach the pinnacle of achievement. Finally, to my beloved fiancee *Shimaa*, I am always thinking of how lucky I am for having you in my life. I am indebted to you for your spiritual support and for choosing to go through this journey together.

TABLE OF CONTENTS

LIST OF FIGURES

LIST OF TABLES

LIST OF ACRONYMS AND ABBREVIATIONS

IAEA	-	International Atomic Energy Agency
NPP	-	Nuclear Power Plant
PWR	-	Pressurized Light-Water Reactor
BWR	-	Boiling Light-Water Reactor
PHWR	-	Pressurized Heavy-Water Reactor
SMR	-	Small Modular Reactor
CNSC	-	Canadian Nuclear Safety Commission
NRC	-	National Research Center
SSI	-	Soil-Structure Interaction
SSSI	-	Structure-Soil-Structure Interaction
SEM	-	Spectral Element Method
FEM	-	Finite Element Method
FDM	-	Finite Difference Method
PSM	-	Pseudo-Spectral Method
PML	-	Perfectly Matched Layer

GLL	-	Gauss-Lobatto Legendre
USGS	-	United States Geological Survey
ASCE	-	American Society of Civil Engineers
SEI	-	Structural Engineering Institute
CSA	-	Canadian Standards Association
OSHA	-	Occupational Safety and Health Administration
RB	-	Reactor Building
ASB	-	Ancillary Services Building
VB	-	Vacuum Buiding
GWe	-	Gigawatt Electrical
MWe	-	Megawatt Electrical
ρ	-	Density of soil
ρ_b	-	Density of backfill soils
λ, μ	-	Lamé constants
u, v, w	-	Displacement in $x-$, $y-$ and $z-$directions
∇^2	-	Laplace operator

$\bar{\varepsilon}$	-	Volumetric strain of soil
ζ	-	Critical damping ratio
ν	-	Poisson's ratio
$\boldsymbol{\Phi}$	-	A potential function to describe dilatation component of Seismic Waves
$\boldsymbol{\Psi}$	-	A potential function to describe rotation component of Seismic Waves
$\Psi(x,z,t)$	-	Avector potential to describe the in-plane displacement field due to shear waves
$\chi(x,z,t)$	-	Avector potential to describe the out-plane displacement field due to shear waves
$F(z)$	-	A function to describe the variation of Φ with depth
$G(z)$	-	A function to describe the variation of Ψ with depth
$\hat{k}_R$	-	Damped rayleigh wavenumber
$\hat{v}_R$	-	Damped rayleigh wave velocity
$\hat{v}_s$	-	Damped shear wave velocity
v_s	-	Shear wave velocity
v_p	-	Primary wave velocity

H	-	Substructure depth
σ_{xx}	-	Normal stress
σ_{xz}	-	Shear stresses
F_{xx}	-	Total seismic earth pressure normal force
F_{xz}	-	Total seismic earth pressure shear force
f	-	Excitation frequency in Hz
ω	-	Excitation frequency in rad/sec
h_i	-	Thickness of soil layer
$\bar{Z}$	-	Location of the point of application of the dynamic thrust measured from the free surface
G	-	Shear Modulus of Soil
k_x	-	Wavenumber in x −direction
k_{z_α}	-	SV-waves wavenumber in $z-$ direction
k_{z_β}	-	P-waves wavenumber in $z-$ direction
$\mathbf{k}$	-	Magnitue of the wavenumber
$[u_{SV}]_{VL}$	-	Displacement in x −direction due to vertically propagating shear waves

$[u_{SV}]_R$	-	Displacement in x −direction due to reflected SV-waves from an inclined backfill boundary
$[u_P]_R$	-	Displacement in x −direction due to reflected P-waves from an inclined backfill boundary
v_{sb}	-	Shear Wave Velocity of the Backfill
θ	-	Angle of Inclination of the Backfill Interface with the Horizontal Axis
L	-	The clear distance between two adjacent structure
x_1	-	The thickness of Backfill 1
x_{sv}	-	The distance between two successive reflections in an SV-wavepath at the upper or lower boundaries of the soil layer
x_p	-	The distance between two successive reflections in a P-wavepath at the upper or lower boundaries of the soil layer
$N_{SV,P}$	-	The total number of branching points along a wavepath and is rounded to the next higher integer
N_U	-	The number of branching points along a wavepath at the upper boundary of the soil layer
N_L	-	The number of branching points along a wavepath at the lower boundary of the soil layer

α_{Ib}	-	Angle of incidence of the vertically propagating shear waves on the inclined surface of Backfill 2
α_{In}	-	Angle of incidence of the reflected SV-waves at the upper or lower boundaries of the soil layer
β_{In}	-	Angle of incidence of the reflected P-waves at the upper or lower boundaries of the soil layer
α_{Tn}	-	Angle of refraction of the reflected SV -waves at the upper or lower boundaries of the soil layer
β_{Tn}	-	Angle of refraction of the reflected P-waves at the upper or lower boundaries of the soil layer

DECLARATION OF ACADEMIC ACHIEVEMENT

This thesis has been prepared in accordance with the guidelines established by the School of Graduate Studies at McMaster University. The thesis adheres to the criteria of acceptance for a "Sandwich Ph.D. Thesis" outlined in sections 1.3 and 5.0 of the guide. The thesis consists of a compilation of three "submitted for peer review" journal papers, as well as introductory and conclusion chapters. The work presented in this thesis has been performed solely by Mahmoud Mohammed, with Professor Peijun Guo, the academic supervisor, providing both technical and editorial feedback and guidance. Data from external references and used in the thesis have been cited in the body text and compiled at the end of each chapter where appropriate. The original contribution of the author to each of the three manuscripts are as follows:

Chapter 2: Madany, M., Guo, P. (2021). "Seismic Earth Pressure Due to Rayleigh Waves in Viscoelastic Media" *Journal of Earthquake Engineering*. (Status: Accepted for Publication).

The main idea of the paper emerged from the thinking of M. Madany, based on critical discussions with Professor P. Guo. The work in this paper was carried out by M. Madany, with technical guidance and feedback provided by Professor P. Guo. The manuscript was prepared by M. Madany and reviewed by Professor P. Guo for technical and editorial comments.

Chapter 3: Madany, M., Guo, P. (2021). "Structure-soil-structure Interaction Analysis for Lateral Seismic Earth Pressure of a Deeply buried Structure in Layered Ground" *International Journal of Geomechanics*. (Status: Accepted for Publication; DOI: 10.1061/(ASCE)GM.1943-5622.0002189).

The main idea of the paper emerged from the thinking of M. Madany, based on critical discussions with Professor P. Guo. The work in this paper was carried out by M. Madany, with technical guidance and feedback provided by Professor P. Guo. The manuscript was prepared by M. Madany and reviewed by Professor P. Guo for technical and editorial comments.

Chapter 4: Madany, M., Guo, P. (2021). "Seismic Interaction Between Deeply Embedded Substructures and nearby Pipelines" *Journal of Geotechnical and Geoenvironmental Engineering*. (Status: Under Review)

The main idea of the paper emerged from the thinking of M. Madany, based on critical discussions with Professor P. Guo. The work in this paper was carried out by M. Madany, with technical guidance and feedback provided by Professor P. Guo. The manuscript was prepared by M. Madany and reviewed by Professor P. Guo for technical and editorial comments.

Chapter 1

INTRODUCTION

1.1. BACKGROUND AND MOTIVATION

Nuclear power has been gaining tremendous interest worldwide as a source of clean energy that can replace a significant portion of fossil fuel and has the potential of dramatically slowing the negative impacts of climate change. As of December 2019, the total number of operating nuclear power reactors reached 443 distributed in 30 countries, with a total power capacity of 392.1 GWe (IAEA 2020). An additional 54 reactors are still under construction in 19 countries, which will increase the global electricity generation by 57.441 GWe. Operating Nuclear Power Plants (NPPs) around the world are not identical but differ according to the type of reactor and the plant configuration. There are several types of nuclear reactors operating under different coolant systems. The most common types are the Pressurized Light-Water Reactor (PWR), Boiling Light-Water Reactor (BWR), and Pressurized Heavy-Water Reactor (PHWR).

Regardless of the type of reactor, the number of reactors in an NPP is not constant but depends on multidisciplinary factors that can be boiled down to the target power capacity and intended operating times. Regarding the power capacity, the size of a single nuclear reactor has grown since the establishment of nuclear power from 60 MWe to more than 1600 MWe. Nuclear reactors can be categorized accordingly into small, medium, and large reactors. There is no international

agreement on the limits of each category. However, according to the International Atomic Energy Agency (IAEA), the definition of a small reactor encompasses any reactor with a power capacity of less than 300 MWe. Small reactors are commonly referred to as the Small Modular Reactor (SMRs), and the large reactors are known as conventional reactors.

At present, SMRs are getting all the attention as the future of nuclear energy in the world. High capital costs and long construction times have always been major drawbacks to the conventional NPPs. However, SMRs technology has proven its ability to efficiently overcome both obstacles and become a fierce competitor to conventional NPPs. Furthermore, SMRs add more layers of safety to the nuclear industry by providing passive nuclear safety features. Perhaps the main advantage of SMRs is the manufacturing and assembly process, where both take place in a central factory with high control management and safe transportation directly to the site of interest. Developing economies can benefit from the balance of capital costs and revenue offered by SMRs throughout the construction phases. For instance, if target power capacity requires a twin SMRs, the user can start collecting the revenue right after installing the first SMR, which would drastically reduce the construction costs of the second SMR and feed the power grid with half the energy target. Moreover, SMR technology is particularly beneficial to the remote areas where energy demand is relatively low and the cost of transmitting electrical power from the nearest NPP is significantly high.

Numerous SMR proposals are still in the design stage or have been released for licensing, which is generally the most challenging stage in the commercial application of SMRs. The licensing process is considered challengeable as the design of the SMRs incorporates several novel approaches that have not been applied in the nuclear industry before, and thus can affect the overall stability and safety of the plant. According to the Canadian Nuclear Safety Commission (CNSC) and the National Research Center (NRC), the integrity of subsurface civil structures is among the concerns raised in general, and against seismic events in particular. A key feature in most of the proposed SMR designs is the partial or full embedment of the containment structure. Such deep embedments address various vulnerabilities associated with natural and sabotage hazards, such as hurricanes and aircraft crashes, respectively. Furthermore, the ground surrounding the reactor acts as a natural barrier to prevent the release of radioactivity into the environment in the event of a nuclear accident. According to discussion paper DIS-16-04 (2016), the design of structures with such deep embedment has not been established yet in the Canadian and American codes and standards for nuclear facilities, specifically for the problem of seismic soil-structure interaction (SSI).

1.2. SEISMIC SOIL-STRUCTURE INTERACTION (SSI)

The problem of seismic SSI has been well established for the design of structures with shallow foundations. Numerous studies have been conducted over the past few decades to identify key parameters of SSI analysis, including site response analysis,

kinematic and inertial interactions, and impedance functions (Mylonakis and Gazetas 2000). However, the available tools lack precision at large embedment depths, which also require further investigation into other aspects such as the effect of surface waves and the interaction with neighbouring structures, as will be discussed in detail. Originally, the main objective of SSI analysis is evaluating the collective response of three linked systems: the soil, the foundation, and the structure. The main steps towards achieving this goal can be summarized in obtaining modified earthquake input motion at the foundation level and replacing surrounded soil with equivalent impedance functions. Two numerical modelling approaches are commonly employed in SSI analysis, namely, direct and substructure approaches (Wolf 1989). The main difference between both approaches lies in the model discretization.

In the direct approach, the superstructure, foundation, and a significant part of the surrounding soil are modelled in the same environment. Conversely, the substructure approach breaks down the total system into independent subsystems, usually: the structure, the soil medium, and the excavated soil. However, each approach has salient features in terms of efficiency, accuracy, and computational effort that make it suitable for some systems but not others. The direct approach is relatively cumbersome, and great computational effort is devoted to analyzing the entire model at once. Nevertheless, the direct approach gives higher accuracy and capable of incorporating advanced modelling considerations, such as material nonlinearity throughout the model and the possibility of soil-foundation separation.

A wide range of numerical methods can be utilized to perform the analysis, including the Spectral Element Method (SEM), Finite Element Method (FEM), among others. A detailed discussion on numerical modelling of a soil-structure system is provided in an upcoming section.

Given the deep embedment and relatively small footprint of the SMR substructure, understanding the soil-structure interaction of similar systems such as caissons is essential to identify potential challenges and give insights into the expected behaviour of the SMR substructure. Different types of caissons are used in bridges and offshore wind turbines, such as gravity and suction caissons. Regarding the SSI problem in the case of caissons, two approaches are generally considered in the analysis: rigid (Jalbi et al. 2018)or flexible (Doherty et al. 2005) caisson in deformable soils. The most popular analytical model used in the previous research was based on Winkler springs distributed over the surface of the caissons to represent the interaction with adjacent soil (Cheng et al. 2010). The soil-structure system represented by a depth-varying ground excitation, considering only body waves. Other parameters such as the separation between caissons and adjacent soils were considered in subsequent research by adding gapping elements to numerical models (Gerolymos and Gazetas 2006). The equivalent stiffness of the Winkler springs were evaluated analytically (Yao and Mao 2010) or using different numerical approaches such as pushover analysis (Cheng et al. 2010). In a relatively recent research, flexibility of the caissons is accounted for in the analysis by introducing macro-elements into the analysis (Skau et al. 2019). The main idea of

the macro-element is to include a stiffness correction to account for the changes in the elastic coupling between horizontal load and moment due to caisson flexibility. Different numerical models were proposed to assess the SSI of caissons in bridges in the time and frequency domains, considering equivalent linear and nonlinear soil behaviour (Gaudio and Rampello 2016; Hubert et al. 2014; Chang et al. 2001). Limited field experimental studies were conducted to investigate the SSI of caisons owing to the high cost and the enormous work required to construct a real case study. In a field experiment conducted in 2014 on root-caissons (Lei et al. 2021), it was found that the ultimate bearing capacity of a root-caisson foundation is greatly larger than that of a traditional caisson foundation. Other lab experiments were also conduscted to investigate the behaviour of suction caissons (W. and J. 2021) and open caissons (Chavda and Dodagoudar n.d.).

1.3. CHALENGES RELATED TO EARTHQUAKES

Regarding earthquake input motion, tectonic ruptures occur at depths range from a few kilometres up to 700 kilometres and propagate through soil layers towards the site (USGS 2009). Earthquakes produce two main types of waves, which are body waves and surface waves. Body waves generally travel through the interior of the earth, unlike surface waves that travel within the earth's crust. The two types of waves can be easily distinguished on a seismogram in terms of arrival times and frequencies, where body waves are the first to reach the site with a broad spectrum of high frequencies in the three dimensions. Body waves can be decomposed into

Primary waves (P-waves) and Secondary, or Shear, waves (S-waves). On the other hand, there are several types of surface waves, but the two main types are Rayleigh waves (R-waves) and Love waves (L-waves).

1.3.1. SEISMIC SURFACE WAVES

Due to the deep embedment of the containment structure, the substructure is more likely to experience the two types of seismic waves: body waves at the bottom and surface waves near the ground surface. The majority of studies and current codes and standards in the nuclear industry devoted a substantial interest to the effect of body waves on different aspects of SSI, such as seismic earth pressure. However, surface waves are more destructive and the primary source of damage to structures as they carry higher amplitudes and last longer than body waves. The amplitudes of surface waves may reach several centimetres in large earthquakes (Teng 1987). Furthermore, surface waves decay at a slower rate with distance than body waves as a result of the geometrical spreading in two dimensions (Lowrie 2007).

The type of surface waves can be inferred by observing the ground movements during an earthquake. Rayleigh wave consists of P- and SV-waves interacting near the ground surface in a vertical plane, and thus particle motion includes both longitudinal and transverse components. On the other hand, Love waves are developed due to SH-waves trapped in a surficial layer of lower shear wave velocity than the bedrock, resulting in particle motion in the horizontal direction only (Kramer 1996). The two types of surface waves are easily

distinguishable on seismograms as Love waves strike earlier than Rayleigh waves, proving that Love waves propagate at a higher speed. However, seismologists consider Rayleigh waves the most important type of surface waves (Longuet-Higgins 1950; Telford et al. 1990). Since Rayleigh waves include both horizontal and vertical particle motions, Rayleigh waves can apply direct normal and shear stresses on the substructure of the SMR (i.e., Seismic earth pressure). With reference to the mathematical derivation of Rayleigh waves, the displacement variation with depth is unique and different from P- and S-waves separately. Consequently, the lateral seismic earth pressure and, in turn, the total seismic force and moment on the substructure are expected to deviate from their counterparts due to body waves. Rayleigh waves can exist in a homogeneous soil layer or a multilayered soil profile, where the SMR's substructure is likely to penetrate several layers of soil due to the deep embedment depth. In the SMR design proposed by NuScale, the substructure depth reaches 30 m (NuScale Power, 2020).

1.3.2. SEISMIC STRUCTURE-SOIL-STRUCTURE INTERACTION

Among the concerns raised by the CNSC and NRC is the conservatism of the vertically propagating shear waves assumption in the seismic design of the SMR's structure (Budnitz et al. 2015; DIS-16-04. 2016). In general, when seismic waves impinge the interface between two layers, part of the seismic energy transmits to the upper layer, and the remaining part is reflected in the same layer. The amplitudes of the reflected and refracted waves depend on the angle of incidence

and mechanical properties of the soil layers. Regardless of the type of seismic waves, the reflected and refracted amplitudes should satisfy the displacement compatibility and stress continuity at the interface between two layers (Mccamy, K. et al. 1962; Zoeppritz 1919). Additionally, the angles of incidence and reflection are identical as they are both developed in the same layer (i.e., Snell's law). The angle of refraction deviates from the angle of incidence due to the variation in mechanical properties of the soil layers. Once the refraction angle reaches 90°, the transmitted waves graze the interface between two layers and the corresponding incidence angle is referred to as the critical angle of incidence. At higher incidence angles, total internal reflections occur and the seismic energy is trapped in the soil layer, leading to the generation of surface waves. Nevertheless, for a seismic wave travelling upward through successively softer soil layers, the ray path of the refracted waves successively deviates towards the normal to the interface. This explains the assumption of vertically propagating shear waves in most civil engineering applications.

The conservatism of the vertically propagating shear waves assumption is invalid in multiple cases, such as obliquely stratified soils, seismic structure-soil-structure interaction, and the interception of waves by artificial boundaries. The latter two cases apply to the SMR's structure, where the engineering backfill represents the artificial boundary, and the adjacent structures are the source of the seismic interaction. Calculation of the appropriate backfill slop depends on the excavation depth and mechanical properties of the adjacent soils. The selected slope

should maintain the overall stability of the open excavation during construction phases. In nuclear power plants, several buildings are located in close proximity to the reactor building. The seismic interaction between these buildings through the soil (i.e., SSSI) is expected to amplify seismic stresses on the substructures and in-structure responses of the below-grade floors. Backfill soils can be a source of further amplification in seismic responses or, on the contrary, can be utilized as a natural isolator to reduce seismic amplitudes transmitted to substructures. This can be achieved by selecting the appropriate backfill slope and material properties. Another parameter that strongly influences SSSI is the clear distance between structures, which can be adequately adjusted to achieve minimal impact on new designs.

1.3.3. SEISMIC SUBSTRUCTURE-PIPELINE INTERACTION

Another artificial barrier that can adversely affect the vertical shear waves assumption and SSSI in NPPs is the buried pipelines. Along the distance between adjacent buildings, buried pipelines of different functionality and diameters are usually located in the immediate vicinity of a substructure or pass between two substructures. Such configuration raises two concerns about the implications of seismic interaction between substructures and buried pipelines. The first concern is associated with the seismic capacity of the substructures to endure the additional seismic loads caused by the pipeline. The pipeline will act as a barrier preventing part of the seismic energy from propagating from one substructure to another.

Furthermore, a series of new wavepaths will be developed across the distance between the pipeline and the substructure. Besides the additional seismic stresses on the substructures, the newly developed wavepaths may be trapped in the soil layer, giving rise to surface waves. The current provisions for seismic design of substructures in nuclear codes and standards do not include any considerations to the seismic interaction between substructures and buried pipelines (ASCE/SEI 4-16; CSA N289.3-10; NP-T-3.20; U.S. NRC).

The second concern is pertaining to the pipeline integrity against seismic energy reflected from the substructures, as well as vertically propagating shear waves. The different parts of safety-related buried piping systems in NPPs are originally designed to withstand ground motions caused by shear waves and Rayleigh waves. The required analysis is either performed by the finite element method or equivalent static method. The interaction between the pipeline and surrounding soils has been suggested by several studies and incorporated into some nuclear standards (ASCE/SEI 4-16; CSA N289.3-10). However, additional seismic forces resulting from interaction with neighbouring infrastructures have yet to be investigated. The magnitude of the additional forces depends essentially on several parameters, including the distance to substructures, soil characteristics, and pipeline depth. Furthermore, non-uniform stress distribution and thus deformations may be developed on the pipeline, depending on the pipeline location and adjacent substructure configurations.

1.4. RESEARCH OBJECTIVES

The main objective of this dissertation is to mitigate hazards associated with earthquakes in the seismic design of the buried portion of the SMR containment structure. The deep embedment depth of the SMR substructure raises concerns about the vulnerabilities in the current provisions for seismic design of substructures in nuclear codes and standards. The primary focus is to thoroughly investigate the lateral seismic earth pressure on substructures that penetrate stratified soils due to surface waves, structure-soil-structure interaction, and the interaction with buried pipelines. Furthermore, effective tools and mathematical expressions are provided to help assess existing safety-related substructures in NPPs against additional seismic earth pressures due to SSSI. A secondary focus is placed on the integrity of buried pipelines against the seismic energy reflected from substructures to ensure the pipelines are capable of maintaining their functionality during and after earthquake events. As such, the objectives of the dissertation can be specified as follows:

- Develop an analytical approach using three-dimensional wave propagation theory to calculate lateral seismic earth pressure induced by Rayleigh waves on a deeply buried substructure in viscoelastic stratified soils,
- Analytically evaluate additional lateral seismic earth pressure on a deeply buried structure due to structure-soil-structure interaction and engineering backfill. In addition, develop an effective procedure using three-dimensional wave propagation theory to track the interference of seismic waves between

adjacent structures and calculate the optimal distance that produces minimal SSSI, and

- Numerically investigate the seismic interaction between substructures and buried pipelines, with a primary focus being placed on the additional lateral seismic earth pressure on substructures and a secondary focus on pipeline integrity.

1.5. THESIS ORGANIZATION

The thesis consists of five chapters, starting with the introductory part, then it is followed by three chapters covering the objectives of the thesis, and finally ending with a concluding chapter that summarizes the main findings of the research. The following paragraphs give a brief description of the content of each chapter.

Chapter 1 provides essential background on the development of Small Modular Reactors and the challenges to actual implementation in the industry, an overview of soil-structure interaction and the relationship to SMR challenges to define the problem statement, specific research objectives, and thesis organization.

Chapter 2 presents an analytical solution to the seismic lateral earth pressure induced by Rayleigh waves on a substructure with a deep embedment depth. A closed-form solution is proposed based on the three-dimensional wave propagation theory in viscoelastic media. The solution is derived for two distinct soil-structure systems: a rigid substructure inserted into a homogeneous half-space and a rigid substructure surrounded by layered soils. Equations are presented as a function of

damping ratio, Poisson ratio, and substructure depth. A comprehensive numerical example is solved using the proposed expressions to investigate the effect of each parameter and illuminate the graphical representation of the seismic earth pressure distribution with depth. In addition, a detailed comparison is performed to examine the effectiveness of the assumption of a homogeneous soil layer as an alternative to the accurate solution using a layered soil profile.

Chapter 3 constructs an analytical solution based on the three-dimensional wave propagation theory to evaluate the additional seismic lateral earth pressure on substructures due to structure-soil-structure interaction, as well as backfill soils. Two adjacent buildings of different buried depths and backfill configurations are considered in the analysis, where one of the substructures represents the deep embedment condition of the SMR containment structure. Substructures are surrounded by N horizontally stratified homogeneous soil layers of isotropic elastic material properties. Seismic excitation is represented by vertically-propagating horizontally-polarized shear waves travelling upward from an elastic half-space to the layered soils. This chapter also assesses the conservatism of the assumption of the vertically propagating shear waves in most civil engineering applications. A simplified procedure based on a guided flow chart is suggested to solve the wave propagation back and forth between the adjacent buildings through the soil, taking into account the excavation slope of both backfills and multi-phases wave propagation between substructures. In addition, the chapter provides an efficient tool for calculating the optimal distance between two adjacent structures that

correspond to minimal SSSI in new designs and can also be utilized in the seismic evaluation of existing situations. Numerical examples are solved to shed light on the graphical representation of the equations and investigate the effect of steep to gentle excavation slopes in amplifying the seismic stresses on substructures. The numerical examples give insight into the selection of appropriate backfill properties as a function of their counterparts of adjacent soil layers.

Chapter 4 examines the seismic interaction between two substructures of different depths and buried pipelines passing in-between. The primary focus is the integrity of the substructures against additional seismic earth pressures induced by the pipeline. As a result of seismic energy reflected from substructures, a secondary focus is placed on the pipeline integrity as a safety-related system to maintain its functionality during and after an earthquake event. Chapter 4 discusses the successful implementation of the three-dimensional wave propagation theory into the Sectral Element Method (SEM) and the essential aspects that should be considered in the numerical modelling of the soil-pipeline-structure system. Qualitative numerical analysis is performed, in which the influence of three main parameters is presented graphically and thoroughly discussed to address the adverse impact of the seismic interaction between the substructures and buried pipeline. Parameters include pipeline location, excitation frequency, and material damping.

Chapter 5 provides a reflective summary of the research, draws out the overall implications of the research and key findings that clearly answer the main

research question, and offers dynamic recommendations for the possibility of future work o the topic.

1.6. REFERENCES

ACI Committee 349. (2010). "ACI 349-06. Code Requirements for Nuclear Safety-Related Concrete Structures and Commentary." *American Concrete Institute (ACI)*.

ASCE/SEI 4-16. (2017). *Seismic analysis of safety-related nuclear structures*. *Seismic Analysis of Safety-Related Nuclear Structures*, American Society of Civil Engineers.

ASME. (2019). *BPVC Section III-Rules for Constructions of Nuclear Facility Components-Subsection NCA-General Requirements for Division 1 and Division 2*.

De Basabe, J. D., and Sen, M. K. (2010). "Stability of the high-order finite elements for acoustic or elastic wave propagation with high-order time stepping." *Geophysical Journal International*, 181(1), 577–590.

Budnitz, R. J., Konstandinidis, D., and Zhou, Z. (2015). *Evaluations of NRC Seismic-Structural Regulations and Regulatory Guidance, and Simulation-Evaluation Tools for Applicability to Small Modular Reactors (SMRs)*.

Canadian Nuclear Safety Commission (CNSC). (2016). *Small Modular Reactors : Regulatory Strategy, Approaches and Challenges*. *Discussion Paper DIS-16-*

04.

Canadian Standards Association (CSA). (2008). *CSA N291-Requirements for safety-related structures for CANDU nuclear power plants*.

Canadian Standards Association (CSA). (2014). *CSA N287.3-Design requirements for concrete containment structures for nuclear power plants*.

Chapman, C. (2004). *Fundamentals of Seismic Wave Propagation*. Cambridge University Press, Cambridge.

Chavda, J. T., and Dodagoudar, G. R. (n.d.). "Experimental studies on a circular open caisson." *International Journal of Physical Modelling in Geotechnics*, 0(0), 1–18.

Cheng, Z., Law, H., and Jiang, Y. (2010). *Soil-Structure Interaction Analysis For Bridge Caisson Foundation*.

CSA N289.3-10. (2015). *Design procedures for seismic qualification of nuclear power plants*. Canadian Standards Association.

Datta, S. K., Shah, A. H., and Wong, K. C. (1984). "Dynamic stresses and displacements in buried pipe." *Journal of Engineering Mechanics*, 110(10), 1451–1466.

Gaudio, D., and Rampello, S. (2016). "Dynamic Soil-structure Interaction of Bridge-pier Caisson Foundations." *Procedia Engineering*, 158, 146–151.

Gerolymos, N., and Gazetas, G. (2006). "Static and dynamic response of massive

caisson foundations with soil and interface nonlinearities—validation and results.” *Soil Dynamics and Earthquake Engineering*, 26(5), 377–394.

Geuzaine, C., and Remacle, J. F. (2009). “Gmsh: A 3-D finite element mesh generator with built-in pre- and post-processing facilities.” *International Journal for Numerical Methods in Engineering*, 79(11), 1309–1331.

Haskell, N. A. (1953). “The dispersion of surface waves on multilayered media.” *Bulletin of the Seismological Society of America*, 43(1), 17–34.

Hubert, L., Po, L. I., and Patrick, W. (2014). “Soil-Structure Interaction for Gravity Caissons in Bridge Seismic Design.” *Structures Congress 2014*, Proceedings.

IAEA. (2020). *Operating Experience with Nuclear Power Stations in Member States*. Operating Experience with Nuclear Power Stations in Member States (CD-ROM), INTERNATIONAL ATOMIC ENERGY AGENCY, Vienna.

Jalbi, S., Shadlou, M., and Bhattacharya, S. (2018). “Impedance functions for rigid skirted caissons supporting offshore wind turbines.” *Ocean Engineering*, 150, 21–35.

John P.wolf. (1994). *Foundation vibrational analysis using simple physical models*. *Prentice Hall*, Englewood Cliffs, New Jersey.

Julian, B. R., and Gubbins, D. (1977). “Three-dimensional seismic ray tracing.” *Journal of Geophysics*.

Karabalis, D. L., and Mohammadi, M. (1998). "3-D dynamic foundation-soil-foundation interaction on layered soil." *Soil Dynamics and Earthquake Engineering*, 17(3), 139–152.

Katayama, T., Kubo, K., and Sato, N. (1975). "Earthquake Damage To Water and Gas Distribution Systems." *Proceedings of the US National Conference on Earthquake Engineering, EERI*, Ann Arbor, 396–405.

Kloukinas, P., Langousis, M., and Mylonakis, G. (2012). "Simple wave solution for seismic earth pressures on nonyielding walls." *Journal of Geotechnical and Geoenvironmental Engineering*, 138(12), 1514–1519.

Komatitsch, D., and Tromp, J. (1999). "Introduction to the spectral element method for three-dimensional seismic wave propagation." *Geophysical Journal International*.

Komatitsch, D., and Tromp, J. (2014). "SPECFEM2D User Manual Version 7.0." *Computational Infrastructure for Geodynamics*.

Komatitsch, D., and Vilotte, J.-P. (1998). "The spectral element method: An efficient tool to simulate the seismic response of 2D and 3D geological structures." *Bulletin of the Seismological Society of America*, 88(2), 368–392.

Kouretzis, G. P., Bouckovalas, G. D., and Gantes, C. J. (2006). "3-D shell analysis of cylindrical underground structures under seismic shear (S) wave

action." *Soil Dynamics and Earthquake Engineering*, 26(10), 909–921.

Kramer, S. L. (1996). *Geotechnical Earthquake Engineering*. Prentice Hall, New Jersey.

Lee, M. K. W., and Finn, L. W. D. (1978). "{DESRA}-2: Dynamic effective stress response analysis of soil deposits with energy transmitting boundary including assessment of liquefaction potential." *Soil Mechanics*, 38(38).

Lee, T. H., and Wesley, D. A. (1973). "Soil-structure interaction of nuclear reactor structures considering through-soil coupling between adjacent structures." *Nuclear Engineering and Design*, 24(3), 374–387.

Lei, W., Weiming, G., Yonggao, Y., and Xiaodong, T. (2021). "Field Experimental Study on Vertical Bearing Capacity of Root-Caisson Foundation." *Advances in Soil Dynamics and Foundation Engineering*, Proceedings.

Lin, H. -T, Roesset, J. M., and Tassoulas, J. L. (1987). "Dynamic interaction between adjacent foundations." *Earthquake Engineering & Structural Dynamics*, 15(3), 323–343.

Longuet-Higgins, M. S. (1950). "A theory of the origin of microseisms." *Philosophical Transactions of the Royal Society of London. Series A, Mathematical and Physical Sciences*, 243(857), 1–35.

Lowrie, W. (2007). *Fundamentals of Geophysics*. Cambridge University Press,

New York, NY, USA.

Mccamy, K., Meyer, R.P., and Smith, T. J. (1962). "Generally applicable solutions of Zoeppritz' amplitude equations." *Bulletin of the Seismological Society of America*, 52(4), 923–955.

Mononobe, N., and Matsuo, H. (1929). "On the Determination of Earth Pressures During Earthquakes." *Proceedings of World Engineering Congress*, Tokyo, Japan, 274–280.

Mulliken, J. S., and Karabalis, D. L. (1995). "Discrete Model For Foundation-soil-foundation Interaction." *Soil Dynamics and Earthquake Engineering*, 8, 1–3.

Mylonakis, G., and Gazetas, G. (2000). "Seismic soil-structure interaction: Beneficial or detrimental?" *Journal of Earthquake Engineering*, 4(3), 277–301.

Newmark, N. M., and Hall, W. J. (1975). "Pipeline Design To Resist Large Fault Displacement." 416–425.

NP-T-3.20. (2018). *Buried and Underground Piping and Tank Ageing Management for Nuclear Power Plants*. Vienna.

NuScalePower. (2020). "NuScale Final Safety Analysis Report." <https://www.nrc.gov/docs/ML2022/ML20224A491.pdf>.

O'Rourke, M., and Ayala, G. (1993). "Pipelinpipeline damage due to wave

propagatione." *Journal of Geotechnical Engineering*, 119(9), 1490–1498.

Okabe, S. (1926). "General theory of earth pressure." *Journal of the Japanese Society of Civil Engineers*, 12(1), 1277–1323.

P., D. J., T., H. G., and J., D. A. (2005). "Stiffness of Flexible Caisson Foundations Embedded in Nonhomogeneous Elastic Soil." *Journal of Geotechnical and Geoenvironmental Engineering*, American Society of Civil Engineers, 131(12), 1498–1508.

Padrón, L. A., Aznárez, J. J., and Maeso, O. (2011). "3-D boundary element-finite element method for the dynamic analysis of piled buildings." *Engineering Analysis with Boundary Elements*, 35(3), 465–477.

Peter, D., Komatitsch, D., Luo, Y., Martin, R., Le Goff, N., Casarotti, E., Le Loher, P., Magnoni, F., Liu, Q., Blitz, C., Nissen-Meyer, T., Basini, P., and Tromp, J. (2011). "Forward and adjoint simulations of seismic wave propagation on fully unstructured hexahedral meshes." *Geophysical Journal International*, 186(2), 721–739.

Reese, C. D., and Eidson, J. V. (2006). *Handbook of OSHA Construction Safety and Health*. *Handbook of OSHA Construction Safety and Health*.

Rizzo, F. J., Shippy, D. J., and Rezayat, M. (1985). "A boundary integral equation method for radiation and scattering of elastic waves in three dimensions." *International Journal for Numerical Methods in Engineering*.

Rodríguez-Castellanos, A., Rodríguez-Sánchez, J. E., and Carbajal-Romero, M. (2010). "Coupled response for rigid foundations." *Journal of Geotechnical and Geoenvironmental Engineering*, 135(12), 1971–1975.

Scott, R. F. (1973). "Walls, Earthquake-Induces Earth pressures by Retaining." *5thWorld Conference on Earthquake Engineering*, Tokyo, Japan, 1611–1620.

Seed, H. B., and Whitman, R. V. (1970). "Design of Earth Retainig Structures for Dynamic Loads." *ASCE Specialty Conference on Lateral Stresses in the Ground and Design of Earth-Retaining Structures*, Cornell Univ., Ithaca, New York, 103–147.

Skau, K. S., Jostad, H. P., Eiksund, G., and Sturm, H. (2019). "Modelling of soil-structure-interaction for flexible caissons for offshore wind turbines." *Ocean Engineering*, 171, 273–285.

Stacey, R. (1988). "Improved transparent boundary formulations for the elastic-wave equation." *Bulletin of the Seismological Society of America*, 78(6), 2089–2097.

Steedman, R. S., and Zeng, X. (1990). "The influence of phase on the calculation of pseudo-static earth pressure on a retaining wall." *Geotechnique*, 40(1), 103–112.

Stein, S., and Wysession, M. (2003). *An Introduction to Seismology, Earthquakes,*

and Earth Structure. *Seismological Research Letters*, Blackwell Publishing Ltd., Malden, USA.

Takada, S., and Tanabe, K. (1987). "Three-dimensional seismic response analysis of buried continuous or jointed pipelines." *Journal of Pressure Vessel Technology, Transactions of the ASME*, 109(1), 80–87.

Telford, W. M., Geldart, L. P., and Sheriff, R. E. (1990). *Applied Geophysics*. *Cambridge University Press.*

Teng, T.-L. (1987). *Geophysics - Field Measurements*. *Methods in Experimental Physics*.

Thomson, W. T. (1950). "Transmission of elastic waves through a stratified solid medium." *Journal of Applied Physics*, 21, 89–93.

Triantafyllidis, T., and Prange, B. (1988). "Rigid circular foundation: Dynamic effects of coupling to the half-space." *Soil Dynamics and Earthquake Engineering*, 7(1), 40–52.

Trifonov, O. V., and Cherniy, V. P. (2010). "A semi-analytical approach to a nonlinear stress-strain analysis of buried steel pipelines crossing active faults." *Soil Dynamics and Earthquake Engineering*, 30(11), 1298–1308.

U.S. NRC. (2013). *Standard Review Plan for the Review of Safety Analysis Reports for Nuclear Power Plants: LWR Edition. Section 3.7.3 Seismic Subsystem Analysis Review Responsibilities*. *NUREG 0800*.

USGS. (2009). “Determining the Depth of an Earthquake.” *Earthquake Information Bulletin (USGS)*, 9(4), 16.

Veletsos, A. S., and Younan, A. H. (1994). “Dynamic soil pressures on rigid vertical walls.” *Earthquake Engineering & Structural Dynamics*, 23(3), 275–301.

W., G., and J., C. (2021). “Experimental Study of Installation of Concrete Suction Caisson in Clay.” *IFCEE 2015*, Proceedings.

Warburton, G. B., Richardson, J. D., and Webster, J. J. (1971). “Forced vibrations of two masses on an elastic half space.” *Journal of Applied Mechanics, Transactions ASME*, 38(1), 148–156.

Whitman RV. (1969). “Current Status of Soil Dynamics.” *Applied Mechanics Reviews*, 22, 1–8.

Wolf, J. P. (1989). “Soil-structure-interaction analysis in time domain.” *Nuclear Engineering and Design*.

Wood, J. H. (1973). *Earthquake-induced soil pressures on structures*. *PhD Thesis*, Pasadena, CA.

Yao, W. A., and Mao, L. (2010). “Symplectic system based analytical solution for bending of rectangular plates on Winkler foundation.” *The IES Journal Part A: Civil & Structural Engineering*, Taylor & Francis, 3(1), 28–37.

Zoeppritz, K. (1919). “Über Erdbebenwellen Part VII b . Über Reflexion und

Durchgang seismischer Wellen durch Unstetigkeitsflächen.” *Nachrichten von der Gesellschaft der Wissenschaften zu Göttingen, Mathematisch-Physikalische Klasse*, 66–84.

Chapter 2

SEISMIC EARTH PRESSURE DUE TO RAYLEIGH WAVES IN VISCOELASTIC MEDIA

2.1. ABSTRACT

This paper presents an analytical solution to calculate the seismic earth pressure induced by Rayleigh wave in viscoelastic media using the three-dimensional wave propagation theory. Two soil-structure systems are considered: a substructure inserted into homogeneous soil layer, and a substructure surrounded by a multilayered soil profile. Closed-form solutions are proposed as functions of damping ratio, Poisson's ratio, and the height of the substructure. Furthermore, two special cases were investigated to examine the influences of a soft and a stiff thin layer in the layered soil profiles. The results obtained for different scenarios were compared systematically in a comprehensive numerical example.

Keywords: seismic earth pressure; Rayleigh waves; soil structure interaction; multilayered soils.

2.2. INTRODUCTION

Over the past decades, the determination of seismic earth pressure has gained considerable interest in earthquake geotechnical engineering due to its importance in the safety of major facilities such as Nuclear Power Plants (NPPs) or transportation infrastructure systems. Numerous analytical, numerical, and

experimental studies have been performed to study the dynamic behavior of the seismic-prone retained structures. Depending on the wall movement and the soil stresses, the analytical methods for seismic earth pressure can be classified into three categories: rigid plastic (limit state method), elastic, and elastoplastic methods. The limit state methods assume that the wall movement is large enough and hence the soil behind the wall reaches its failure state (or limit state). The equilibrium equations of the sliding soil wedge are formulated by considering the shear strength of soil. The elastic methods assume small wall displacements and employ the theory of elasticity to analyze the soil-structure system, where appropriate boundary conditions are used to capture the interaction with the substructure. The elastoplastic methods consider small-to-large wall displacements and the hysteretic behavior of the soil.

After the devastating impact of the Great Kanto earthquake in Japan in 1923, Okabe (1926) proposed the General Theory of Earth Pressure to calculate seismic earth pressure based on the limit state assumption. Okabe's method can be considered as an extension of Coulomb's theory that assumes a sliding soil wedge behind the wall. For a soil wedge subjected to horizontal and vertical seismic forces, Okabe (1926) suggested an expression for the total seismic force and defined the coefficient of lateral earth pressure K_{ae}. Okabe's work was verified by a shaking table experiment conducted by Mononobe and Matsuo(1929). The expressions given by Okabe (1926) were later simplified by Seed and Whitman (1970) by dividing the total force into static and dynamic components. In addition, Seed and

Whitman (1970) suggested that the point of application of the total seismic force is located at a height between 0.5H and 0.7H from the base of the wall. As an extension of the Mononobe-Okabe method, Steedman and Zeng (1990) employed the sinusoidal wave propagation throughout the backfill to calculate the seismic earth pressure distribution on a retaining wall founded on rock. They noted that the Mononobe-Okabe method gives reasonable evaluation of the total seismic load, but the seismic earth pressure distribution is very different from that assumed by the M-O method. In a relatively recent study, Choudhury et al. (2014) employed the limit equilibrium method to estimate the seismic earth pressure on a rigid wall that retains cohesionless soil, taking into account both vertical and horizontal accelerations.

The most common elastic method was developed by Wood (1973), currently known as the exact analytical solution. Wood (1973) derived a general solution for the seismic earth pressure on perfectly rigid and deformable walls supporting homogeneous elastic soil. By treating the soil as a one-dimensional shear beam attached to rigid walls by Winkler springs to consider soil-structure interaction, Scott (1973) provided expressions for the seismic earth pressure, the total seismic load, and the total moment acting on the wall. In the work of Veletsos and Younan (1994), the soil was modeled as a series of elastically supported bars with a distributed mass, which resulted in an expression for the dynamic increment in the lateral earth pressure. Considering the horizontal earthquake shaking, Lee and Finn (1978) developed charts for the design of seismic earth pressure against a

rigid wall retaining uniform and nonuniform backfills. Using Ritz functions and variable separation method, Kloukinas et al. (2012) solved the wave propagation equations and provided a closed-form solution for the seismic earth pressure. However, due to the mathematical complexity of this solution, its application in engineering practice is limited.

Regarding the earthquake excitation of the above-mentioned methods, various assumptions have been made in the literature. For example, the M-O method used uniform excitation throughout the backfill, while Steedman and Zeng (1990) assumed sinusoidal distribution of the acceleration in the horizontal direction. The closed-form solution by Wood (1973) is based on the analysis for vertically propagating shear waves in soil. Choudhury and Nimbalkar (2005, 2006) introduced closed-form solutions for the seismic active earth pressure and seismic passive resistance for a rigid retaining wall using a pseudo-dynamic approach, taking into account the horizontal and vertical accelerations, as well as primary and shear wave velocities. Using a modified pseudo-dynamic approach, Rajesh and Choudhury (2017) considered the primary and shear waves in the analysis to develop a generalized expression of the seismic active thrust on a rigid wall retaining submerged backfill. The same authors adopted the modified pseudo-dynamic approach to evaluate the stability of seawalls subjected to the joint action of a tsunami and seismic aftershock (Rajesh and Choudhury 2018). The horizontal and vertical accelerations were also employed by Bellezza (2014, 2015) to define

the seismic active soil thrust on a rigid retaining wall using a new pseudo-dynamic approach, considering visco-elastic soil behaviour.

In terms of seismic waves in soil, earthquakes produce two main types of waves: body waves and surface waves. Body waves travel through the inner layers of the Earth. Contrarily, a surface wave exists only in the surficial layers and reach the site after the arrival of body waves due to its relatively low propagation velocity. Surface waves can be more destructive than body waves as they propagate at a slower rate and can have a much larger amplitude in strong earthquakes. Also, surface waves geometrically attenuate at a much slower rate than body waves, with the attenuation rates being proportional to $1/r$ and $1/\sqrt{r}$ for the body waves and surface waves (Lowrie, 1997), respectively. Body waves include Primary waves (P-waves) and Secondary waves (S-waves), while Surface waves include Rayleigh waves and Love waves. Figure 2.1 shows both types of waves and elucidates the difference in the magnitudes and the arrival times.

Motivated by the lack of research in seismic earth pressure induced by surface waves, in this paper we present a closed-form solution to calculate the seismic earth pressure due to Rayleigh wave propagation in viscoelastic media. Starting with a simple case of a rigid substructure buried in a homogeneous viscoelastic soil layer, we first derive the expressions for shear and normal stresses against a rigid wall as well as the magnitude and the location of the total force. The derivation is then extended to a more general case, in which a rigid substructure is inserted into a multilayered soil profile. Two special cases are investigated to explore the influence

of a soft and a stiff thin layer in multilayered profiles. A comprehensive parametric study is performed, and valuable conclusions were drawn.

2.3. EARTH PRESSURE DUE TO RAYLEIGH WAVES IN HOMOGENOUS VISCOELASTIC SOIL LAYER

2.3.1. ASSUMPTIONS AND LIMITATIONS

Figure 2.2 shows a rigid substructure surrounded by isotropic homogeneous viscoelastic soil. Viscoelasticity is considered in the analysis by introducing the correspondence principle (Wolf 1985), where the damped solution can be obtained by replacing the elastic constants with the corresponding complex counterparts. Regarding radiation damping, it is assumed that the boundaries at the right and bottom edges of the soil profile domain have complete absorption of seismic energy that reaches the boundary, either reflected from the soil-structure system or propagating towards the unbounded soil medium. The contact between a substructure and the surrounding soil can be maintained for deeply buried structure owing to the high horizontal earth pressure, which implies the compatibility of displacement on the soil-substructure interface. For strong ground motion induced by earthquake, separation of soil from the substructure may take place near the ground surface. However, this is beyond the scope of this research. The base of the rigid structure and the homogeneous soil layer is underlain by rigid rock where horizontal and vertical displacements are restrained. In other words, neither vertical nor horizontal displacements are allowed at depth H. At the free surface, the total

traction is zero, which implies the normal and shear stresses vanish. In an advanced section in the paper, the derivation is extended to include a substructure inserted into multilayered soils. Soil layers are assumed to be horizontally stratified, and the stress continuity and displacement compatibility should be satisfied at the interface between soil layers.

2.3.2. EQUATIONS OF MOTION

As a plane wave, Rayleigh wave is a combination of the P- and SV-waves near the surface. For a plane wave traveling in the $x-$direction, particle displacement is only in the $x-$ and $z-$directions. When using u, v, w to represent displacement in $x-$, $y-$ and $z-$directions, one has $u = u(x,z,t)$, $v = 0$, $w = w(x,z,t)$. Consider an infinitesimal element of isotropic, linear, elastic soil, as depicted in Figure 2.2a. The equations of motion in the $x-z$ plane can be expressed as a function of the corresponding displacements and strains together with the two *Lamé* constants λ and μ as:

$$\rho\frac{\partial^2 u}{\partial t^2} = (\lambda+\mu)\frac{\partial \bar{\varepsilon}}{\partial x} + \mu\nabla^2 u \tag{1.a}$$

$$\rho\frac{\partial^2 w}{\partial t^2} = (\lambda+\mu)\frac{\partial \bar{\varepsilon}}{\partial z} + \mu\nabla^2 w \tag{1.b}$$

where ∇^2 is Laplace operator, and $\bar{\varepsilon}$ is the volumetric strain of soil.

When a seismic wave propagating through a medium, attenuation of wave amplitude may occur owing to different mechanisms, typically geometrical damping (radiation damping) and material damping (where the material is not linear

elastic). Radiation damping occurs due to the spread of stress waves over unbounded soil medium, resulting in decrease in the density of energy or intensity of motion. Material damping is induced by non-elastic relative movement between soil particles, which converts part of the elastic energy to heat (or energy dissipation) accompanied by decreasing in the amplitude of the stress waves. This energy dissipation mechanism is known as hysteretic damping. As mentioned earlier, material damping is accounted for by introducing the correspondence principle, but radiation damping is neglected. Therefore, the damped version of Equations (1) can be written as

$$\rho \frac{\partial^2 u}{\partial t^2} = \left(\hat{\lambda} + \hat{\mu}\right) \frac{\partial \bar{\varepsilon}}{\partial x} + \hat{\mu} \nabla^2 u \tag{2.a}$$

$$\rho \frac{\partial^2 w}{\partial t^2} = \left(\hat{\lambda} + \hat{\mu}\right) \frac{\partial \bar{\varepsilon}}{\partial z} + \hat{\mu} \nabla^2 w \tag{2.b}$$

where $\hat{\lambda}$ and $\hat{\mu}$ are the complex *Lamé* constants. When introducing the damping ratio $\boldsymbol{\zeta}$ of the soil, $\hat{\lambda}$ and $\hat{\mu}$ are given as

$$\hat{\mu} = \mu(1 + 2i\zeta) \tag{3.a}$$

$$\hat{\lambda} = \hat{\mu}\, \mathcal{F}^2, \;\; \mathcal{F}^2 = \frac{2\nu}{1 - 2\nu} \tag{3.b}$$

2.3.3. POTENTIAL FUNCTIONS OF RAYLEIGH WAVES

For a plane wave travels in homogeneous soil in the $x - z$ plane, the displacements in the $x -$ and $z -$directions, $u = u(x, z, t)$ and $w = w(x, z, t)$ respectively, can be described by two potential functions Φ and Ψ as (Pavlis, 2003)

$$u(x,z,t) = \frac{\partial \Phi}{\partial x} + \frac{\partial \Psi}{\partial z} \tag{4.a}$$

$$w(x,z,t) = \frac{\partial \Phi}{\partial z} - \frac{\partial \Psi}{\partial x} \tag{4.b}$$

The two potential functions Φ and Ψ represent the dilatation and rotation components of the seismic wave, respectively. For a Rayleigh wave, Φ and Ψ are specifically expressed as (Pavlis, 2003)

$$\Phi(x,z,t) = F(z)e^{i(\omega t - \hat{k}_R x)} \tag{5.a}$$

$$\Psi(x,z,t) = G(z)e^{i(\omega t - \hat{k}_R x)} \tag{5.b}$$

where $\hat{k}_R$ is the complex Rayleigh wavenumber. Functions $F(z)$ and $G(z)$ describe the variation in the amplitude of Φ and Ψ with depth. By substituting equations (5) and (4) into equations (2) and solving both equations simultaneously for $F(z)$ and $G(z)$, the general solution can be written in the exponential form as:

$$F(z) = A_1 e^{-\hat{q}z} + B_1 e^{\hat{q}z} \tag{6.a}$$

$$G(z) = A_2 e^{-\hat{s}z} + B_2 e^{\hat{s}z} \tag{6.b}$$

$$\hat{q}^2 = \hat{k}_R^2 \left[1 - \left(\frac{\hat{v}_R}{\alpha\, \hat{v}_s}\right)^2\right], \quad \hat{s}^2 = \hat{k}_R^2 \left[1 - \left(\frac{\hat{v}_R}{\hat{v}_s}\right)^2\right], \quad \alpha^2 = \frac{2-2}{1-2} \tag{6.c}$$

where $\hat{v}_R$ is the damped Rayleigh wave velocity, and $\hat{v}_s$ is the damped shear wave velocity, and $\alpha\hat{v}_s$ represents the damped primary wave velocity $\hat{v}_p$. Substitution of Equations (6) and (5) into Equations (4) gives the horizontal and vertical displacements as:

$$u(x,z,t) = -i\hat{k}_R e^{-\hat{q}z}A_1 - i\hat{k}_R e^{\hat{q}z}B_1 - \hat{s}e^{-\hat{s}z}A_2 + \hat{s}e^{\hat{s}z}B_2 \quad (7.a)$$

$$w(x,z,t) = -\hat{q}e^{-\hat{q}z}A_1 + \hat{q}e^{\hat{q}z}B_1 + i\hat{k}_R e^{-\hat{s}z}A_2 + i\hat{k}_R e^{\hat{s}z}B_2 \quad (7.b)$$

where A_1, B_1, A_2, and B_2 represent the seismic displacement amplitudes of different wave components in different directions.

2.3.4. BOUNDARY CONDITIONS AND DAMPED RAYLEIGH WAVE VELOCITY

For the soil-structure system shown in Figure 2.2, the horizontal and vertical displacements are restrained, and the shear and normal stresses vanish at the free surface. Therefore,

$$u(z=H)=0 \qquad -i\hat{k}_R e^{-\hat{q}H}A_1 - i\hat{k}_R e^{\hat{q}H}B_1 - \hat{s}e^{-\hat{s}H}A_2 + \hat{s}e^{\hat{s}H}B_2 = 0 \quad (8.a)$$

$$w(z=H)=0 \qquad -\hat{q}e^{-\hat{q}H}A_1 + \hat{q}e^{\hat{q}H}B_1 + i\hat{k}_R e^{-\hat{s}H}A_2 + i\hat{k}_R e^{\hat{s}H}B_2 = 0 \quad (8.b)$$

$$\sigma_{zz}(z=0) = \hat{\lambda}\bar{\varepsilon} + 2\hat{\mu}\varepsilon_{zz} = 0 \qquad \hat{\mu}\left[\left(\alpha^2\hat{q}^2 - \mathcal{F}^2\hat{k}_R^2\right)(A_1+B_1) - 2i\hat{k}_R\hat{s}(A_2-B_2)\right] = 0 \quad (8.c)$$

$$\sigma_{xz}(z=0) = \hat{\mu}\varepsilon_{xz} = 0 \qquad \hat{\mu}\left[2i\hat{k}_R\hat{q}(A_1-B_1) + \left(\hat{k}_R^2+\hat{s}^2\right)(A_2+B_2)\right] = 0 \quad (8.d)$$

The above equations can be written in the matrix form as follows:

$$\begin{bmatrix} -i\hat{k}_R e^{-\hat{q}H} & -i\hat{k}_R e^{\hat{q}H} & -\hat{s}e^{-\hat{s}H} & \hat{s}e^{\hat{s}H} \\ -\hat{q}e^{-\hat{q}H} & \hat{q}e^{\hat{q}H} & i\hat{k}_R e^{-\hat{s}H} & i\hat{k}_R e^{\hat{s}H} \\ \alpha^2\hat{q}^2 - \mathcal{F}^2\hat{k}_R^2 & \alpha^2\hat{q}^2 - \mathcal{F}^2\hat{k}_R^2 & -2i\hat{k}_R\hat{s} & 2i\hat{k}_R\hat{s} \\ 2i\hat{k}_R\hat{q} & -2i\hat{k}_R\hat{q} & \hat{k}_R^2 + \hat{s}^2 & \hat{k}_R^2 + \hat{s}^2 \end{bmatrix} \begin{Bmatrix} A_1 \\ B_1 \\ A_2 \\ B_2 \end{Bmatrix} = 0 \quad (9)$$

The determinant of the coefficient matrix in Equation (9) represents the characteristic function for the Rayleigh waves to propagate in the soil layer shown in Figure 2.2. Given the frequency of the waves (ω), the solution of Equation (9) gives the phase velocity ($\hat{v}_R$) of Rayleigh waves. The characteristic equation is a function of the Poisson's ratio, damping ratio, and height of the rigid wall. The damped Rayleigh wave velocity is implicitly a function of damped shear and primary waves velocities expressed as $v_s\sqrt{1+2i\zeta_s}$ and $v_p\sqrt{1+2i\zeta_s}$, respectively. Moreover, attenuation of Rayleigh wave owing to damping is frequency dependent. As mentioned earlier, the damping ratios of shear and primary waves are assumed to be equal, and hence a global damping ratio of ζ is employed in the paper. However, for $\zeta_s \neq \zeta_p$, the Rayleigh wave displacements are no longer 90° out of phase (Wolf, 1985). Even though the damping characterizing the attenuation of Rayleigh wave can be determined without explicit expression, this paper made no effect to determine it.

2.3.5. SEISMIC EARTH PRESSURE

The seismic earth pressure on a substructure consists of two components: the normal stress σ_{xx} and the shear stress σ_{xz}. For a frictionless wall, the shear stress

component can be neglected, and the total seismic earth pressure is evaluated only by normal stresses. Otherwise, the total earth pressure should be calculated as the square root of the sum of the squares of the shear and normal stress components with an angle of inclination with respect to the horizontal. The shear and normal stresses on the wall (i.e., at $x = 0$) are determined from the stress-strain relation as:

$$\sigma_{xx}(z,t) = \hat{\mu}\big[\big(-\alpha^2\hat{k}_R^2 + \mathcal{F}^2\hat{q}^2\big)\big(e^{-\hat{q}z}A_1 + e^{\hat{q}z}B_1\big) + i\hat{s}\hat{k}_R(\alpha^2 - \mathcal{F}^2)\big(e^{-\hat{s}z}A_2 - e^{\hat{s}z}B_2\big)\big]\, e^{i\omega t} \tag{10.a}$$

$$\sigma_{xz}(z,t) = \hat{\mu}\big[2i\hat{k}_R\hat{q}\big(e^{-\hat{q}z}A_1 - e^{\hat{q}z}B_1\big) + \big(\hat{k}_R^2 + \hat{s}^2\big)\big(e^{-\hat{s}z}A_2 + e^{\hat{s}z}B_2\big)\big]\, e^{i\omega t} \tag{10.b}$$

The total seismic load on the wall can be calculated by integrating the normal and shear stresses along the total height of the wall H, which leads to

$$F_{xx} = \hat{\mu}\left[\frac{\big(-\alpha^2\hat{k}_R^2 + \mathcal{F}^2\hat{q}^2\big)}{\hat{q}}\Big(\big(1 - e^{-\hat{q}H}\big)A_1 + \big(e^{\hat{q}H} - 1\big)B_1\Big) + i\hat{k}_R(\alpha^2 - \mathcal{F}^2)\Big(\big(1 - e^{-\hat{s}H}\big)A_2 - \big(e^{\hat{s}H} - 1\big)B_2\Big)\right] \tag{11.a}$$

$$F_{xz} = \hat{\mu}\left[2i\hat{k}_R\Big(\big(1 - e^{-\hat{q}H}\big)A_1 - \big(e^{\hat{q}H} - 1\big)B_1\Big) + \frac{\big(\hat{k}_R^2 + \hat{s}^2\big)}{\hat{s}}\Big(\big(1 - e^{-\hat{s}H}\big)A_2 + \big(e^{\hat{s}H} - 1\big)B_2\Big)\right] \tag{11.b}$$

To gain further insight into the graphical representation and the physical significance of the equations, the seismic lateral earth pressure is calculated for the

soil-structure system shown in Figure 2.2, considering the geometrical and mechanical properties listed in Table 2.1. It should be noted that a typical damping ratio of soil ranges approximately from 0 to 25% (Bolton et al. 1986). However, the higher damping ratios were considered in Table 2.1 to give insights into the behaviour of special backfill materials with high energy absorption capabilities, such as rubber concrete backfill, induced by Rayleigh waves.

Substitution of the properties from Table 2.2 into the characteristic equation of the system gives Rayleigh wave velocity. The relationship between the seismic amplitudes A_1, B_1, A_2, and B_2 can then be determined by substituting the Rayleigh wave velocity into the system of linear homogeneous Equation (9). Therefore, all seismic responses can be calculated as a ratio of one of the seismic amplitudes (e.g., u_0 and w_0 at the ground surface).

Figure 2.3 shows the effect of damping ratio and Poisson's ratio on the horizontal and vertical components of Rayleigh wave displacements. The vertical axis represents the depth of soil, and the horizontal axis represents Rayleigh wave displacements normalized to the amplitude at the free surface. In general, the displacements at $z = H$ meet the boundary conditions, where the base of the soil-structure system is assumed fixed. Damping has little effect on the vertical displacement up to 20% damping ratio, after which it gradually increases at higher ratios. For the horizontal displacement component, the effect of damping appears clearly between depths $2.5\,m$ and $9\,m$, where its effect beyond this range is

minimal. In Figure 2.3b, the effect of the Poisson's ratio is significant in both the horizontal and vertical displacements. The concentration of the horizontal displacement near the free surface increases as the Poisson's ratio increases, while the opposite occurs in the vertical displacement.

The seismic lateral earth pressure on the substructure can be readily obtained by Substituting the Rayleigh wave velocity and the characteristics of the soil-structure system listed in Table 2.2 into Equations (10). Figure 2.4 shows the effect of damping ratio and the Poisson's ratio on the normal and shear stress distributions on the substructure. The horizontal axis represents the normal/shear stresses normalized to shear modulus of the soil. Regarding the effect of damping on seismic earth pressure, some similarities can be found between the shear and normal stresses in Figure 2.3 and Rayleigh wave displacements in Figure 2.4a. It can be seen that the effect of damping is prominent near the free ground surface up to a depth of $6\,m$, after which the variation in stresses due to damping is minimal. Furthermore, the normal stresses change direction at different depths such as z_1 in Figure 2.4a, depending on the selected damping ratio. Moreover, at certain depths such as z_2, depending on the selected Poisson's ratio, the effect of damping is reversed where higher damping ratios tend to amplify seismic earth pressure.

In Figure 2.4b, the normal and shear stresses increase gradually as the Poisson's ratio increases. However, the direction of the normal stresses on the substructure is reversed at depth z_3, which implies potential separation between the substructure and the soil (depending on the original static horizontal stress). It

should be emphasized that the depths z_1, z_2, and z_3 are not constant but vary according to the selected damping ratio and Poisson's ratio.

Figure 2.5 compares the results of the present study with the solution suggested by Choudhury et al. (2014) at different Poisson ratios. The Choudhory method is referred to as C-Method in Figure 2.5. The seismic earth pressure using the C-method was calculated considering a full horizontal and vertical accelerations. The angle of inclination of failure surface and the soil friction angle were taken as 35° and 33°, respectively, which are consistent with the soil properties given in Table 2.1. Since the C-method is a limit equilibrium method, it produces higher seismic earth pressure than the present study based on seismic wave propagation. The highest discrepancies occur near the free surface and vanish gradually with depth. In addition, the discrepancies reduce as Poisson's ratio increases.

2.4. EARTH PRESSURE DUE TO RAYLEIGH WAVES IN MULTI-LAYERED SOILS

Rayleigh wave may also develop in layered soils, which are frequently encountered in engineering practice. For the analysis of Rayleigh wave in layered soils, the general principles for homogeneous soils as presented in previous sections are still valid. However, the stress continuity and deformation compatibility on the interface of soil layers should be applied to determine the constants in the potential functions and the wave velocity. Figure 2.6 shows a substructure inserted into a soil profile consists of N homogeneous horizontally stratified soil layers. The wall of the

substructure is assumed rigid, and the base of the soil-structure system is underlain by rigid rock where horizontal and vertical displacements are restrained. Layers and interfaces are number away from the surface.

Following the analysis of wave propagation in continuum, the problem of seismic earth pressure in a multi-layered soil involves two separate steps: Modal analysis and response solutions. Modal analysis gives the dynamic characteristics of the soil profile and is a function of the geometrical and mechanical properties of the soil layers. The dynamic characteristics include mode shapes and dispersion curves, which are combinations of natural frequencies and phase velocities. The response solution gives the displacements in the soil layers and the stresses on the substructure.

2.4.1. MODAL SOLUTION

In soil layer m, following the Transfer Matrix approach (Haskell, 1953 and Thomson, 1950), the displacement in the $x-z$ plane in equations (8) and the pertinent normal and shear stresses can be written in the matrix form as:

$$\begin{Bmatrix} u/\hat{k}_R \\ w/\hat{k}_R \\ \sigma_{zz}/\hat{\mu} \\ \sigma_{xz}/\hat{\mu} \end{Bmatrix} = \tag{12}$$

$$\begin{bmatrix} -ie^{-\hat{q}z} & -ie^{\hat{q}z} & -\hat{s}e^{-\hat{s}z} & \hat{s}e^{\hat{s}z} \\ -\hat{q}e^{-\hat{q}z} & \hat{q}e^{\hat{q}z} & ie^{-\hat{s}z} & ie^{\hat{s}z} \\ (\alpha^2\hat{q}^2 - \mathcal{F}^2\hat{k}_R^2)e^{-\hat{q}z} & (\alpha^2\hat{q}^2 - \mathcal{F}^2\hat{k}_R^2)e^{\hat{q}z} & -2i\hat{s}e^{-\hat{s}z} & 2i\hat{s}e^{-\hat{s}z} \\ 2i\hat{q}e^{-\hat{q}z} & -2i\hat{q}e^{\hat{q}z} & (\hat{s}^2+1)e^{-\hat{s}z} & (\hat{s}^2+1)e^{\hat{s}z} \end{bmatrix} \begin{Bmatrix} A_1 \\ B_1 \\ A_2 \\ B_2 \end{Bmatrix} e^{i(\omega t - \hat{k}_R x)}$$

The components of the coefficient matrix in Equation (12) are implicitly functions of the Poisson's ratio, frequency, and Rayleigh wave velocity. By enforcing the displacement compatibility and stress continuity at the interface between soil layers, the responses at two subsequent interfaces can be written as:

$$\left\{\frac{u}{k_R}, \quad \frac{w}{k_R}, \quad \frac{\sigma_{zz}}{\mu}, \quad \frac{\sigma_{xz}}{\mu}\right\}_m = [D]_{m,B}[D]_{m,T}^{-1} \left\{\frac{u}{k_R}, \quad \frac{w}{k_R}, \quad \frac{\sigma_{zz}}{\mu}, \quad \frac{\sigma_{xz}}{\mu}\right\}_{m-1} \tag{13}$$

where $[D]$ is the coefficient matrix at the top and bottom boundaries of the m^{th} layer. The subscripts T and B refer to the top and bottom boundaries of the soil layer, respectively. By setting the origin z at the top of the m^{th} layer, the coefficient matrices at the top and bottom of the layer can be calculated by setting z equals to zero and h_m, respectively, as:

$$[D]_{m,T} = \begin{bmatrix} -i & -i & -\hat{s} & \hat{s} \\ -\hat{q} & \hat{q} & i & i \\ \left(\alpha^2\hat{q}^2 - \mathcal{F}^2\hat{k}_R^2\right) & \left(\alpha^2\hat{q}^2 - \mathcal{F}^2\hat{k}_R^2\right) & -2i\hat{s} & 2i\hat{s} \\ 2i\hat{q} & -2i\hat{q} & (\hat{s}^2+1) & (\hat{s}^2+1) \end{bmatrix} \tag{14.a}$$

$$[D]_{m,B} = \begin{bmatrix} -ie^{-\hat{q}h_m} & -ie^{\hat{q}h_m} & -\hat{s}e^{-\hat{s}h_m} & \hat{s}e^{\hat{s}h_m} \\ -\hat{q}e^{-\hat{q}h_m} & \hat{q}e^{\hat{q}h_m} & ie^{-\hat{s}h_m} & ie^{\hat{s}h_m} \\ \left(\alpha^2\hat{q}^2 - \mathcal{F}^2\hat{k}_R^2\right)e^{-\hat{q}h_m} & \left(\alpha^2\hat{q}^2 - \mathcal{F}^2\hat{k}_R^2\right)e^{\hat{q}h_m} & -2i\hat{s}e^{-\hat{s}h_m} & 2i\hat{s}e^{-\hat{s}h_m} \\ 2i\hat{q}e^{-\hat{q}h_m} & -2i\hat{q}e^{\hat{q}h_m} & (\hat{s}^2+1)e^{-\hat{s}h_m} & (\hat{s}^2+1)e^{\hat{s}h_m} \end{bmatrix} \tag{14.b}$$

Regarding the boundary conditions of the soil-structure system shown in Figure 2.6, the vertical and horizontal displacements are restrained at the base, while the shear and normal stresses at the free ground surface are both zero. The modal solution can be determined by applying the boundary conditions. When utilizing Equations (14), the displacements and stresses at the very bottom of the soil profile can be related to the displacements at the free ground surface via:

$$\begin{Bmatrix} 0 \\ 0 \\ \sigma_{zz}/\mu \\ \sigma_{xz}/\mu \end{Bmatrix}_n = \prod_{i=1}^{n} \left([D]_B[D]_T^{-1}\right)_i \begin{Bmatrix} u/k_R \\ w/k_R \\ 0 \\ 0 \end{Bmatrix}_0 \tag{15}$$

By partitioning the above matrix into sub-matrices, the characteristic function of the multilayered soil system can be expressed as:

$$\begin{bmatrix} Q_{11} & Q_{12} \\ Q_{21} & Q_{22} \end{bmatrix} \begin{Bmatrix} u \\ w \end{Bmatrix}_0 = \begin{Bmatrix} 0 \\ 0 \end{Bmatrix} \tag{16}$$

where $[Q]$ is the product of the coefficient matrices in Equation (15).

Given the properties of the soil profile shown in Figure 2.6, the characteristic function depends on the frequency and Rayleigh wave velocity. The solution of the characteristic function gives numerous combinations of frequencies and Rayleigh wave velocities, which form the dispersion curves of the layered soil system. The common criteria to develop the dispersion curves is by fixing one of the two variables (the frequency and phase velocity) such as the frequency and solving the characteristic function for the phase velocities. Substitution of the frequency and the corresponding velocities into Equation (12) yields the mode shapes of Rayleigh wave propagation in the soil system.

We next present a numerical example to compare the difference between the responses of a multilayer soil system and a single homogeneous soil layer. Table 2.2 shows the characteristics of the soil-structure system used in the analysis. To allow a fair comparison, the total depth of the layers is selected to be equal to the thickness of the single layer. In addition, the mechanical properties of the single layer represent approximately the average value of the layered system in Table 2.2.

At the frequency varying from 15 Hz to 70 Hz, the characteristic function was solved, and the dispersion curves were developed, as shown in Figure 2.7. The vertical axis represents Rayleigh wave velocity, while the horizontal axis represents the frequency. Each curve represents a unique mode of Rayleigh wave propagation in the soil-structure system shown in Figure 2.6. For instance, at a frequency of 50 Hz, the corresponding phase velocities are 189.50, 312.50, 386.10, and

$491.32\ m/s$, respectively. It should be noted that the majority of the earthquake frequencies are mostly in the range of 0.2 to 20 Hz. However, the 50 Hz frequency has been adopted in the current analysis to shed light on different mode shapes of Rayleigh waves in the soil-structure system shown in Figure 2.7 and for the purposes of comparison with the homogeneous soil layer, which produces only one mode shape.

When substituting the wave velocities into Equation (12), we obtain the natural mode shapes for soil motion in the horizontal and vertical directions and the results are presented in Figure 2.8. The horizontal axis represents the horizontal/vertical displacement at depth z normalized to the displacement at the free surface, while the vertical axis represents the depth of soil. By utilizing Equation (16), the seismic amplitudes $A_1, B_1, A_2,$ and B_2 at the top layer can be determined by solving the following homogeneous system of linear equations:

$$\begin{aligned} C_{11}A_1 + C_{12}B_1 + C_{13}A_2 + C_{14}B_2 &= 0 \\ C_{21}A_1 + C_{22}B_1 + C_{23}A_2 + C_{24}B_2 &= 0 \\ J_{31}A_1 + J_{32}B_1 + J_{33}A_2 + J_{34}B_2 &= 0 \\ J_{41}A_1 + J_{42}B_1 + J_{43}A_2 + J_{44}B_2 &= 0 \end{aligned} \tag{17}$$

where $[C]$ is the product of $[Q]$ and $[D_1]_T$, and $[J]$ represents $[D_1]_T$.

Figure 2.8 shed light on the correlation between the phase velocity corresponding to each mode shape and the shear wave velocities for the soil profile with properties given in Table 2.2. For Rayleigh wave propagation, the fundamental mode is affected significantly only in the top layer and then attenuates exponentially with depth. This observation implies that the higher modes become dominant as the depth increases, leading to higher frequency responses compared to the assumption of an equivalent homogeneous soil layer. Furthermore, the effect of each mode increases as the phase velocity approaches the shear wave velocity of the relevant soil layer. It should be mentioned that the number of mode shapes shown in Figure 2.8 is not constant but increases at higher frequencies as shown in Figure 2.7.

2.4.2. SEISMIC EARTH PRESSURE ON THE WALL

In this section, we determine the total displacements of the soil particles and the total seismic earth pressure on the wall of a rigid substructure induced by Rayleigh waves. The total shear and normal stresses on the wall due to all mode shapes at layer n can be determined from the stress-strain relationships as:

$$\sigma_{xx_n} = \sum_{i=1}^{m} \Big[\left(\mathcal{F}^2 \hat{q}_i^2 - \alpha^2 \hat{k}_{R_i}^2 \right) \left(e^{-\hat{q}_i z} A_1 + e^{\hat{q}_i z} B_1 \right) + 2i\hat{s}\hat{k}_{R_i} \left(e^{-\hat{s}_i z} A_2 - e^{\hat{s}_i z} B_2 \right) \Big] \mu e^{i\omega t} \tag{18.a}$$

$$\sigma_{xz_n} = \sum_{i=1}^{m} \Big[2i\hat{q}_i \big(e^{-\hat{q}_i z} A_1 - e^{\hat{q}_i z} B_1 \big) + (\hat{s}_i^2 + 1) \big(e^{-\hat{s}_i z} A_2 + e^{\hat{s}_i z} B_2 \big) \Big] \mu e^{i\omega t} \tag{18.b}$$

To distinguish between the effect of each mode shape on the seismic earth pressure, the shear and normal stresses on the wall of the substructure in Figure 2.6 were calculated and plotted for each individual mode, with the results being presented in Figure 2.9. The horizontal axis in Figure 2.9 represents the normal/shear stresses in MPa, while the vertical axis represents the depth of the soil. It can be seen that the distributions of the normal and shear stresses are generally consistent with the mode shapes in Figure 2.8, where higher modes have significant effect on the earth pressure as depth increases compared to the fundamental mode. The shear stresses due to the fundamental mode shape and that in the single homogeneous layer are almost identical. Furthermore, the shear stress distribution is small compared to normal stresses, except for mode shapes whose phase velocities approach the shear wave velocity of the relevant soil layer.

To compare the earth pressure developed in the layered soil system and homogeneous soils, the shear and normal stresses from Figure 2.4 at $\nu = 0.3$ and $\zeta = 20\%$ were extracted and plotted against their counterparts for multilayered soils in Figure **2.9**. Material properties of the homogeneous soil layer can be considered as the mean value of their counterparts in the layered system (see Table 2.2). In general, the assumption of homogeneous soil layer can significantly

underestimate the actual seismic earth pressure on the substructure. This can be attributed to the contribution of higher modes in the total earth pressure.

The normal stress distribution in the single homogeneous layer is close to the distribution due to the fundamental frequency of the layered soil system. However, the contribution of the fundamental frequency in the total earth pressure is minimal compared to higher modes, especially at increased depths. The total shear and normal stresses in the layered soil system is the superposition of the responses in individual modes, while there is only one mode in the homogeneous single layer. Therefore, neglecting the effect of higher modes when adopting the single homogeneous layer assumption may result in unrealistic total forces on the substructure, and therefore an unreliable seismic design.

2.4.3. EFFECT OF THIN LAYERS ON THE SEISMIC EARTH PRESSURE

In engineering practice, a thin layer of soft or stiff soil may be between two layers of the soil-structure system shown in Figure 2.6 is often encountered. It is generally understood that a thin layer may have certain influence on the magnitude and distribution of the seismic earth pressure varies depending on the location, thickness, and stiffness of the layer. However, this influence is often neglected. In this section, a parameter study is presented to examine the influence of thin layers on the seismic responses of the soil-structure system.

The procedure outlined in the seismic earth pressure of a layered soil system will be utilized to investigate two separate cases of a thin soil layer with different

stiffnesses. In either case, the thickness of the thin layer is $0.5\ m$ and is allocated between Layers (2) and (3). The material properties are assumed as $\rho_S = 5000\ kg/m^3$ and $v_{sS} = 1000\ m/s$ for the stiff thin layer and $\rho_L = 1000\ kg/m^3$ and $v_{sL} = 100\ m/s$ for the soft thin layer, respectively. For the sake of comparison with the homogeneous and layered soil profiles, the damping ratio and Poisson's ratio are taken as $20\ \%$ and 0.3 respectively.

Modal analysis was performed, and the corresponding mode shapes and phase velocities were determined. Table 2.3 shows a comparison between the phase velocities calculated at a frequency of $50\ Hz$ in the following four different cases:

- Case (1): Single homogenous viscoelastic soil layer, as shown in Figure 2.2
- Case (2): Multilayered viscoelastic soil profile (reference case), as shown in Figure 2.6
- Case (3): Multilayered viscoelastic soil profile + Stiff thin layer located between Layer (2) and (3)
- Case (4): Multilayered viscoelastic soil profile + Soft thin layer located between Layer (2) and (3)

The data summarized in Table 2.3 show that the fundamental mode shape remains constant for all cases. In the single homogeneous layer, only the fundamental mode exists, and its variation with depth was presented in Figure 2.3. Regardless of the fundamental mode shape, thin soft layer tends to reduce phase velocities of the reference multilayered system (i.e., Case 2). Contrarily, the thin

stiff layer leads to higher velocities, except for the last mode which cannot exceed the shear wave velocity of the bottom soil layer. Regarding the wavelengths in Mode (1), the wavelength of Case (1) is approximately twice the wavelength of the other cases. However, the ratios of the phase velocities to the shear wave velocity of the relevant layer are almost identical, which equal 0.927 and 0.947 for the single homogeneous and multilayered cases, respectively.

Figure 2.10 shows the distribution of the absolute total normal and shear stresses on the substructure corresponding to the four cases listed in Table 2.3. The horizontal axis represents the magnitude of the normal/shear stresses, while the vertical axis represents the depth of the soil. In general, the assumption of an equivalent homogeneous soil layer significantly underestimates the total seismic earth pressure as a result of neglecting the contribution of higher modes. The presence of a stiff thin layer (Case 3) in the layered soil profile shown in Figure 2.6 has marginal effect on the earth pressure distribution in the first layer. Discrepancies appear in Layers (2) and (3), where the stiff thin layer tends to decrease the earth pressure on the substructure. However, instantaneous spikes on the distribution curves of the normal and shear stresses are observed at the location of the thin layer. Regarding the thin soft layer (Case 4), the normal and shear stresses are amplified along the depth of the substructure, except at the location of the thin layer where the upper and lower layers absorbed most of the energy.

2.4.4. POINT OF APPLICATION OF THE DYNAMIC THRUST

According to the literature review, the height of the active thrust varies from $H/3$ (Okabe 1926) to $0.6H$ (Seed and Whitman 1970) measured from the base of the wall. Conceptually, this range is expected to be changed due to the uniqueness of Rayleigh waves propagation either in homogenous or multilayered soils. Considering a frictionless rigid wall surrounded by a viscoelastic homogenous soil (as shown in Figure 2.2), the location of the point of application measured as the depth from the free surface is given by

$$\bar{Z} = \frac{\hat{\mu}\left(-\alpha^2\hat{k}_R^2 + \mathcal{F}^2\hat{q}^2\right)}{\hat{q}^2}\left[\left(-H\hat{q}e^{-\hat{q}H} - e^{-\hat{q}H} + 1\right)A_1 + \left(H\hat{q}e^{\hat{q}H} - e^{\hat{q}H} + 1\right)B_1\right] + \frac{2i\hat{\mu}\hat{k}_R}{\hat{s}}\left[\left(-H\hat{s}e^{-\hat{s}H} - e^{-\hat{s}H} + 1\right)A_2 - \left(H\hat{s}e^{\hat{s}H} - e^{\hat{s}H} + 1\right)B_2\right] \quad (19)$$

For a given wall height (H), the above equation is implicitly a function of the Poisson's ratio and damping ratio. As mentioned before, the total earth pressure in multilayered soils is the sum of the forces due to each mode shape individually. As a result, it would be challenging to express the location of the point of application in a closed form solution. Instead, this location can be determined numerically or estimated as the average of that for each mode shape. The latter assumption will be assessed against the exact solution in the following section.

Figure 2.11 shows the location of the active thrust for the cases listed in Table 2.3 when considering different Poisson's ratios and damping ratios. The

location is expressed as the depth normalized by the wall height. The horizontal axis represents the Poisson's/damping ratio, and the vertical axis represents the height of the point of application measured from the base of the wall. The height h_i for Case (1) was calculated directly from Equation (19). However, for cases involving multilayered soils, i.e., cases (2) to (4), the height h_i was calculated numerically by integrating the total earth pressure across the depth H and identifying the centroid of the earth pressure distribution. The point of application in the homogeneous soil layer is always higher than that in the multilayered soils, except for Cases (2) and (3) at zero damping ratio. At a constant damping ratio, the point of application moves towards the base as the Poisson's ratio increases for the single layer system (Case 1), while the opposite occurs in multilayered soil cases. In Figure 2.11b, soil layers with higher energy absorption rate tend to reduce the concentration of particle displacement near the free surface. As a result, the application location of total force from the normal stresses moves downwards, which is in line with the variation of the normal stresses with damping ratio presented in Figure 2.4a.

Figure 2.11 also sheds light on the influence of the number of mode shapes, which can drastically change the location and the magnitude of the dynamic thrust. Referring to Figure 2.11a for Case (4) at $\nu = 0.45$ and Figure 2.11b for Cases (2) and (3) at zero damping, the location of thrust application does not follow the same trend as the previous results. This can be attributed to the number of mode shapes

developed from the modal analyses in which all cases produced four mode shapes except the previously mentioned special cases that have three mode shapes.

For single homogeneous and multilayered soils, the location of the active thrust due to Rayleigh waves inherently depends on the geometrical and mechanical properties of the soil layers. Therefore, it is not acceptable to draw a general conclusion on the exact location of the dynamic thrust. However, according to the results in Figure 2.11, the active thrust on a wall in a single homogeneous soil layer is located between $0.7H$ to $0.8H$, which is not within the predefined ranges $H/3$ and $0.6H$ from the base of the wall. For a system of multilayered soils, the point of application varies from $0.4H$ to $0.8H$ from the base of the wall.

To gain more insight into the differences between the four cases, the total earth pressure force and moment due to all mode shapes were calculated, with the results being summarized in Table 2.4. The multilayered soils develop considerably higher forces than a single layered soil, which is a direct consequence from the number of modes, especially at high frequencies. Regarding the multilayered soils, the existence of a stiff thin layer reduces the total force on the substructure. However, the location of the active thrust does not appear to cause strong variations in the total moment at the base (see Figure 2.11). For instance, the moment in Case (4) is higher than that in Case (3), even though the point of application in Case (4) is lower than that in Case (3).

Regarding the calculation of the location of the active thrust as the average of all mode shapes, the average location for Case 2 was calculated for different Poisson and damping ratios. The height h_i was calculated numerically, as explained earlier, for the earth pressure distribution due to each mode shape of Case (2) separately, then the average height was determined. The results were compared to the exact solutions in Figure 2.11. Table 2.5 shows the error in calculating the location of the dynamic thrust using the average location assumption. The positive sign means that the point of application is located at a height higher than the exact solution, and vice versa for the negative sign. The average height assumption gives higher location of application in most cases and hence higher moments at the base. However, the opposite occurred at zero damping ratio for cases corresponding to the Poisson ratios of 0.3 and 0.4. This can be attributed to the number of mode shapes in these cases. For cases with positive and negative signs, the number of mode shapes is four and three, respectively. Essentially, higher mode shapes tend to bring the point of application towards the base, as shown in Figure 2.8. In addition, the discrepancy in the location of thrust application decreases as the damping ratio and the Poisson ratio increase.

2.5. CONCLUSIONS

The integrity of the substructures in major facilities such as conventional Nuclear Power Plants (NPPs) and Small Modular Reactors (SMRs) during an earthquake is the first line of defense against any disaster. The earth pressure induced by

earthquake plays an important role in the performance of the substructures of these facilities. For the two main types of seismic waves (i.e., body waves and surface waves), most research focused on the earth pressure distribution due to body waves. However, surface waves can be more destructive than body waves as they propagate at a slower velocity and tend to have a larger amplitude in strong earthquakes.

This paper provides an analytical solution for the seismic earth pressure induced by Rayleigh wave propagating in viscoelastic media, using the three-dimensional wave propagation theory. Two soil-structure systems were investigated: a substructure in homogeneous viscoelastic soil layer and a substructure surrounded by a multilayered soil profile. For both cases, the total displacements in the $x - z$ plane and the seismic earth pressure on the wall are determined as functions of damping ratio and the Poisson ratio of the soil as well as the height of the substructure.

A parametric study was performed with numerical examples to inspect the responses of homogeneous single layer and multilayered soils. Two special cases were also examined to explore the effect of soft and stiff thin layers in a multi-layered soil system. Modal analyses were performed to determine the phase velocities and mode shapes. The modal characteristics were then used to calculate different responses for four selected cases, focusing on the horizontal and vertical soil displacements, the normal and shear stresses on the substructure, as well as the magnitude and location of the total dynamic force induced by Rayleigh waves.

In general, the homogeneous single layer assumption considerably underestimates seismic forces on the substructure and hence gives unreliable seismic design. The existence of soft thin layers in the soil profile leads to amplified forces on the substructure compared to the stiff thin layer, except at the location of the thin layer. Regarding the point of application of the dynamic thrust, the homogeneous single layer gives higher heights measured from the base, compared to the multilayered soils. The existence of soft thin layers brings the point of application towards the base, and vice versa for the stiff thin layer. An alternative approach to calculate the height of the dynamic thrust is by taking the average height due to each mode shape separately. The latter assumption was compared with the exact solution, where higher heights of the point of application were obtained due to the average height assumption and hence higher moments at the base.

At a constant damping ratio, the earth pressure on the substructure increases as the Poisson's ratio increases. At a constant Poisson's ratio, the effect of damping is prominent near the free surface where the earth pressure on the substructures decreases as damping ratio increases. However, the effect of damping vanishes at large depths. Lastly, the seismic earth pressure distribution is also a function of the height of the substructure. However, the required depth of the substructure is controlled by other engineering requirements rather than earthquake geotechnical engineering.

2.6. ACKNOWLEDGEMENT

The financial support for the study was provided through the Canadian Nuclear Energy Infrastructure Resilience under Systemic Risk (CaNRisk) – Collaborative Research and Training Experience (CREATE) program of the Natural Science and Engineering Research Council (NSERC) of Canada.

2.7. REFERENCES

ACI Committee 349. (2010). "ACI 349-06. Code Requirements for Nuclear Safety-Related Concrete Structures and Commentary." *American Concrete Institute (ACI)*.

ASCE/SEI 4-16. (2017). *Seismic analysis of safety-related nuclear structures*. *Seismic Analysis of Safety-Related Nuclear Structures*, American Society of Civil Engineers.

ASME. (2019). *BPVC Section III-Rules for Constructions of Nuclear Facility Components-Subsection NCA-General Requirements for Division 1 and Division 2*.

De Basabe, J. D., and Sen, M. K. (2010). "Stability of the high-order finite elements for acoustic or elastic wave propagation with high-order time stepping." *Geophysical Journal International*, 181(1), 577–590.

Budnitz, R. J., Konstandinidis, D., and Zhou, Z. (2015). *Evaluations of NRC Seismic-Structural Regulations and Regulatory Guidance, and Simulation-Evaluation Tools for Applicability to Small Modular Reactors (SMRs)*.

Canadian Nuclear Safety Commission (CNSC). (2016). *Small Modular Reactors : Regulatory Strategy, Approaches and Challenges*. *Discussion Paper DIS-16-04*.

Canadian Standards Association (CSA). (2008). *CSA N291-Requirements for safety-related structures for CANDU nuclear power plants*.

Canadian Standards Association (CSA). (2014). *CSA N287.3-Design requirements for concrete containment structures for nuclear power plants*.

Chapman, C. (2004). *Fundamentals of Seismic Wave Propagation*. Cambridge University Press, Cambridge.

Chavda, J. T., and Dodagoudar, G. R. (n.d.). "Experimental studies on a circular open caisson." *International Journal of Physical Modelling in Geotechnics*, 0(0), 1–18.

Cheng, Z., Law, H., and Jiang, Y. (2010). *Soil-Structure Interaction Analysis For Bridge Caisson Foundation*.

CSA N289.3-10. (2015). *Design procedures for seismic qualification of nuclear power plants*. Canadian Standards Association.

Datta, S. K., Shah, A. H., and Wong, K. C. (1984). "Dynamic stresses and displacements in buried pipe." *Journal of Engineering Mechanics*, 110(10), 1451–1466.

Gaudio, D., and Rampello, S. (2016). "Dynamic Soil-structure Interaction of

Bridge-pier Caisson Foundations." *Procedia Engineering*, 158, 146–151.

Gerolymos, N., and Gazetas, G. (2006). "Static and dynamic response of massive caisson foundations with soil and interface nonlinearities—validation and results." *Soil Dynamics and Earthquake Engineering*, 26(5), 377–394.

Geuzaine, C., and Remacle, J. F. (2009). "Gmsh: A 3-D finite element mesh generator with built-in pre- and post-processing facilities." *International Journal for Numerical Methods in Engineering*, 79(11), 1309–1331.

Haskell, N. A. (1953). "The dispersion of surface waves on multilayered media." *Bulletin of the Seismological Society of America*, 43(1), 17–34.

Hubert, L., Po, L. I., and Patrick, W. (2014). "Soil-Structure Interaction for Gravity Caissons in Bridge Seismic Design." *Structures Congress 2014*, Proceedings.

IAEA. (2020). *Operating Experience with Nuclear Power Stations in Member States*. Operating Experience with Nuclear Power Stations in Member States (CD-ROM), INTERNATIONAL ATOMIC ENERGY AGENCY, Vienna.

Jalbi, S., Shadlou, M., and Bhattacharya, S. (2018). "Impedance functions for rigid skirted caissons supporting offshore wind turbines." *Ocean Engineering*, 150, 21–35.

John P.wolf. (1994). *Foundation vibrational analysis using simple physical models*. *Prentice Hall*, Englewood Cliffs, New Jersey.

Julian, B. R., and Gubbins, D. (1977). “Three-dimensional seismic ray tracing.” *Journal of Geophysics*.

Karabalis, D. L., and Mohammadi, M. (1998). “3-D dynamic foundation-soil-foundation interaction on layered soil.” *Soil Dynamics and Earthquake Engineering*, 17(3), 139–152.

Katayama, T., Kubo, K., and Sato, N. (1975). “Earthquake Damage To Water and Gas Distribution Systems.” *Proceedings of the US National Conference on Earthquake Engineering, EERI*, Ann Arbor, 396–405.

Kloukinas, P., Langousis, M., and Mylonakis, G. (2012). “Simple wave solution for seismic earth pressures on nonyielding walls.” *Journal of Geotechnical and Geoenvironmental Engineering*, 138(12), 1514–1519.

Komatitsch, D., and Tromp, J. (1999). “Introduction to the spectral element method for three-dimensional seismic wave propagation.” *Geophysical Journal International*.

Komatitsch, D., and Tromp, J. (2014). “SPECFEM2D User Manual Version 7.0.” *Computational Infrastructure for Geodynamics*.

Komatitsch, D., and Vilotte, J.-P. (1998). “The spectral element method: An efficient tool to simulate the seismic response of 2D and 3D geological structures.” *Bulletin of the Seismological Society of America*, 88(2), 368–392.

Kouretzis, G. P., Bouckovalas, G. D., and Gantes, C. J. (2006). "3-D shell analysis of cylindrical underground structures under seismic shear (S) wave action." *Soil Dynamics and Earthquake Engineering*, 26(10), 909–921.

Kramer, S. L. (1996). *Geotechnical Earthquake Engineering*. Prentice Hall, New Jersey.

Lee, M. K. W., and Finn, L. W. D. (1978). "{DESRA}-2: Dynamic effective stress response analysis of soil deposits with energy transmitting boundary including assessment of liquefaction potential." *Soil Mechanics*, 38(38).

Lee, T. H., and Wesley, D. A. (1973). "Soil-structure interaction of nuclear reactor structures considering through-soil coupling between adjacent structures." *Nuclear Engineering and Design*, 24(3), 374–387.

Lei, W., Weiming, G., Yonggao, Y., and Xiaodong, T. (2021). "Field Experimental Study on Vertical Bearing Capacity of Root-Caisson Foundation." *Advances in Soil Dynamics and Foundation Engineering*, Proceedings.

Lin, H. -T, Roesset, J. M., and Tassoulas, J. L. (1987). "Dynamic interaction between adjacent foundations." *Earthquake Engineering & Structural Dynamics*, 15(3), 323–343.

Longuet-Higgins, M. S. (1950). "A theory of the origin of microseisms." *Philosophical Transactions of the Royal Society of London. Series A,*

Mathematical and Physical Sciences, 243(857), 1–35.

Lowrie, W. (2007). *Fundamentals of Geophysics*. Cambridge University Press, New York, NY, USA.

Mccamy, K., Meyer, R.P., and Smith, T. J. (1962). "Generally applicable solutions of Zoeppritz' amplitude equations." *Bulletin of the Seismological Society of America*, 52(4), 923–955.

Mononobe, N., and Matsuo, H. (1929). "On the Determination of Earth Pressures During Earthquakes." *Proceedings of World Engineering Congress*, Tokyo, Japan, 274–280.

Mulliken, J. S., and Karabalis, D. L. (1995). "Discrete Model For Foundation-soil-foundation Interaction." *Soil Dynamics and Earthquake Engineering*, 8, 1–3.

Mylonakis, G., and Gazetas, G. (2000). "Seismic soil-structure interaction: Beneficial or detrimental?" *Journal of Earthquake Engineering*, 4(3), 277–301.

Newmark, N. M., and Hall, W. J. (1975). "Pipeline Design To Resist Large Fault Displacement." 416–425.

NP-T-3.20. (2018). *Buried and Underground Piping and Tank Ageing Management for Nuclear Power Plants*. Vienna.

NuScalePower. (2020). "NuScale Final Safety Analysis Report."

<https://www.nrc.gov/docs/ML2022/ML20224A491.pdf>.

O'Rourke, M., and Ayala, G. (1993). "Pipelinpipeline damage due to wave propagatione." *Journal of Geotechnical Engineering*, 119(9), 1490–1498.

Okabe, S. (1926). "General theory of earth pressure." *Journal of the Japanese Society of Civil Engineers*, 12(1), 1277–1323.

P., D. J., T., H. G., and J., D. A. (2005). "Stiffness of Flexible Caisson Foundations Embedded in Nonhomogeneous Elastic Soil." *Journal of Geotechnical and Geoenvironmental Engineering*, American Society of Civil Engineers, 131(12), 1498–1508.

Padrón, L. A., Aznárez, J. J., and Maeso, O. (2011). "3-D boundary element-finite element method for the dynamic analysis of piled buildings." *Engineering Analysis with Boundary Elements*, 35(3), 465–477.

Peter, D., Komatitsch, D., Luo, Y., Martin, R., Le Goff, N., Casarotti, E., Le Loher, P., Magnoni, F., Liu, Q., Blitz, C., Nissen-Meyer, T., Basini, P., and Tromp, J. (2011). "Forward and adjoint simulations of seismic wave propagation on fully unstructured hexahedral meshes." *Geophysical Journal International*, 186(2), 721–739.

Reese, C. D., and Eidson, J. V. (2006). *Handbook of OSHA Construction Safety and Health*. *Handbook of OSHA Construction Safety and Health*.

Rizzo, F. J., Shippy, D. J., and Rezayat, M. (1985). "A boundary integral equation

method for radiation and scattering of elastic waves in three dimensions." *International Journal for Numerical Methods in Engineering*.

Rodríguez-Castellanos, A., Rodríguez-Sánchez, J. E., and Carbajal-Romero, M. (2010). "Coupled response for rigid foundations." *Journal of Geotechnical and Geoenvironmental Engineering*, 135(12), 1971–1975.

Scott, R. F. (1973). "Walls, Earthquake-Induces Earth pressures by Retaining." *5thWorld Conference on Earthquake Engineering*, Tokyo, Japan, 1611–1620.

Seed, H. B., and Whitman, R. V. (1970). "Design of Earth Retainig Structures for Dynamic Loads." *ASCE Specialty Conference on Lateral Stresses in the Ground and Design of Earth-Retaining Structures*, Cornell Univ., Ithaca, New York, 103–147.

Skau, K. S., Jostad, H. P., Eiksund, G., and Sturm, H. (2019). "Modelling of soil-structure-interaction for flexible caissons for offshore wind turbines." *Ocean Engineering*, 171, 273–285.

Stacey, R. (1988). "Improved transparent boundary formulations for the elastic-wave equation." *Bulletin of the Seismological Society of America*, 78(6), 2089–2097.

Steedman, R. S., and Zeng, X. (1990). "The influence of phase on the calculation of pseudo-static earth pressure on a retaining wall." *Geotechnique*, 40(1),

103–112.

Stein, S., and Wysession, M. (2003). *An Introduction to Seismology, Earthquakes, and Earth Structure*. *Seismological Research Letters*, Blackwell Publishing Ltd., Malden, USA.

Takada, S., and Tanabe, K. (1987). "Three-dimensional seismic response analysis of buried continuous or jointed pipelines." *Journal of Pressure Vessel Technology, Transactions of the ASME*, 109(1), 80–87.

Telford, W. M., Geldart, L. P., and Sheriff, R. E. (1990). *Applied Geophysics*. *Cambridge University Press.*

Teng, T.-L. (1987). *Geophysics - Field Measurements*. *Methods in Experimental Physics*.

Thomson, W. T. (1950). "Transmission of elastic waves through a stratified solid medium." *Journal of Applied Physics*, 21, 89–93.

Triantafyllidis, T., and Prange, B. (1988). "Rigid circular foundation: Dynamic effects of coupling to the half-space." *Soil Dynamics and Earthquake Engineering*, 7(1), 40–52.

Trifonov, O. V., and Cherniy, V. P. (2010). "A semi-analytical approach to a nonlinear stress-strain analysis of buried steel pipelines crossing active faults." *Soil Dynamics and Earthquake Engineering*, 30(11), 1298–1308.

U.S. NRC. (2013). *Standard Review Plan for the Review of Safety Analysis*

Reports for Nuclear Power Plants: LWR Edition. Section 3.7.3 Seismic Subsystem Analysis Review Responsibilities. *NUREG 0800*.

USGS. (2009). "Determining the Depth of an Earthquake." *Earthquake Information Bulletin (USGS)*, 9(4), 16.

Veletsos, A. S., and Younan, A. H. (1994). "Dynamic soil pressures on rigid vertical walls." *Earthquake Engineering & Structural Dynamics*, 23(3), 275–301.

W., G., and J., C. (2021). "Experimental Study of Installation of Concrete Suction Caisson in Clay." *IFCEE 2015*, Proceedings.

Warburton, G. B., Richardson, J. D., and Webster, J. J. (1971). "Forced vibrations of two masses on an elastic half space." *Journal of Applied Mechanics, Transactions ASME*, 38(1), 148–156.

Whitman RV. (1969). "Current Status of Soil Dynamics." *Applied Mechanics Reviews*, 22, 1–8.

Wolf, J. P. (1989). "Soil-structure-interaction analysis in time domain." *Nuclear Engineering and Design*.

Wood, J. H. (1973). *Earthquake-induced soil pressures on structures*. *PhD Thesis*, Pasadena, CA.

Yao, W. A., and Mao, L. (2010). "Symplectic system based analytical solution for bending of rectangular plates on Winkler foundation." *The IES Journal Part*

A: Civil & Structural Engineering, Taylor & Francis, 3(1), 28–37.

Zoeppritz, K. (1919). "Über Erdbebenwellen Part VII b . Über Reflexion und Durchgang seismischer Wellen durch Unstetigkeitsflächen." *Nachrichten von der Gesellschaft der Wissenschaften zu Göttingen, Mathematisch-Physikalische Klasse*, 66–84.

2.8. TABLES

Table 2.1. Characteristics of the soil-structure system shown in Figure 2.2

$H\ (m)$	$\rho\ (kg/m^3)$	$v_s\ (m/s)$	$f\ (Hz)$	ν	$\zeta\ (\%)$
15	1900	350	50	$0.1-0.4$	$0-80$

Table 2.2. Properties of Soil Layers

Layer #	Layer Thickness $h_f\ (m)$	Density ρ (kg/m^3)	V_s (m/s)	Poisson's Ratio ν	Damping $\zeta\ (\%)$
1	3	1500	200	0.3	20
2	5	1900	350	0.3	20
3	7	2100	500	0.3	20
Equivalent homogeneous layer	15	1900	350	0.3	20

Table 2.3. Modal analysis results of the Single and Layered soil profiles at $f = 50\ Hz$, $\zeta = 20\%$, and $\nu = 0.3$

	Phase Velocity (m/s)				Wavelength (m)			
	Mode (1) v_{R1}	Mode (2) v_{R2}	Mode (3) v_{R3}	Mode (4) v_{R4}	Mode (1) v_{R1}	Mode (2) v_{R2}	Mode (3) v_{R3}	Mode (4) v_{R4}
Case (1)	324.60	N/A	N/A	N/A	6.50	N/A	N/A	N/A
Case (2)	189.45	312.50	385.1	491.32	3.79	6.25	7.70	9.83
Case (3)	189.45	314.40	395.34	465.35	3.79	6.29	7.91	9.31
Case (4)	189.45	300.56	356.6	485.6	3.79	6.01	7.13	9.71

Table 2.4. Total earth pressure force on the substructure and the total moment at the base

	Total x10^3 (kN)	Moment x10^3 ($kN.m$)
Case (1)	0.0736	0.254
Case (2)	3.4146	22.786
Case (3)	2.1865	13.053
Case (4)	4.0250	28.972

Table 2.5. Discrepancies between the average height assumption and the exact solution in calculating the location of the dynamic thrust from the base of the wall

		Poisson's Ratio (ν)			
		0.1	0.2	0.3	0.4
Damping Ratio (ζ) %	00	+38.96%	+37.26%	-03.29%	-02.80%
	20	+38.35%	+36.80%	+33.60%	+19.95%
	40	+37.43%	+36.33%	+32.90%	+22.26%
	60	+34.91%	+33.78%	+30.56%	+22.69%

	Poisson's Ratio (ν)			
	0.1	0.2	0.3	0.4
80	+32.42%	+28.35%	+27.60%	+20.78%

2.9. FIGURES

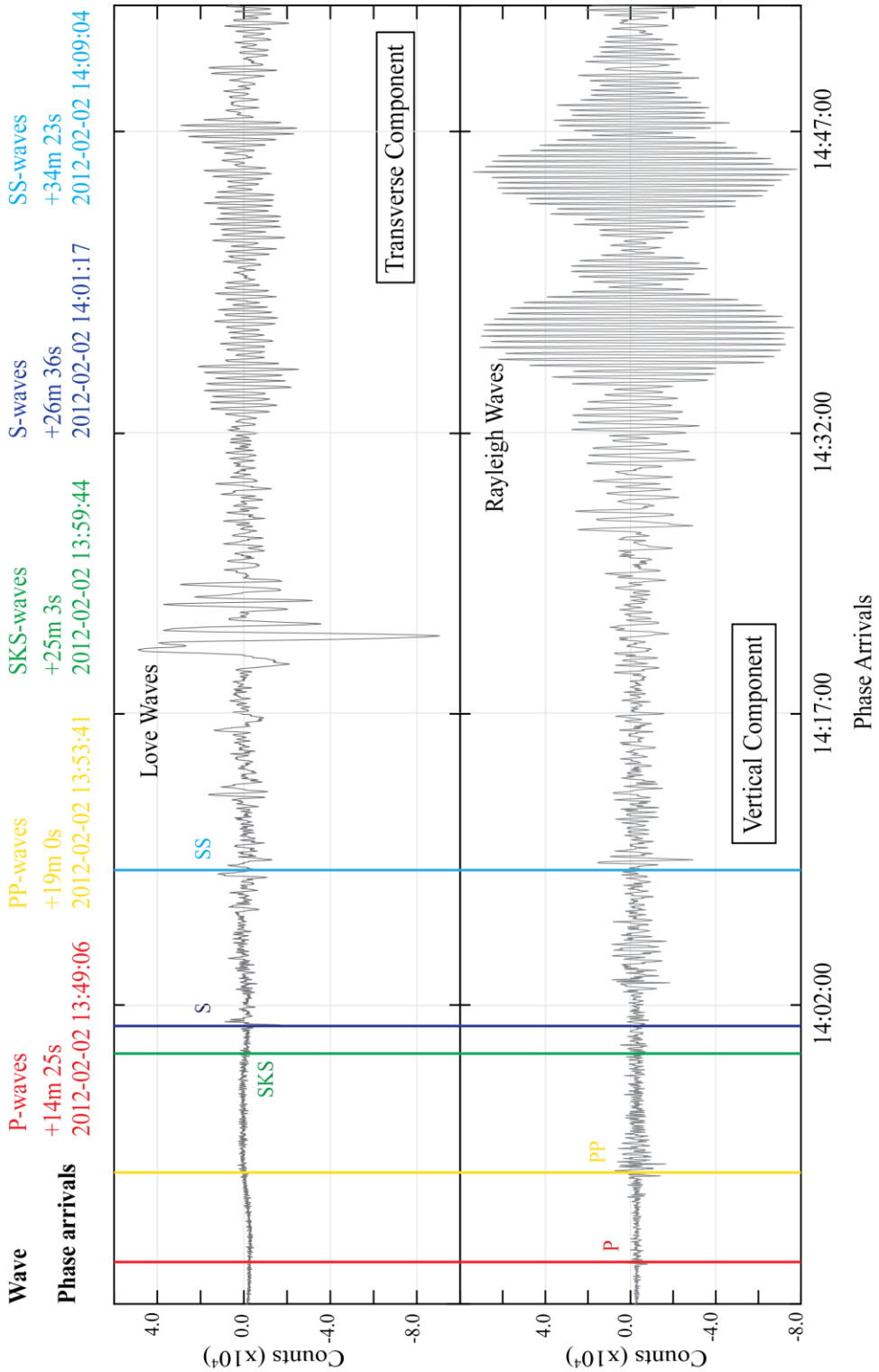

Figure 2.1. Two-component seismogram for an earthquake of a magnitude $M_w = 7.0$ recorded in the Vanuatu trench at station CCM

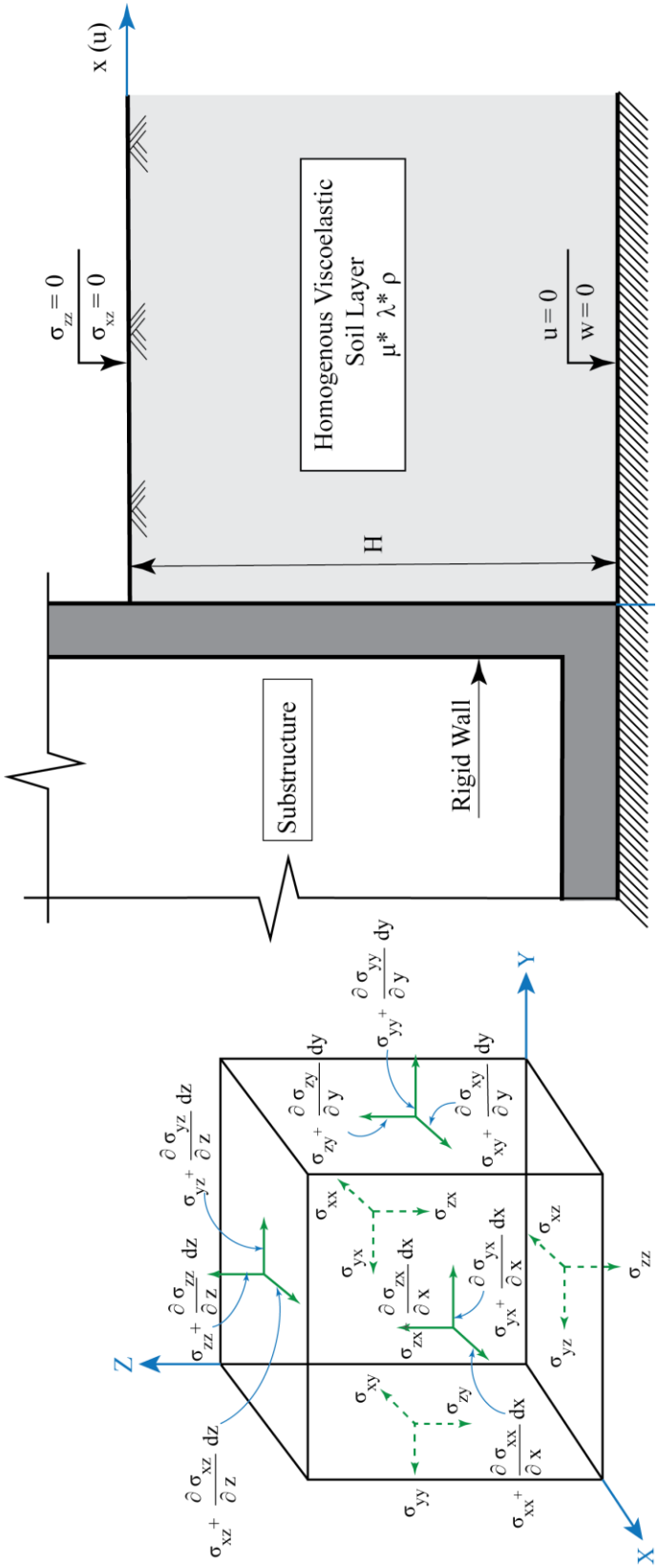

Figure 2.2. a) Stress components on an infinitely loaded cubic element; b) A rigid wall retained homogeneous viscoelastic soil subjected to Rayleigh waves

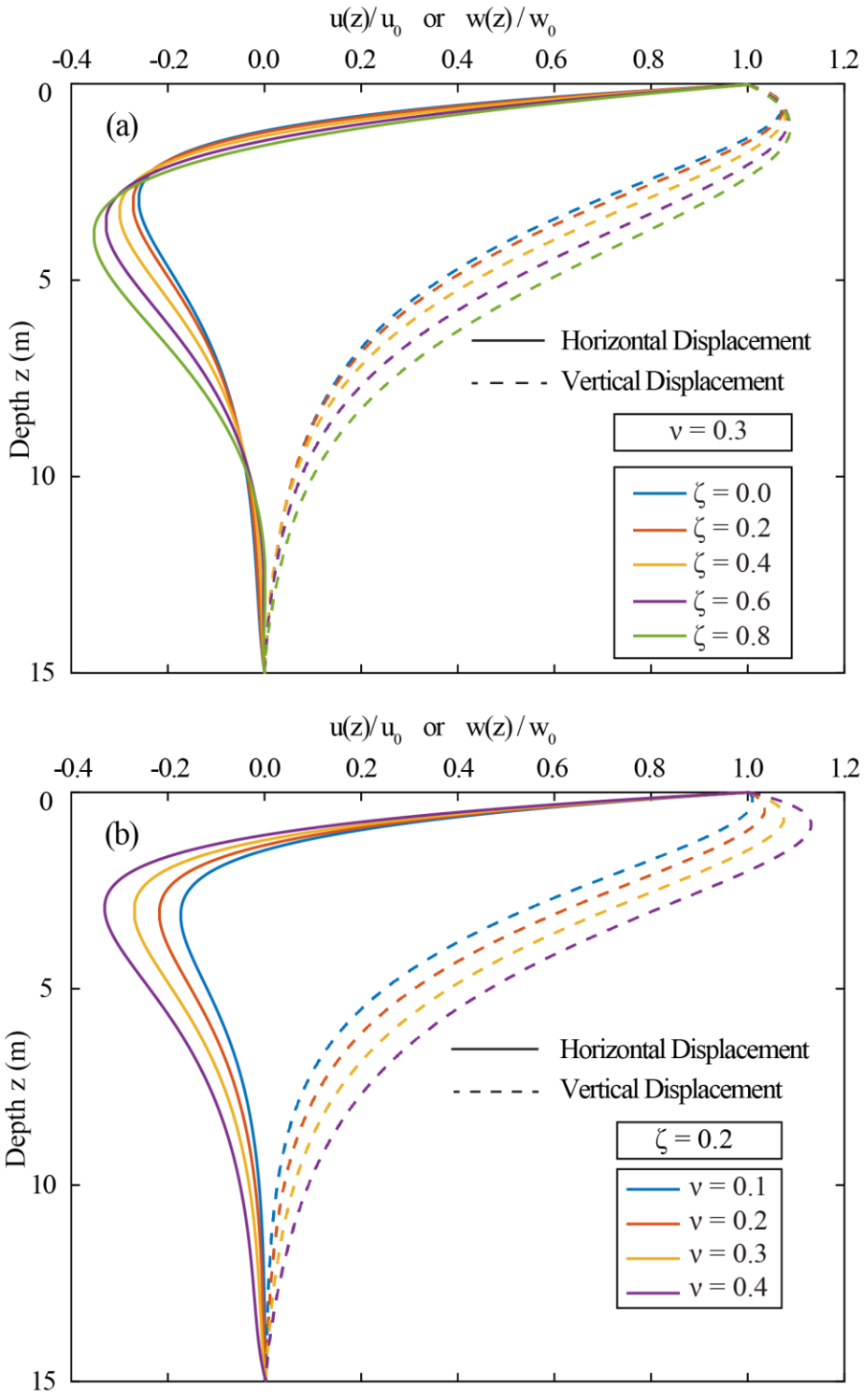

Figure 2.3. Variation of Rayleigh wave displacement with depth for different a) Damping Ratios; and b) Poisson's Ratios

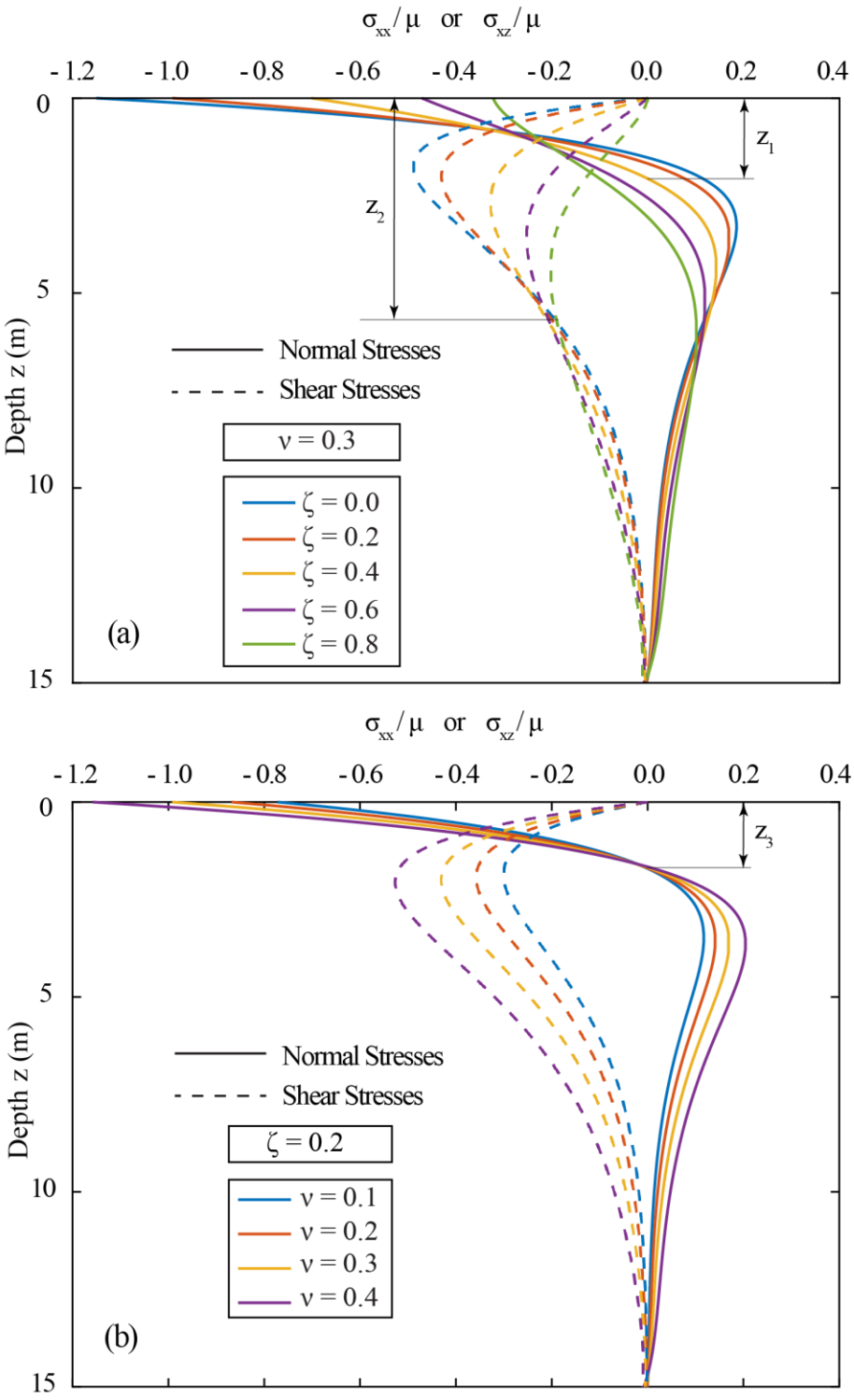

Figure 2.4. Variation of shear and normal stresses with depth for different: a) Damping Ratios; and b) Poisson's Ratios

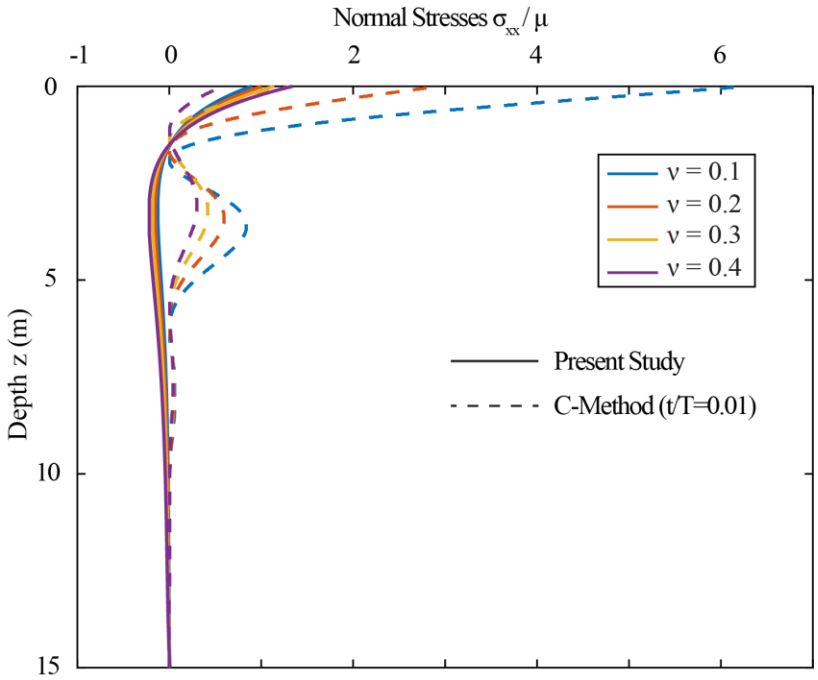

Figure 2.5. Variation of earth pressure with depth due to Rayleigh waves using C-method and this study.

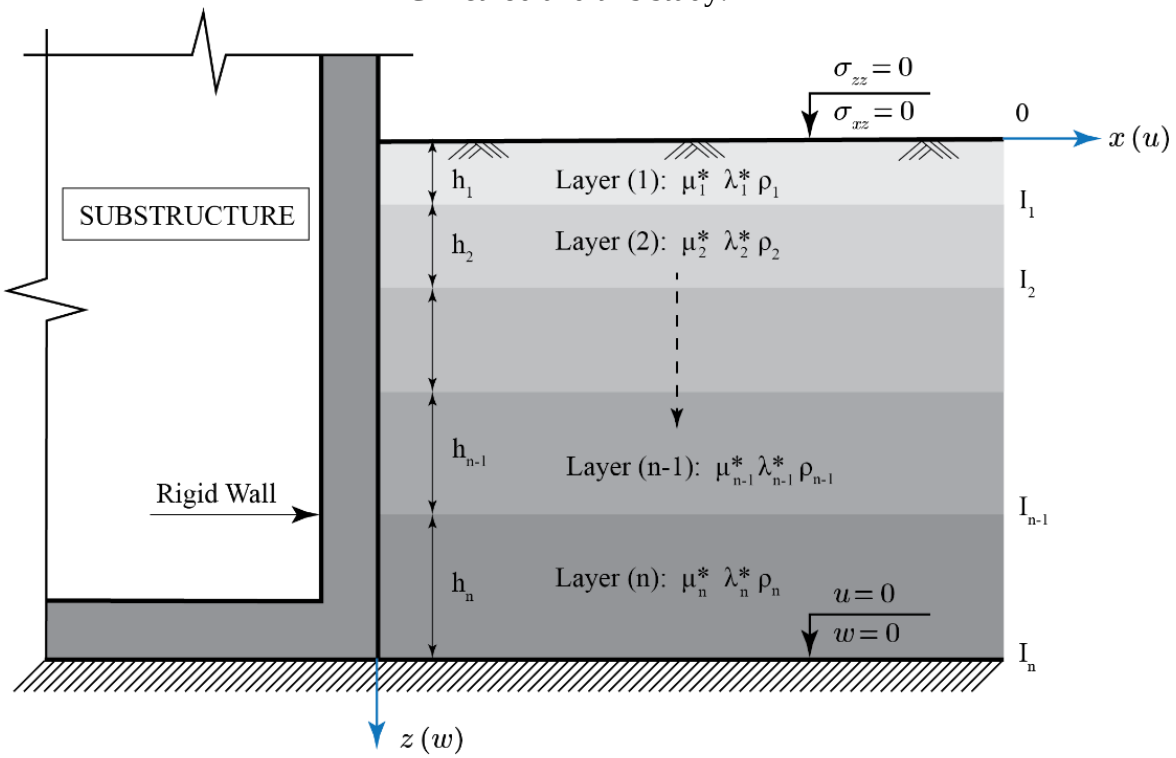

Figure 2.6. A substructure with rigid wall in multilayered viscoelastic soil subjected to Rayleigh waves.

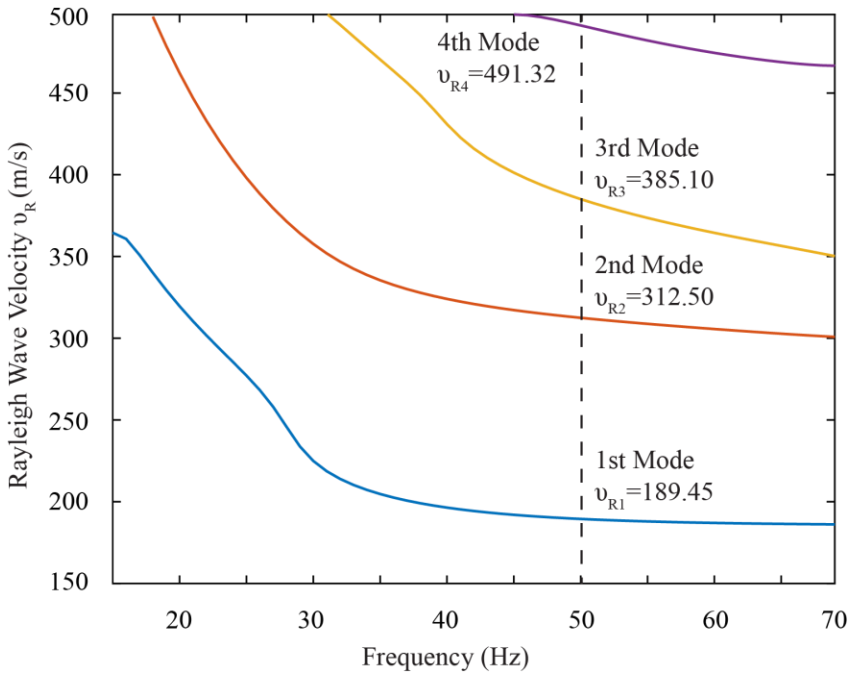

Figure 2.7. Dispersion curves of the soil system defined in Table **2.2**

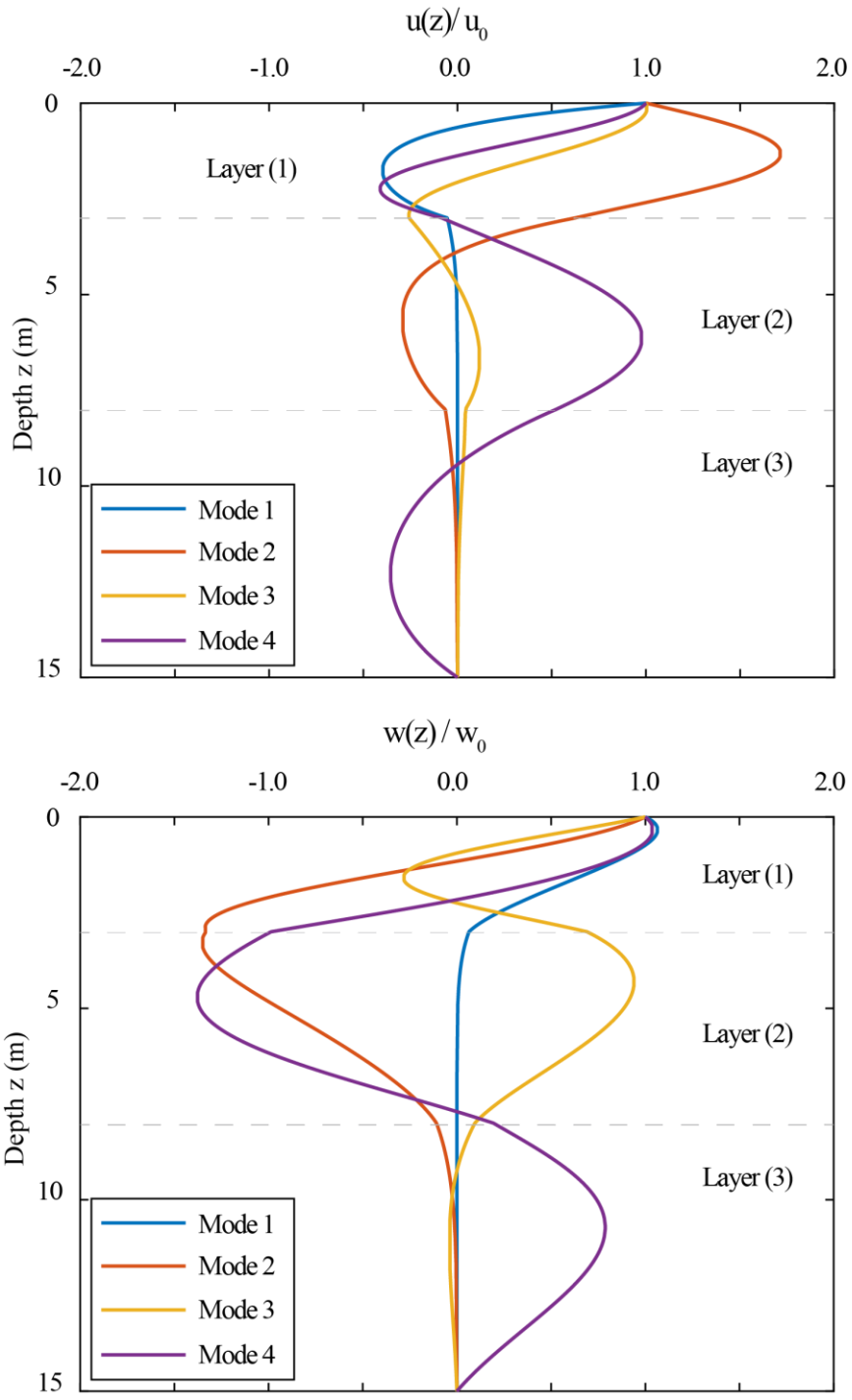

Figure 2.8. Natural mode shapes of Rayleigh waves at 50 Hz for the soil system defined in Table **2.2**

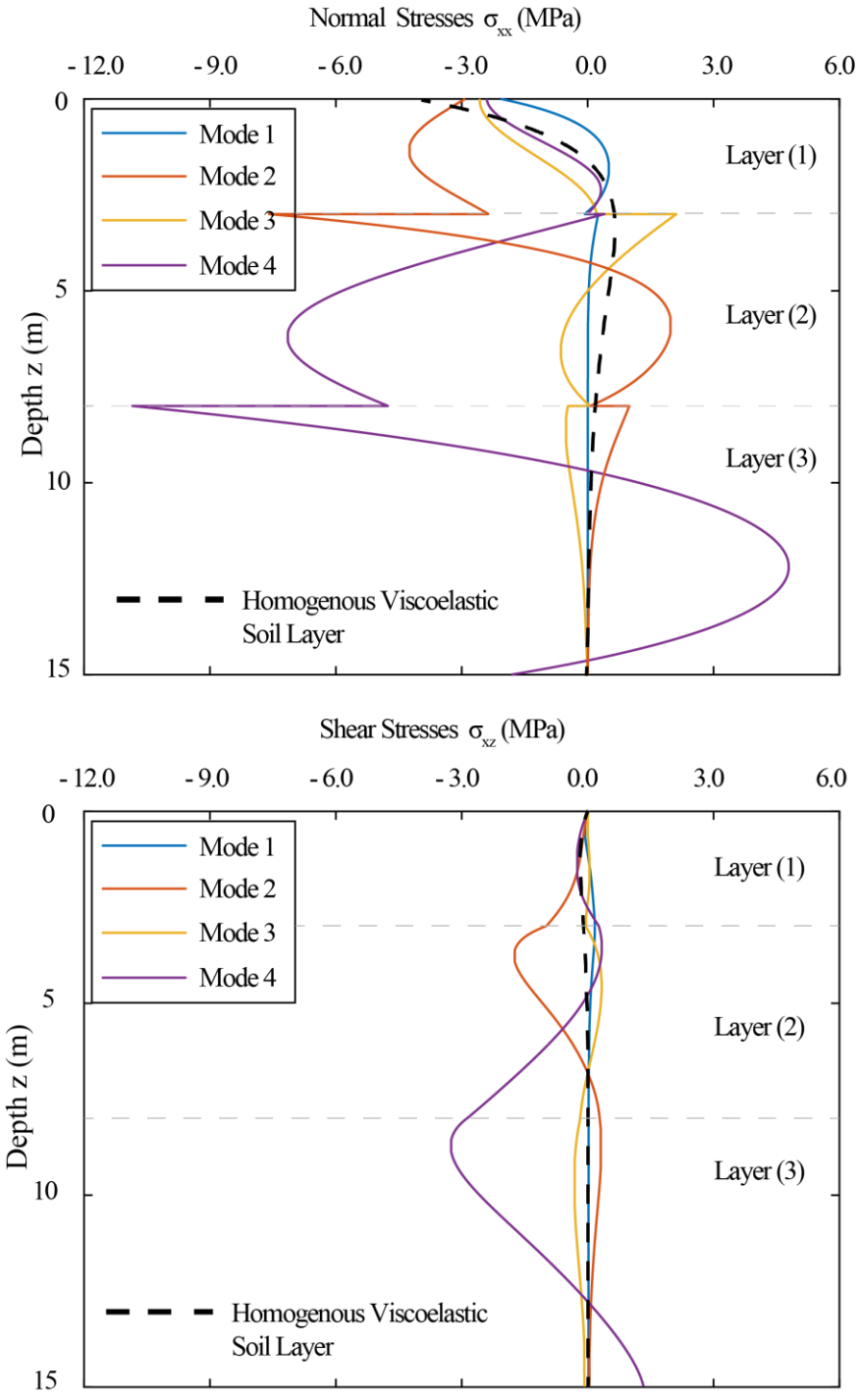

Figure 2.9. Distribution of normal and shear stresses on the substructure due to the first three mode shapes at a frequency of 50 Hz

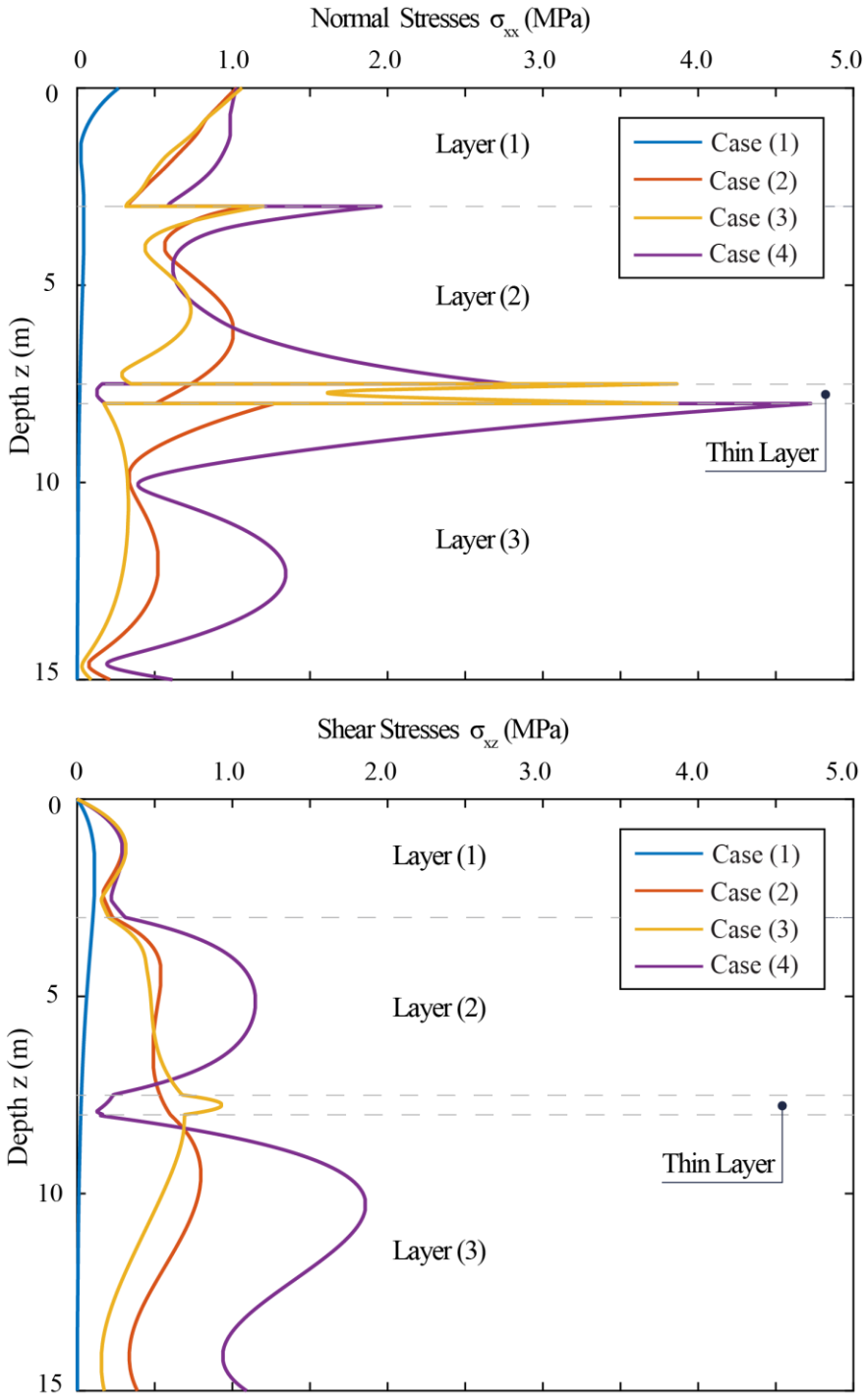

Figure 2.10. Distributions of absolute normal and shear stresses for different cases listed in Table **2.3**

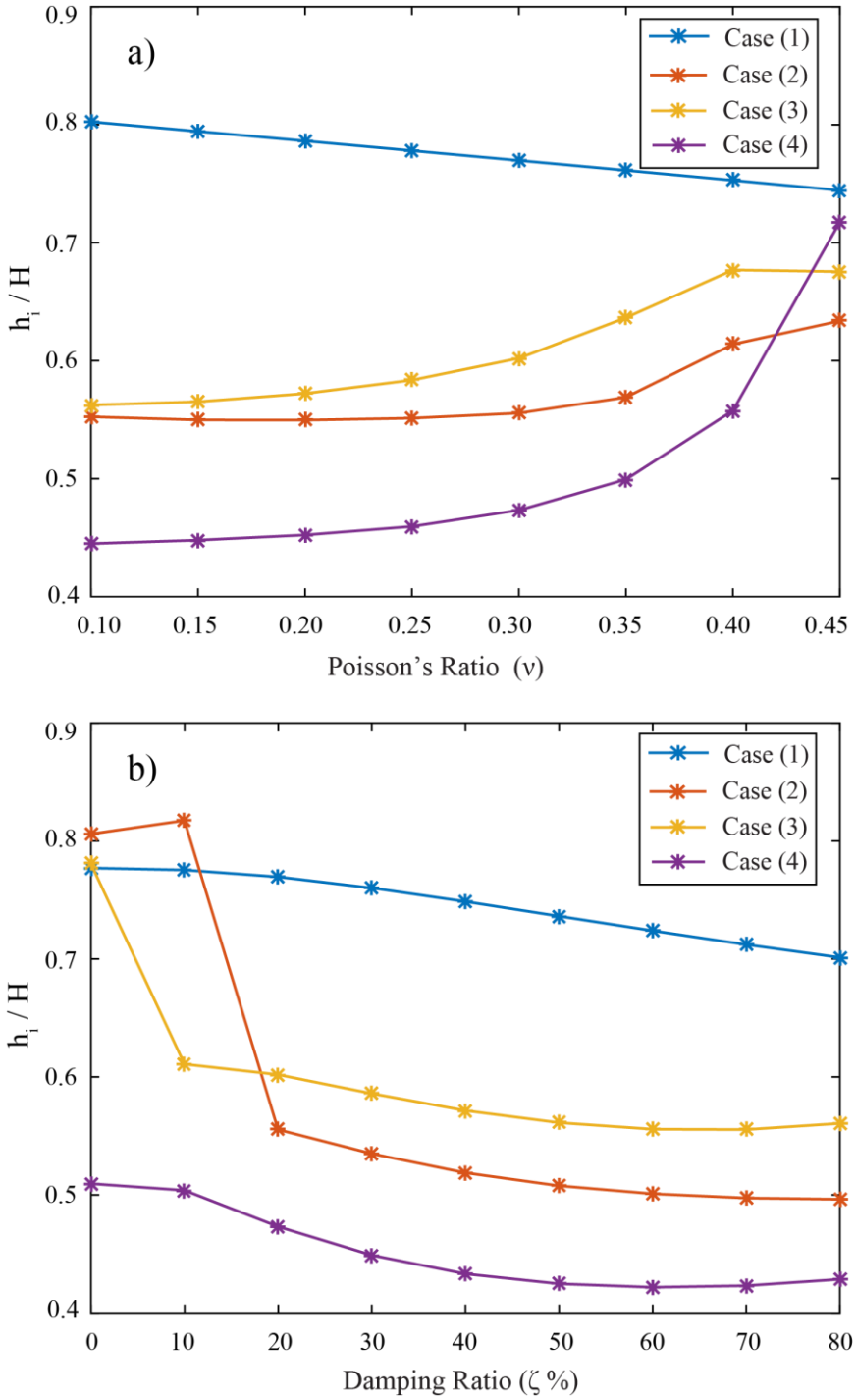

Figure 2.11. The location of the point of application of dynamic thrust measured from the base of the soil-structure system at a) $\zeta = 20\%$, and b) $\nu = 0.3$

Chapter 3

STRUCTURE-SOIL-STRUCTURE INTERACTION ANALYSIS FOR LATERAL SEISMIC EARTH PRESSURE OF DEEPLY BURIED STRUCTURE IN LAYERED GROUND

3.1. ABSTRACT

Based on the theory of three-dimensional wave propagation, this paper proposed a method to evaluate the amplified seismic responses of two adjacent structures in horizontally stratified ground owing to seismic Structure-Soil-Structure Interaction (SSSI) and backfill soils. A guided flowchart was used to simplify the analysis for the propagation of seismic wave between adjacent substructures and its interference in the soil layers. Using the proposed method, a parametric study was performed to examine the influence of three parameters (namely, the slope of the excavation boundary, the distance between structures, and material properties of the backfill) on the amplification of seismic earth pressure on the substructures. An optimal distance between adjacent substructures was determined that conform to the minimum SSSI.

Author keywords: Structure-soil-structure interaction; Seismic lateral earth pressure; Shear waves; Primary Waves; Wave propagation; Backfill.

3.2. INTRODUCTION

In seismic ground motion analysis, the seismic excitation is generally assumed as vertically propagating horizontally polarized shear waves. With this assumption, the total energy of the waves is concentrated in the horizontal direction. However, this assumption may become invalid for substructures surrounded by backfill. Two main characteristics are generally used to define backfill: the soil properties and the excavation slope. The orientation of the excavation boundaries may vary from vertical to inclined, depending on the overall stability of the open excavation. Vertically propagating shear waves travel parallel to the boundary of the vertical backfill, while impinging the interface of the inclined backfill at an angle equal to the slope of the interface. As a result, part of the incident energy is transmitted to the structure through the backfill while the rest is reflected in the soil layer. The propagation direction of the reflected waves varies with the slope of the interface and soil properties, which makes the effectiveness of the assumption of vertically propagating shear waves invalid.

A new nuclear technology, called the Small Modular Reactors (SMRs), has been developed recently. The SMR's substructure is likely to burry deep in the ground. For example, in the SMR design proposed by NuScale, the substructure depth reaches 30 m (NuScale Power, 2020). Deeply embedded structures with a relatively small footprint are expected to be more sensitive to seismic excitations and waves induced by engineering backfill. In a nuclear Power

Plant (NPP) housing SMRs, two buildings with foundations at different levels and different backfill configurations may be located in close proximity. When seismic waves impinge adjacent buildings, part of the seismic energy is absorbed by the substructures and the remainder is reflected back into the soil and undergoes phases of wave propagation back and forth between the substructures. Along the distance between the substructures, the reflected seismic waves are subjected to a series of reflections and refractions at the upper and lower boundaries of the soil layer, resulting in amplified seismic stresses on the substructures. This interaction between the substructures is referred to as seismic Structure-Soil-Structure Interaction (SSSI), and is affected by various factors, such as characteristics of the soil profile and the spacing between adjacent structures. SSSI and backfill soils can amplify the total seismic forces transmitted to the substructure and influence the floor response spectra of the below-grade floors. In addition, under certain circumstances, backfilling may cause energy to be trapped in the soil layer near the free surface, resulting in surface waves.

Since Whitman (1969) raised concerns about SSSI, studies have been performed to investigate this phenomenon. Owing to the challenges in physical modelling of SSSI (e.g., Kitada et al. 1999), the majority of the studies are based on semi-analytical or numerical methods due to the complexity of the analytical solution (e.g., Lou et al. 2011). However, solutions have been proposed for simple cases such as two identical cylindrical foundations resting on an elastic half-space (Warburton et al. 1971) or a set of closely spaced footings (Hesham et al. 2018).

In semi-analytical methods, the soil-structure system is idealized as a series of springs, masses, and dampers (Lu et al. 2020; Luco and Contesse 1973). The excitation is applied as a fixed or harmonic force at one of the structures (Kobori et al. 1973), or the whole system is subjected to vertical or oblique shear waves (Murakami and Luco 1977; Mulliken and Karabalis 199s8; Alexander et al. 2013; Vicencio and Alexander 2018). Regardless of the excitation type, some studies focus on the spatial variation of the ground motion (e.g., Alam and Kim 2014). A homogeneous soil layer rested on elastic half-space is the most common configuration in semi-analytical methods, considering the elastic (Liang et al. 2017, 2018) and viscoelastic (Behnamfar and Sugimura 1999) behaviour of the soil. In general, the analytical and semi-analytical studies did not exceed the level of complexity of two masses attached to an elastic half-space (Hesham et al. 2018) or a shallow foundation buried in an elastic half-space (Luco and Contesse 1973; Vicencio and Alexander 2019).

In numerical methods, two approaches are generally used: the direct approach and the substructuring approach. The substructure approach breaks down the total system into independent subsystems, usually: the structure, the soil medium, and the excavated soil (Wolf 1989). In the direct approach, the structures and part of the surrounding soil are modelled in the same environment. Two numerical methods are commonly used: the Finite Element Method “FEM” (Lin et al. 1987; Wang et al. 2013; Roy et al. 2015; Bybordiani and Arici 2019) and the Boundary Element Method “BEM” (Karabalis and Mohammadi 1998; Wong and

Luco 1986). With the development of computational mechanics and computer technology, the FEM and BEM can be integrated into a single environment to take advantage of the FEM in modelling the near-field soil and BEM in modelling the far-field soil (Álamo et al. 2015; Lehmann and Antes 2001; Padrón et al. 2011).

Motivated by the literature review above, this paper investigates the seismic interaction between a deeply buried structure in a layered ground and adjacent structures (i.e., SSSI), taking into account the effect of surrounding backfills. In a layered stratum, the reflected waves from the inclined boundary of an excavation may be further reflected and transmitted at the soil layer interfaces. Furthermore, under some circumstances, the wave energy may even be trapped in a soil layer, resulting in more complex SSSI. The three-dimensional wave propagation theory in an elastic medium is employed to determine the additional seismic amplitudes, displacements, and lateral earth pressure on the substructure. Moreover, a simplified technique for resolving seismic wave interference between adjacent structures is proposed, which can also be used to determine the adequate spacing between structures to mitigate the seismic SSSI.

3.3. CONFIGURATION OF THE STRUCTURE-SOIL-STRUCTURE SYSTEM

Figure 3.1 shows two rigid substructures with different burial depths in a layered ground, where the distance between the structures is L. Structure 1 represents an

existing structure (i.e., SMR) with a deep embedment of H_1 and vertical backfill of width X_1 (i.e., Backfill 1). Structure 2 represents a newly added structure to the site with a burial depth of H_2 and inclined backfill (i.e., Backfill 2). The soil profile consists of N horizontally stratified layers of homogeneous, isotropic linear elastic soils with different shear wave velocities and thicknesses. The soil layers are underlain by an elastic half-space, which is considered as the bedrock. Since the primary objective of the present work is the development of a method to determine the additional seismic earth pressure induced by SSSI using the three-dimensional wave propagation theory, the soils are considered as linear elastic with the consideration that seismic strain level in the ground is lower than approximately 10^{-4} and no failure occurs. Neglecting material damping and soil nonlinearity (i.e., reduction of shear modulus as seismic strain level increases) tends to affect the calculated particle movements. In particular, neglecting material damping tends to yield larger particle movement, while neglection of strain-level dependency of stiffness tends to under-predict particle movement at high strain levels. However, the method developed in the following sections can be easily extended to take into account soil damping and nonlinearity.

Regarding boundary conditions of the soil-structure system shown in Figure 3.1, stress continuity and deformation compatibility must be satisfied at the interface of soil layers or/and between the backfills and adjacent soil layers. At the free surface, the total traction is zero, which implies the normal and shear stresses vanish. In addition, the radiation damping is neglected, while the boundaries at the right,

bottom, and left edges of the soil profile domain (marked in red in Figure 3.1) have complete absorption of seismic energy that reaches the boundary, either reflected from the soil-structure system or propagating towards the unbounded soil medium. It should be noted that deformation compatibility can be easily satisfied at soil interfaces in ground with horizontal soil layers. The contact between a substructure and the surrounding soil can be maintained for deeply buried structure owing to the high horizontal stress, which implies the compatibility of displacement on the soil-substructure interface. For strong ground motion induced by earthquake, separation of soil from the substructure may take place near the ground surface. However, this is beyond the scope of this research.

We examine the soil-structure interaction when shear waves (SV-waves) travel vertically in the $x-z$ plane from the bedrock across the soil layers. The $x-$axis is horizontal and pointing to the right of the origin, while the positive $z-$axis is vertical and pointing downward. The labelling system used for the soil layers, backfill, and the two structures is shown in Figure 3.1 and is utilized in the upcoming analysis.

For a plane wave propagating in the $x-z$ plane, the displacements can be written as a function of time using a scalar potential function ϕ with two vector potential functions Ψ and χ as:

$$u(x,z,t) = \nabla\phi(x,z,t) + \nabla \times \Psi(x,z,t) + \nabla \times \nabla \times \chi(x,z,t) \qquad (1)$$

where $\phi(x,z,t)$ is a scalar potential to describe the displacement field due to the primary waves (P-waves). $\Psi(x,z,t)$ and $\chi(x,z,t)$ are vector potentials to describe the in-plane and out-of-plane displacement field, respectively, due to the shear waves (Stein and Wysession 2003). According to the three-dimensional wave propagation theory (Chapman 2004), an incident SV-wave at the interface between two different materials produces four types of waves: reflected SV- and P-waves and transmitted SV- and P-waves, as illustrated in Figure 3.2. Assuming the amplitudes of the SV- and P- waves are A and B, respectively, the harmonic solutions of both waves in the $x-z$ plane are given as (Stein and Wysession 2003):

$$\Psi(x,z,t) = A\exp\left[i\left(\omega t - k_x x \pm k_{z_\alpha} z\right)\right]$$
$$\phi(x,z,t) = B\exp\left[i\left(\omega t - k_x x \pm k_{z_\beta} z\right)\right] \quad (2)$$

where k_x and k_z are the wavenumbers in $x-$ and $z-$ directions, respectively, and ω is the angular frequency of the seismic wave. The direction of wave propagation is usually determined by the wave vector **k** with the magnitude $|\mathbf{K}| = \sqrt{k_x^2 + k_z^2}$, while the direction is perpendicular to the wavefront. The $\pm$ signs stand for waves travelling upward and downward, respectively. By applying the linear elastic stress-strain relationship and substituting Equation (2) into Equation (1), the displacements and pertinent stresses in the $x-z$ plane due to the SV- and P-waves can be expressed as:

$$\begin{Bmatrix} u_x \\ u_z \\ \sigma_{xz} \\ \sigma_{xx} \end{Bmatrix} = E \begin{bmatrix} -iW_s k_{z_s} & \frac{ik_{z_s}}{W_s} & -ik_x W_p & -\frac{ik_x}{W_p} \\ -ik_x W_s & -\frac{ik_x}{W_s} & ik_{z_p} W_p & -\frac{ik_{z_p}}{W_p} \\ \mu(k_{z_s}^2 - k_x^2) W_s & \frac{\mu(k_{z_s}^2 - k_x^2)}{W_s} & 2\mu k_x k_{z_p} W_p & -\frac{2\mu k_x k_{z_p}}{W_p} \\ -2\mu k_x k_{z_s} W_s & \frac{2\mu k_x k_{z_s}}{W_s} & -[(\lambda + 2\mu)k_x^2 + \lambda k_{z_p}^2] W_p & \frac{\left[-(\lambda + 2\mu)k_x^2 + \lambda k_{z_p}^2\right]}{W_p} \end{bmatrix} \begin{Bmatrix} A_+ \\ A_- \\ B_+ \\ B_- \end{Bmatrix} \quad (3)$$

where A_+ and B_+ are the amplitudes of the upgoing SV- and P- waves, A_- and B_- are the amplitudes of the downgoing SV- and P- waves, λ and μ are Lame constants of the material. The wavenumbers of the SV- and P- waves are given by:

$$k_{z_s} = (\omega^2/v_s^2 - k_x^2)^{0.5} \qquad k_{z_p} = \left(\omega^2/v_p^2 - k_x^2\right)^{0.5} \quad (4)$$

and

$$W_s = e^{ik_{z_s}z} \qquad W_p = e^{ik_{z_p}z} \qquad E = e^{i(\omega t - k_x x)} \quad (5)$$

in which v_s and v_p are the S- and P-wave velocities, respectively. Since the focus of this paper is on the effect of Structure 2 on the seismic demand of Structure 1 (i.e., SMR), the propagation of the transmitted waves A_T^b and B_T^b in Backfill 2 is neglected, as shown in Figure 3.2. Accordingly, all forthcoming derivations and analyses will focus on the amplified seismic forces on Structure 1 by taking into account the SSSI via analyzing how the reflected waves from the backfill boundaries propagating through horizontal soil layers. However, it should not be overlooked that Backfill 2 is vulnerable to basin-edge effects, particularly the hazards of locally developed surface waves. These effects have a destructive

influence due to the amplification of long-period components of seismic ground motions (Koketsu and Miyake 2008) and cause more damage to structures of low natural frequencies (Abraham et al. 2016). In a nuclear power plant, a wide variety of structures, systems, and components with different natural frequencies ranging from low to high may exist in the vicinity of the backfill. Therefore, great attention should be devoted to the selection of the Backfill 2 configuration, including its slope and material properties.

3.4. TOTAL DISPLACEMENTS

The total displacement u_T on the interface between the soil and Structure 1 can be decomposed into two parts: the first part represents the displacement in the $x-$direction due to the originally vertically propagating shear waves (without SSSI) and denoted by $[u_{SV}]_{VL}$. The second part has two components in the $x-z$ plane: $[u_{SV}]_R$ and $[u_P]_R$ due to the reflected SV- and P-waves from the inclined boundary of backfill 2, respectively. In other words, $[u_{SV}]_R$ and $[u_P]_R$ are the additional displacements owing to SSSI. As a result, u_T is expressed as:

$$u_T = [u_{SV}]_{VL} + [u_{SV}]_R + [u_P]_R \tag{6}$$

where u_T is either in the $x-$ or $z-$direction, depending on the wavenumber of the seismic waves at the desired location, as will be explained in detail in the following sections.

3.5. DISPLACEMENTS DUE TO VERTICALLY PROPAGATING SHEAR WAVES

The first part, $[u_{SV}]_{VL}$, can be determined from Equation (3) after introducing the necessary modifications to simulate vertically propagating shear waves. Since SV-waves propagate parallel to the vertical interface between Backfill 1 and soil layers, no transmitted or reflected P-waves are produced. Thus, the amplitudes B_+ and B_- vanish in Equation (3). In addition, the direction of propagation is defined only by the wavenumber k_z. Therefore, the horizontal displacement in Backfill1 can be expressed as:

$$[u_{SV}]_{VL} = u_{x_n}(z,t)|_{VL} = -iA_v \frac{\omega}{v_{sb}} e^{i(\omega t + \frac{\omega}{v_{sb}} z)} \tag{7}$$

where v_{sb} is the shear wave velocity of Backfill 1, and ω is the angular frequency of the shear waves. A_v is the amplitude of the SV-waves transmitted to Backfill 1 at its bottom from Layer N. A_v can be written as a function of the impedance ratio of the Backfill 1 to Layer N as:

$$A_v = \frac{2}{1 + (\rho_b \, v_b / \rho_N \, v_N)} A_N \tag{8}$$

As shear waves approaching the interface between soil layers and Backfill 2, part of the incident waves is transmitted to the backfill, and the remainder is reflected in the soil layer. The transmitted waves undergo several reflections at the backfill boundaries. It is possible that these waves are trapped in the backfill if total

internal reflections occur, depending on the wavelength "λ", material properties of the soil profile, and the size of the soil medium. According to Snell's Law, when these transmitted waves are incident upon the interface at an angle of incidence greater than the critical angle, no transmission of seismic waves occurs, and the waves are reflected in the backfill. Furthermore, the wavelength should be short enough, which corresponds to high wave frequency, to propagate through the soil medium. Surface waves of different phase velocities can be found within a certain range of propagation along the depth. The variation of the phase velocities as a function of the wavelength is usually referred to as dispersion curves, where higher wavelengths produce higher phase velocities. Moreover, surface waves with higher wavelength decay at greater depths than their lower wavelength counterparts for the same soil medium size (Foti et al. 2018). However, as clearly stated earlier, wave propagation in Backfill 2 is not within the scope of this thesis.

3.6. DISPLACEMENTS DUE TO REFLECTED SV- AND P-WAVES

Induced by the SV- and P-waves reflected from the Backfill 2, $[u_{SV}]_R$ and $[u_P]_R$ are additional displacements that represent the contribution of Structure 2 to amplify Structure1 responses. Essentially, this part requires tracking the reflected SV- and P-waves until reaching Structure 1. The reflected waves undergo several phases of propagation back and forth in the soil layer between the two structures. Within each phase, the reflected waves experience several reflections/refractions with the upper and lower boundaries of the soil layer before reaching any of the

structures. The number of phases and the amplitudes of the final waves transmitted to both structures depend on various factors, including the distance between the structures, material properties of the soil layer, and the slope of both backfills.

From the geometry in Figure 3.2, the SV-waves impinge the inclined boundary of Backfill 2 at an angle equal to the slope of the interface. The satisfaction of the displacement compatibility and stress continuity at the interface between two soils leads to a set of coupled equations to calculate the amplitudes of the transmitted and reflected waves (Zoeppritz 1919). Equations (9) shows these amplitudes in terms of the angle of inclination of the backfill interface θ:

$$\begin{bmatrix} \sin\theta & \sin\theta & \cos(\text{asin}(\mathcal{F}_n \sin\theta)) & -\cos[\text{asin}(V\mathcal{F}_b \sin\theta)] \\ \cos\theta & -\cos\theta & \mathcal{F}_n \sin\theta & V\mathcal{F}_b \sin\theta \\ \cos 2\theta & \cos 2\theta & -\frac{1}{\mathcal{F}_n}\sin[2\,\text{asin}(\mathcal{F}_n \sin\theta)] & \frac{V\mathcal{R}}{\mathcal{F}_b}\sin[2\,\text{asin}(V\mathcal{F}_b \sin\theta)] \\ -\sin 2\theta & \sin 2\theta & \mathcal{F}_n \cos 2\theta & V\mathcal{R}\mathcal{F}_b \cos[2\,\text{arcsin}(V\sin\theta)] \end{bmatrix}$$

$$\begin{bmatrix} -V\sin\theta \\ -\cos[\text{asin}(V\sin\theta)] \\ -V\mathcal{R}\cos[2\,\text{asin}(V\sin\theta)] \\ V\mathcal{R}\sin[2\,\text{asin}(V\sin\theta)] \end{bmatrix} \begin{Bmatrix} A_{I_n} \\ A_{R_n} \\ B_{R_n} \\ B_{T_b} \\ A_{T_b} \end{Bmatrix} = \begin{Bmatrix} 0 \\ 0 \\ 0 \\ 0 \\ 0 \end{Bmatrix} \quad (9)$$

where V is the ratio of the shear wave velocity of the backfill v_{sb} to that of the soil layer v_{sn}, $\mathcal{R}$ is the ratio of the mass density of the backfill ρ_b to that of the soil layer ρ_n, and A_{Rn}, B_{Rn}, B_{Tb}, and A_{Tb} are the amplitudes of the reflected SV-wave, reflected P-wave, transmitted P-wave, and transmitted SV-wave, respectively. The

values of $\mathcal{F}_b$ and $\mathcal{F}_n$ depend on the Poisson ratios (ν) of the backfill and soil layers, respectively. $\mathcal{F}$ is generally given by:

$$\mathcal{F} = \sqrt{\frac{2-2\nu}{1-2\nu}} \tag{10}$$

Equation (9) indicates that the seismic amplitudes transmitted to Structure 2 (A_{T_b} and B_{T_b}) or the change in the seismic demand of the existing structure (A_{R_n} and B_{R_n}) are primarily controlled by the angle of inclination θ and the material properties of the backfill. The angle of inclination θ is inherently dependent on the maximum allowable slope of the excavation required to maintain the overall stability of the open excavation during construction phases.

3.6.1. Interaction of Seismic Waves with the Layer Boundaries and a Guided Flowchart

Along the distance L, the amplitudes of the SV- and P-waves reflected from Backfill 2 reduce successively until the waves reach the vertical backfill due to different mechanisms, including material damping and reflection/refraction of seismic energy at the interface between two layers, as shown in Figure 3.2. Since material damping is not included in this study, the final amplitude is closely related to the number of reflections at the upper and lower interfaces. Figure 3.3 shows the interaction of a reflected SV-wave with the upper and lower boundaries, as well as the interference of seismic waves. Figure 3.3 Also shows a flowchart that simplifies

the interference of waves by mapping all data into a guided diagram, as will be explained in detail. For clarity, the transmitted waves are not shown in Figure 3.3, and only the first three reflected SV- and P-waves are illustrated.

As mentioned before, part of the incident energy is transmitted to the upper/lower layer, as shown in Figure 3.2. However, the transmitted waves to the upper and lower layers are not included in the current analysis, and the proposed procedure is limited to the reflected waves. As will be explained in a quantitative evaluation in subsequent sections, the final amplitudes of waves transmitted to Structure 1 mainly depend on the wavepaths generated from the SV- and P-waves reflected from the inclined backfill. Furthermore, the waves transmitted to the upper and lower layers undergo another series of interactions with the layer boundaries, resulting in much lower amplitudes compared to the original shear waves and the waves reflected from the inclined backfill boundary.

In the flow chart shown in Figure 3.3, the waveform is divided into two sets of wavepaths, namely SV-wavepath and P-wavepath corresponding to the reflected SV- and P-waves, respectively. Each wavepath is characterized by an initial amplitude and number of reflections at the upper and lower boundaries. Both parameters are functions of soil properties, layer thickness, and the slope of Backfill 2. The wavepaths are labelled and given different line styles to distinguish the wavepath number. The starting point of a wavepath is located either on the upper

or lower boundary of the soil layer, while the endpoint is always at the boundary of Backfill 1.

3.6.2. NUMBER OF REFLECTIONS AT THE UPPER AND LOWER BOUNDARIES

Figure 3.3 shows that each wavepath branches off at different locations on the upper and lower boundaries, resulting in a new wavepath different in wave type and spacing between the reflecting locations or branching points. The location of a branching point represents the starting point of a new wavepath and correlates with the number of reflections along the parent wavepath before reaching Backfill 1. The order in which the branched wavepaths is generated from the parent wavepath is indicated by m_{ij} below each branch in the flowchart. The total number of reflections for each wavepath can be calculated as:

$$N_{SV,P} = \frac{L - x_1 - x_2 - \sum\left(m_{ij}x_{sv} + n_{ij}x_p\right)}{x_{sv,p}} \tag{11}$$

$$x_{sv} = h_n\, tan(\alpha_{In}) \quad x_p = h_n \tan(\beta_{In}) \tag{12}$$

where $N_{SV,P}$ is the total number of branching points along the wavepath and is rounded to the next higher integer, h_n is the layer thickness and x_1 is the thickness of Backfill 1. Distance x_2 varies depending on the location of the incident waves on the inclined backfill and can be readily defined from the geometry in Figure 3.2. x_{sv} and x_p are the distances between two successive reflections in the SV- and P-wavepaths, respectively. Angles α_{In} and β_{In} are defined in Figure 3.2. For

instance, the summation term in Equation (11) for the P_{10} wavepath in Figure 3.3 can be written as:

$$\sum \left(m_{ij} x_{sv} + n_{ij} x_p\right)_{P10} = m_{02}\, x_{sv0} + n_{22} x_{p2} + m_{41} x_{sv4} \tag{13}$$

Since the soil layers are assumed to be homogeneous, the spacings x_{sv} and x_p are constant for all branched SV- and P-wavepaths, and for the main wavepaths SV_0 and P_0. Zero values of $N_{SV,P}$ mean that the wavepath does not encounter any interaction with the upper and lower boundaries of the soil layer before reaching Backfill 1. Due to the variation in the material properties of the soil profile (see Figure 3.1, it is more convenient to define the number of reflections at the upper and lower boundaries separately, as follows:

$$N_{SV,P} = \begin{cases} Even: & N_U = N_L = N_{SV,P}/2 \\ Odd: & if\ \mathbf{k} = \begin{cases} +\boldsymbol{ve}: & N_U = (N_{SV,P}+1)/2\,,\ N_L = \left(N_{SV,P}-1\right)/2 \\ -\boldsymbol{ve}: & N_U = (N_{SV,P}-1)/2\,,\ N_L = \left(N_{SV,P}+1\right)/2 \end{cases} \end{cases} \tag{14}$$

where **k** is the wave vector, with positive values corresponding to upward wave propagation and negative values representing downward propagation.

The wavepaths are clearly affected by the slope of the excavation boundary. According to OSHA standards (Reese and Eidson 2006), the typical excavation slopes vary from 34 to 53 degrees. At an angle of 45 degrees, two important observations are obtained. Firstly, the reflected SV-waves propagate horizontally in the soil layer towards the existing structure (i.e., Structure 1) without any

interaction with the upper and lower boundaries. Secondly, by applying Snell's Law at the interface between Backfill 2 and soil layers and examining different Poisson ratios, it can be found that a post-critical situation occurs, and the reflected P-waves always travel along the interface and decay away from the interface. In other words, no reflected plane P-waves are developed in the soil layer.

3.6.3. INITIAL AMPLITUDE OF WAVES ALONG DIFFERENT WAVEPATH

The amplitudes A and B in the flow chart in Figure 3.3 represent the initial wave amplitudes corresponding to each wavepath. Given the characteristics of the soil profile and the angle of inclination θ, Equation (9) can be used with minor modifications to calculate the amplitudes of the SV-wave. The slope angle θ and the backfill material properties are replaced by the angle of reflection α_{In} and the material properties of the upper or lower soil layers (Figure **3.2** and Figure 3.3). For the P-wavepaths, Equation (9) is no longer valid and should be replaced by the following equation (Zoeppritz 1919),

$$\begin{bmatrix} \sin\beta_{In} & -\sin\beta_{In} & \cos\alpha_{In} & -\sin\beta_{Tn} & \cos\alpha_{Tn} \\ \cos\beta_{In} & \cos\beta_{In} & \sin\alpha_{In} & -\cos\beta_{Tn} & -V\sin\alpha_{Tn} \\ -\sin 2\beta_{In} & -\sin 2\beta_{In} & \mathcal{F}\cos 2\alpha_{In} & VR\sin 2\beta_{Tn} & -VR\cos 2\alpha_{Tn} \\ -\cos 2\alpha_{In} & \cos 2\alpha_{In} & \frac{1}{\mathcal{F}}\sin 2\alpha_{In} & VR\cos 2\alpha_{Tn} & -VR\sin 2\alpha_{Tn} \end{bmatrix} \begin{Bmatrix} B_I \\ B_R \\ A_R \\ B_T \\ A_T \end{Bmatrix} = \begin{Bmatrix} 0 \\ 0 \\ 0 \\ 0 \\ 0 \end{Bmatrix} \quad (15)$$

where B_I, B_R, A_R, B_T, and A_T are the amplitudes of the incident P-wave, reflected P-wave, reflected SV-wave, transmitted P-wave, and transmitted SV-wave, respectively; α_{Tn} and β_{Tn} are the angles of refraction of the SV- and P-waves, and can be determined using Snell's law (Kramer 1996). Since soil layers are assumed to be homogeneous and horizontally stratified, the ratios of the transmitted and reflected wave amplitudes to the incident wave amplitude are constant for the interface between two layers. For convenience, these ratios are referred to as listed in Table 3.1, in which the subscripts $V, I, U,$ and L denote the interface between the soil layer and Backfill 1, Backfill 2, upper layer, and lower layer, respectively. Accordingly, the ratio of the initial amplitude of waves along any branched wavepath (see Figure 3.3) to the amplitude of the vertically propagating shear wave are given in Equation (16).

$$f = f_{RI} \prod_{j=1}^{N_w} \left[f_{RU}^{e_u} \, f_{RL}^{e_l} \, f_R' \right]_j \tag{16}$$

where f_R' depends on the location of the starting point of the wavepath on the inclined backfill. For upgoing waves, f_R' represents f_{RL}' in Table 3.1, and equals f_{RU}' for downgoing waves. Assume a parent wavepath consists of N branching points, and a new wavepath is developed at the m^{th} point. N_w represents the number of branching points up to the m^{th} point. e_U and e_L are the numbers of branching points along the j-wavepath at the upper and lower boundaries of the soil layer, respectively, up to the starting point of the current wavepath. e_U and e_L can be

calculated from Equation (14), while the total number $N_{SV,P}$ is given by Equation (11).

3.6.4. FINAL AMPLITUDES OF WAVES TRANSMITTED TO THE EXISTING STRUCTURE

The seismic amplitudes on the interface of soil and Structure 1 can be directly determined as a function of the amplitude of the vertically propagating shear waves A_n as:

$$\begin{Bmatrix} A_f \\ B_f \end{Bmatrix} = f\ (f_{RL})^{N_L} (f_{RU})^{N_U} \begin{Bmatrix} f_{TV} \\ f'_{TV} \end{Bmatrix} A_n \tag{17}$$

where A_f and B_f are the amplitudes of the SV- and P-waves transmitted to the vertical backfill. Each wavepath impinges the boundary of Backfill 1 at different locations across the layer thickness. The distance h_f depends on the angle of incidence. For an SV-wavepath, h_f is given by:

$$h_{fi} = (L - x_1 - x_2 - (N_{svi} - 1)x_{svi}) \cot \alpha_n \tag{18}$$

For P-wavepaths, Equation (18) is still valid, but x_{sv} and α_n should be replaced by x_p and β_n corresponding to the P-wavepath.

3.6.5. OPTIMAL DISTANCE L FOR MINIMUM SSSI

As mentioned earlier, the change in the seismic demand of the existing building, Structure 1, due to the insertion of Structure 2 depends on three main factors: the

angle of inclination and mechanical properties of the new backfill and the distance between the two buildings. In addition to controlling the excavation slope and backfill material, the distance between buildings can also be adjusted to achieve minimal seismic amplitudes on Structure 1. The desired distance is related to the target amplitude on Structure 1, which in turn depends on the seismic overcapacity of the structural system. Given N_U and N_L are equal, the minimum distance between the two structures required to achieve the target transmitted amplitude "**A**" due to an SV-wavepath is given by:

$$L_{req} = x_1 + x_2 + x_{sv} \log_{(f_{RL}\, f_{RU})} \left(\frac{\mathbf{A}/A_n}{f f_V} \right) \tag{19}$$

where $f_V = \max(f_{TV},\ f'_{TV})$. Equation (19) reveals that the final transmitted amplitudes generally decrease as the distance between structures increases. Since the logarithmic term can never reach zero, there will always be an increase in the seismic responses of Structure 1. However, an approximate zero-transmission condition can be achieved when $\mathbf{A}/A_n$ has minimal value. As a threshold for the $\mathbf{A}/A_n$, the spacing between the two structures should meet other engineering requirements, including the minimum distance between two foundations and the spread mechanism of the vertical load through soil layers. Regarding the minimum distance corresponding to P-waves, Equation (19) is still valid with x_{sv} being replaced by x_p. Therefore, the minimum distance between Structure 1 and Structure 2 is the larger of L_{req} corresponding to SV- and P-wavepaths.

3.6.6. MULTI-PHASES WAVE PROPAGATION

Part of the incident waves on the vertical backfill (i.e., Backfill 1) will reflect and travel back towards the inclined backfill, leading to another phase of wave propagation. The effectiveness of considering the multiple phases of wave propagation depends mainly on the amplitudes of the reflected waves from both backfills. Besides, the multi-phase condition increases the complexity of the solution since each reflected wave follows the same procedure illustrated in Figure 3.3, leading to a large number of wavepaths. However, the final transmitted amplitudes due to an SV-wavepath, considering multi-phases wave propagation, can be expressed as:

$$\begin{Bmatrix} A_f \\ B_f \end{Bmatrix} = f\, f_{RL}^{N_L}\, f_{RU}^{N_U} \left(\prod_{i=1,3,..}^{S} \left(f_{RV}\, F_{RL}^{N_L}\, F_{RU}^{N_U} \right)_i \left(f_{RI}\, F_{RL}^{N_L}\, F_{RU}^{N_U} \right)_{i+1} \right) \begin{Bmatrix} f_{TV} \\ f'_{TV} \end{Bmatrix} A_n \qquad (20)$$

where S is the total number of phases. Since wave propagation from Backfill 2 to Backfill 1 occurs at every other phase, the counter i in the above equation is given odd numbers.

3.6.7. TOTAL DISPLACEMENT

Recall the reflection and refraction of the vertical SV-waves at the boundary of Backfill 2, the procedure illustrated in Figure 3.3 should be repeated to evaluate the contribution of the reflected P-waves. The total seismic amplitudes due to the SV-

and P-wavepaths must be combined separately, as the resulting wavefronts have different wavevectors **k**. Therefore,

$$\begin{Bmatrix}\mathbf{A}\\ \mathbf{B}\end{Bmatrix} = \sum\left(f(f_{RL})^{N_L}(f_{RU})^{N_U}\begin{Bmatrix}f_{TV}\\ f'_{TV}\end{Bmatrix}A_n\right)_{SV} + \sum\left(f(f_{RL})^{N_L}(f_{RU})^{N_U}\begin{Bmatrix}f'_{TV}\\ f_{TV}\end{Bmatrix}A_n\right)_{P} \quad (21)$$

The total displacement at any point along the boundary of Backfill 1 combines displacements from the vertically propagated shear waves (i.e., Equation (7)) and the SV- and P waves reflected from Backfill 2. The total displacements can be calculated by substituting Equations (7) and (21) into equations (3) and (6):

$$u_T = \left(-iA_v\frac{\omega}{v_s}e^{i\frac{\omega}{v_{sb}}z}\right)e^{i\omega t} - \left(i\mathbf{B}k_x e^{\pm ik_{z_p}z} \pm i\mathbf{A}k_{z_s}e^{\pm ik_{z_s}z}\right)e^{i(\omega t - k_x x)} \quad (22)$$

$$w_T = \left(\pm i\mathbf{B}k_{z_p}e^{\pm ik_{z_p}z} - i\mathbf{A}k_x e^{\pm ik_{z_s}z}\right)e^{i(\omega t - k_x x)} \quad (23)$$

where the positive exponents represent the upgoing waves, and the negative exponents represent the downgoing waves. Besides the increase in the amplitudes of the horizontal displacements, Equation (23) implies that Backfill 1 encounters vertical displacements only due to the presence of Structure 2. Regarding the horizontal component, two wave vectors **k** are identified. The first is associated with the vertically propagating SV-waves, where its magnitude equals ω/v_s and its direction is parallel to the vertical axis. The second is pertinent to the wavenumbers k_x and k_z of the reflected SV- and P-waves, with the magnitude being $\sqrt{k_x^2 + k_z^2}$ and the direction normal to the wavefront.

3.7. SEISMIC EARTH PRESSURE DISTRIBUTION DUE TO SSSI

With the soil displacements being determined, the seismic earth pressure on Structure 1 can be readily calculated. For a vertical frictionless wall, the normal stresses σ_{xx} represents the distribution of seismic lateral earth pressure on the wall. From the stress-strain relationships of an isotropic linear material, the additional seismic earth pressure on Structure 1 due to the reflected waves from Structure 2 (i.e., SSSI) can be expressed as:

$$\sigma_{xx} = \left(\left[\mp\lambda k_{z_\beta}^2 - (\lambda + 2\mu)k_x^2\right]\mathbf{B}\, e^{\pm ik_{z_\beta}z} \mp 2\mu k_x k_{z_\alpha}\mathbf{A}\, e^{\pm ik_{z_\alpha}z}\right) e^{i(\omega t - k_x x)} \quad (24)$$

If the wall is not smooth, the total seismic earth pressure is the sum of the normal stresses σ_{xx} and shear stresses σ_{zx}, which is given by:

$$\sigma_{zx} = \left(\mu\left(k_{z_\alpha}^2 - k_x^2\right)F_{sv}e^{\pm ik_{z_\alpha}z} \pm 2\mu k_x k_{z_\beta}F_p e^{\pm ik_{z_\beta}z}\right) e^{i(\omega t - k_x x)} \quad (25)$$

3.8. EVALUATION OF THE PROPOSED PROCEDURE

The following sections provide a quantitative evaluation of the proposed procedure by calculating the additional seismic earth pressure induced by SSSI. For this purpose, the general layout of the soil-structure system shown in Figure 3.1 is employed in the analysis, where L=30 m and the thicknesses and material properties of the soil profile are given in Table 3.2. It should be mentioned that the Poisson ratio of 0.25 is assumed across the soil profile to simplify the calculations and focus on the effect of three parameters: the distance L between substructures 1 and 2, the slope angle θ, and the backfill material properties. According to Lamb and

Whitman (1979) and Bowles (1988), the typical values of Poisson's ratio for most intact rocks vary in the range of 0.2 to 0.3. The Poisson's ratio of soil, on the other hand, varies with the type of soil density, strain level and drainage conditions, with the typical values varying in the range of 0.2 to 0.4. More particularly, $\nu = 0.2$-0.3 for sandy clay and stiff clay, and 0.2 to 0.35 for dense sand. Without considering the presence of soft soil layer, we choose $\nu = 0.25$ as representative value for all soil layers and the elastic half-space.

The shear wave velocities adopted in the analysis correspond to dense to stiff soil conditions as classified by Pacific Earthquake Engineering Research Center (Wair et al. 2012). Regarding Backfill 2, three different slopes are to be investigated, namely $1.5\colon 1$, $1\colon 1$, and $1\colon 0.75$. The change in the seismic responses of Backfill 1 will be calculated, considering vertically propagating shear waves impinge the inclined interface between Backfill 2 and the ground soil. The following analysis considers only one phase of wave propagation from Substructure 2 to Substructure1.

3.8.1. CASE (1): BACKFILL 2 WITH SLOPE OF $1.5\colon 1$

In the first case, vertically propagating shear waves impinge the inclined interface (Backfill 2) at an angle of 34 degrees with the normal to the interface. The angles of reflection of the SV- and P-wave are 34° and 75.5° respectively. Based on the resulting angles of reflection, the reflected P-waves initially travel upward towards the upper boundary of the soil layer. At the same time, the SV-waves propagate

towards the lower boundary. By tracking the wavepaths as illustrated in Figure 3.3, eight P-wavepaths and six SV-wavepaths are identified, as shown in Figure 3.4.

According to Figure 3.4, the main SV-wavepath (i.e., $SV0$-wavepath) does not branch off at the upper and lower boundaries. This can be attributed to the critical angle of incidence that does not produce reflected P-waves. By applying Snell's law, the critical angle of incidence to produce reflected P-waves is 35.3°, while the actual angle of incidence of the $SV0$ wavepath is 38°.

The final seismic amplitudes transmitted to the existing structure due to all wavepaths were calculated using Equations (11) to (18). Due to the large number of wavepaths, only the results of four wavepaths are presented. The selected wavepaths are the two main wavepaths $SV0$ and $P0$, and the two branched wavepaths $SV1$ and $SV2$. Table 3.3 shows the final transmitted amplitudes normalized to the amplitude of the original vertically propagating shear waves in different soil layers. The positive sign represents upgoing waves, while the negative sign represents downgoing waves. The depth h_f represents the location at which a wavepath impinges the boundary of Backfill 1 and is measured from the top of the soil layer. The amplitudes A_f and B_f and depth h_f were calculated at three different distances (L = 30 m, 25 m and 15 m) to investigate the variation of the seismic responses with the distance L.

It can be seen from Table 3.3 that the final amplitudes decrease as the distance between two buildings increases. The amplitudes of the branched

wavepaths $SV1$ and $P1$ are much smaller than those of the two main wavepaths $SV0$ and $P0$. Accordingly, the main wavepaths can be used solely to evaluate the increase in the seismic responses of Structure 1, with the influence of the branched wavepaths being neglected. Moreover, the amplitude of some wavepaths such as the $SV0$ remains constant at L = 25 m and 30 m, but the depth h_f has different values. This can be traced back to the spacing between two successive reflections along a single wavepath. For instance, the difference between the two distances $L = 25\ m$ and $30\ m$ is not sufficient for a new branching point to be developed at the upper or the lower boundaries. Therefore, the amplitude of the wave remains constant, recalling that the soil is considered as linear elastic and no energy dissipation occurs during the process of wave propagation.

When examining the values of h_f for all wavepaths, it is noticed that two or more wavepaths may impinge the boundary of the vertical backfill at the same location. In such cases, all possible amplitudes should be combined to determine the total amplitude at this location, taking into account the direction of propagation of each wave. For instance, the wavepaths P_2, P_5, and P_7 are incident on the boundary of the vertical backfill at point $\boldsymbol{X}$ with h_f = 1.717 m measured from the top of Layer 2, as shown in Figure 3.4. The total displacement at point $\boldsymbol{X}$ is the sum of all displacements induced by P_2, P_5, and P_7.

The second factor that influences the results is the mechanical properties of the backfill. Figure 3.5 and Figure 3.6 show the effect of the backfill density and

shear wave velocity, respectively, on the final amplitudes corresponding to P0, P1, SV0, and SV1-wavepaths. The given amplitudes were calculated on Structure 1 in the range of Layer 3, where distance L is $15\ m$ and both backfills are of the same material. The vertical axis represents the final amplitudes of the transmitted waves normalized to the amplitude of the original vertically propagating shear waves. The bottom horizontal axes in both figures represent the ratio of the backfill density and shear velocity to their counterparts of Layer 3. The upper horizontal axis represents the ratio of the backfill shear modulus to that of Layer 3. Amplitudes A and B are defined in Equation (3).

Generally, both the backfill density and shear wave velocity have a significant effect on the final seismic amplitude due to the main wavepaths. In contrast, the amplitudes associated with the branched wavepaths show small variations. At smaller ratios of density and shear wave velocity, the amplitude B of the wavepath P0 in Figure 3.5.a and Figure 3.6.a decreases significantly as the density and shear wave velocity ratios increase. The amplitude B reaches its minimum at $\rho_b/\rho_{L3} = 1.18$ and $v_{sb}/v_{sL3} = 0.924$, but a further increase in these ratios amplifies the amplitude. The density and shear wave velocity ratios corresponding to B_{min} can be considered as critical ratios after which the reflected amplitudes in Equations (15) have an imaginary term. Consequently, the actual physical amplitude became the square root of the sum of the squares of the imaginary and real parts (McCamy et al. 1962).

Figure 3.5(b) shows that the amplitude A of the SV0-wavepath experiences an initial increase up to a density ratio of 0.381. Then, it gradually decreases with a further increase in the density ratio. In Figure 3.6(b), the variation of amplitude A is similar to that in Figure 3.5(b) to a certain degree. An initial increase in amplitude A occurs up to a shear velocity ratio of 0.257, and then the amplitude degrades at a higher rate until a shear velocity ratio of 1.031. Recalling the critical density ratio, the imaginary terms appear in the current case in Equation (9) when the shear velocity ratio exceeds 1.031. Therefore, amplitude A in Figure 3.6(b) experiences further amplification at high shear velocity ratios.

Figure 3.5 and Figure 3.6 indicate that the mechanical properties of the backfill soil can be adequately adjusted to eliminate the amplified displacement and stresses caused by the transmitted seismic amplitudes. Generally, backfills with low density (ρ) or lower shear wave velocity (V_s) should be avoided due to its detrimental effect, as illustrated in the figures. Since the shear modulus G is correlated to the density and the shear wave velocity of the soil layer via $G = \rho\, V_s^2$, the shear modulus can be used to select the appropriate backfill type. For the current numerical example, the shear modulus was calculated and placed on the top axes of Figure 3.5 and Figure 3.6. We observe that the backfill with low shear modulus such as loose sand should be avoided in the current case.

After the seismic amplitudes being determined, the total displacements in Backfill 1 can be calculated from equations (22) and (23). For instance, the total displacements at Layer 2 can be expressed as:

$$u_T = -ik_\alpha e^{i(\omega t + \mathrm{k}_\alpha z)} + \left(-0.1834\, e^{ik_{z_s} z} + 0.00066\, e^{-ik_{z_s} z} - 0.004\, e^{ik_{z_p} z} - 0.00476\, e^{-ik_{z_s} z}\right) ik_x A_2 e^{i(\omega t - k_x x)} \text{ (m)}$$

$$w_T = \left(-0.06403\, e^{ik_{z_s} z} - 0.00023\, e^{-ik_{z_s} z} + 0.0058\, e^{ik_{z_p} z} - 0.0067 e^{-ik_{z_p} z}\right) ik_x A_2 e^{i(\omega t - k_x x)} \ (m)$$

where k_α is the wavenumber of the vertically propagating shear wave and equals ω / v_{sb2}. The responses described above are calculated based on an incident SV-wave impinges the midpoint of the interface between the Backfill 2 and soil layer. In fact, the wavefront impinges all points on the interface simultaneously, resulting in continuous reflections from Backfill 2 to Backfill 1. A time lag is expected between the reflected waves at the Backfill 1 interface due to the inclined surface of Backfill 2. However, the thickness of the soil layer is relatively small compared to the shear wave velocity of the soil. Therefore, the time lag can be neglected, and assuming all inclined backfill points are excited at the same time is acceptable. Furthermore, the variation of the final amplitudes on Backfill 1 is firmly dependent on the spacing between two successive reflections on the upper/lower boundaries. In most cases, depending on the excavation slope and layer thickness, the horizontal segment of the inclined backfill may not be sufficient for a new interaction point to be created at the upper/lower boundaries. Therefore, the responses calculated from the mid-point reflection can be considered the representative or average of the entire layer.

The normal and shear components of the additional seismic earth pressure are calculated according to equations (24) and (25), respectively. At Layer 2, normal and shear stresses can be written as:

$$\sigma_{xx} = \left(-382.14\, e^{ik_{z_s}z} + 1.37\, e^{-ik_{z_s}z} - 15.84\, e^{ik_{z_p}z} + 1.64\, e^{-ik_{z_p}z}\right) k_x^2\, A_2\, e^{i(\omega t - k_x x)}$$

$$\sigma_{zx} = \left(480.50\, e^{ik_{z_s}z} + 1.73\, e^{-ik_{z_s}z} + 12.00\, e^{ik_{z_p}z} - 14.00\, e^{-ik_{z_p}z}\right) k_x^2\, A_2\, e^{i(\omega t - k_x x)}$$

In analogy to Layer 2, the additional seismic earth pressure on Structure 1 at layers 1 and 3 can be determined. The graphical representation of these equations is illustrated in Figure 3.7 along with the soil strata identified in Table 3.2. The vertical axis represents the embedment depth of Structure 1 in Layers 1 to 3, while the horizontal axis is the magnitude of the normal or shear stresses. In Figure 3.7(a), the normal stresses calculated using the proposed method are compared with the static earth pressure and seismic earth pressure calculated by other methods. Two methods are used in the comparison: the semi-empirical Seed and Whitman (1970) method and the Spectral Element Method. For that purpose, the open-source SPECFEM2D software is employed in the analysis, in which the three-dimensional wave propagation theory is incorporated using the Spectral Element Method (Komatitsch and Tromp 2014).

The proposed method is generally in good agreement with the additional earth pressure numerically calculated by SPECFEM2D. However, the discrepancies are noticeable at some depths in the third layer, which can be attributed to neglecting the contribution of the transmitted waves in the proposed

method. In comparison with the total seismic earth pressure using the S-W method and SPECFEM2D, the SSSI effect is significant in Layer 3, which corresponds to the highest variation between the mechanical properties of the soil layers and backfill (see Figure 3.5 and Figure 3.6). In addition, the static earth pressure is included in the comparison in Figure 3.7(a) to reveal that the magnitude of the additional earth pressure induced by SSSI is considerable, which in the current case reaches or exceeded the static earth pressure at different locations.

3.8.2. CASE (2): BACKFILL 2 WITH SLOPE OF 1: 1

In the second case, the interface between the soil layers and Backfill 2 makes an angle of 45° with horizontal. Following the same procedure described in Case (1), two important observations can be addressed. Firstly, the SV-waves reflected from Backfill 2 will travel horizontally towards Structure 1 and will not interact with the upper and lower boundaries of the soil layer. Secondly, no reflected P-waves are produced as the angle of incidence of the vertical SV-waves exceeded the critical angle of incidence. Since the reflected SV-waves are horizontally propagating vertically polarized, the wave vector $\mathbf{k_\alpha}$ points accordingly to the horizontal direction, thus the wavenumber k_{z_α} should be canceled from the equations, see Table 3.4.

The wave amplitudes in Table 3.4 are used to calculate the total displacements in Backfill 2 and the additional seismic earth pressure on Structure

1. For instance, the total displacements on the boundary of Backfill 2 at Layer 2 can be written as:

$$u_T = -i\, k_{z_\alpha}\, A_2\, e^{i(\omega t + k_{z_\alpha} z)} \qquad (m)$$

$$w_T = -0.141\, i\, k_x\, A_2\, e^{i(\omega t - k_x x)} \qquad (m)$$

In the equations above, the wavevectors k_x and k_{z_α} equals ω/v_{sb2}. However, k_{z_α} and k_x correspond to waves propagating in the vertical and horizontal directions, respectively. By comparing the total displacements in Cases (1) and (2), we observe that the 45° slope angle of Backfill 2 has no effect on the horizontal component of the total displacement. Therefore, the total horizontal displacement in Case (2) is directly given by Equation (6). Nevertheless, vertical displacements are induced in both cases, but with higher responses in Case (2).

Since Backfill 2 does not induce additional horizontal displacements, there are no additional normal stresses σ_{xx} exerted on Structure 1. The shear stress component σ_{zx} can be calculated by substituting the amplification factors from Table 3.4 into Equation (25). For the sake of comparison with Case (1), the shear stresses on Structure 1 are calculated at Layer 2 and can be expressed as:

$$\sigma_{zx} = -146.92\, A_2 k_x^2\, e^{i(\omega t - k_x x)} \qquad (kPa)$$

A comparison of shear stresses in Cases (1) and (2) reveals that the additional seismic earth pressure in Case (2) is induced by SV wavepaths only. In addition, the exponential terms with the parameter k_{z_s} vanishes as the wavenumber vector of the wavefront is polarized to the horizontal direction. Figure 3.8 shows

the additional seismic shear stresses on Structure 1, along with a comparison with Case (1). For the current case of study, the 45° slope angle of Backfill 2 gives higher shear stresses at layers (1) and (2), but the opposite occurs at Layer (3).

3.8.3. CASE (3): BACKFILL 2 WITH SLOPE OF 1: 0.75

The third case represents a steep excavation slope where the angle of inclination with the horizontal axis is 53°. The reflected SV-waves are incident on the upper and lower boundaries of the soil layer at an angle of 74° with the normal to the interface. The incident angle of the SV-waves at either the inclined boundary of Backfill 2 or the upper and lower boundaries of the soil layer is greater than the critical angle of reflection of the P-waves. Therefore, the SV0 wavepath can be considered the only source of amplification in the seismic responses of Structure 1. Table 3.5 shows the final seismic amplitudes transmitted to Structure 1 for different distances L between the two structures at $\theta = 53°$.

By comparing the data in Table 3.5 and Table 3.3, we observe that Case (3) gives higher transmitted amplitudes A_f than their counterparts in Case (1). However, Case (1) results in slightly higher amplitude B_f at layers (2) and (3) at distance $L = 15\ m$. Since the $SV0$ wavepath in Case (2) does not interact with the upper and lower boundaries of the soil layers, the wave does not experience any reduction in the amplitude. Hence the amplification factors in Case (2) are higher than those in Case (3). When distance L is $15\ m$, the total displacements on the boundary of Backfill 1 at Layer 2 are determined as:

$$u_T = -ik_\alpha e^{i(\omega t + \mathrm{k}_\alpha z)} + \left(0.0764\, e^{-ik_{z_s} z} - 0.0033\, e^{-ik_{z_p} z}\right) ik_x A_2 e^{i(\omega t - k_x x)} \quad (m)$$

$$w_T = \left(-0.0033\, e^{-ik_{z_p} z} - 0.0764\, e^{-ik_{z_s} z}\right) ik_x A_2 e^{i(\omega t - k_x x)} \quad (m)$$

The additional normal and shear stress components of the lateral seismic earth pressure can be determined by substituting A_f and B_f into equations (25) and (26), and can be expressed as:

$$\sigma_{xx} = \left(150.31\, e^{-ik_{z_s} z} + 1.16\, e^{-ik_{z_p} z}\right) A_2\, k_x^2\, e^{i(\omega t - k_x x)} \quad (kPa)$$

$$\sigma_{zx} = \left(4.964\, e^{-ik_{z_\alpha} z} - 0.061\, e^{-ik_{z_\beta} z}\right) A_2\, k_x^2\, e^{i(\omega t - k_x x)} \quad (kPa)$$

The graphical representation of the additional shear and normal stresses on Structure 1 at $\theta = 53°$ is shown in Figure 3.9. The static and seismic earth pressures were added to Figure 3.9(a) in analogy to Figure 3.7(a) to give insights into the calculated stresses at $\theta = 53°$ using the proposed method. By comparing Figure 3.7(a) and Figure 3.9(a), it can be seen that the proposed method still corresponds to the numerically calculated additional earth pressure using SPECFEM2D. However, the discrepancies in layers 1 and 3 decrease as the slope increases. In addition, the additional earth pressure at steep slopes (i.e., $\theta = 53°$) still represents a significant percentage of the original static and total seismic earth pressures. Steep slopes generally give higher additional normal stresses across the three layers, except at local locations.

The variations of the shear stresses across the soil layers according to the three cases are not symmetric. Case (3) produces the highest shear stresses at Layer

3, while the highest stresses at Layers 1 and 2 are accumulated due to Case (2). This can be traced back to the seismic amplitudes shown in Table 3.3 to Table 3.5. Layer 3 produced higher seismic amplitudes of SV-wavepaths than the upper two layers and is accompanied by a relatively high amplitude of P-wavepath compared to Layer 2. In other words, shear stresses in layers 1 and 2 are mainly caused by one type of the two wavepaths, either P- or SV-wavepath, but in Layer 3 both wavepaths have a significant contribution to the resulting shear stresses. This can be attributed to the geometrical and mechanical properties of the soil layer specified in Table 3.2. On the other hand, at a 45° angle of inclination, shear stresses are only induced by SV-wavepaths, with no contribution from P-wavepaths. However, it should be emphasized that these results are not constant for any soil profile but vary depending on several factors, including the soil properties and excavation slope.

While the effect of material damping and transmitted waves are taken into account, the results discussed above may be slightly affected. This is because material damping is expected to reduce the overall additional earth pressure on the substructures; however, the transmitted waves have the tendency to amplify the earth pressure slightly for the reasons previously discussed.

3.9. CONCLUSIONS

The theory of the three-dimensional wave propagation is employed to evaluate the amplified seismic responses of two adjacent structures due to seismic SSSI, as well as backfill soils. Based on a guided flowchart, a simplified technique is proposed

to calculate the additional seismic amplitudes and earth pressures on the substructures due to SSSI. The soil profile considered in the analysis consists of N horizontally stratified layers of homogeneous, isotropic linear elastic soils rested above an elastic half-space. Seismic energy propagating towards the unbounded soil is fully absorbed by the boundaries incorporated at the left, bottom, and right edges of the soil-structure system to account for radiation damping. Expressions for additional seismic earth pressure are proposed based on reflections of seismic waves in soil layers, with the effect of the transmitted waves being neglected. In addition, a closed-form solution is proposed to calculate the optimal distance between two substructures that conform to the minimum SSSI.

A quantitative evaluation of the proposed procedure was presented to shed light on the effect of SSSI induced by inclined backfill, considering a single phase of wave propagation between two adjacent substructures. It was found that the main P- and SV-wavepaths can be solely used to evaluate the amplified seismic forces on the substructures, with the influence of the branched wavepaths being neglected. In addition, the amplitudes of seismic waves transmitted to an existing structure decrease as the distance between the two buildings increases.

Depending on the characteristics of the soil-structure system used in the current configuration, steep excavation slopes tend to amplify the seismic amplitudes at a higher rate than gentle slopes. At a slope of $1{:}\,1$, the reflected SV wave does not undergo any interactions with the upper and lower boundaries of the soil layers and thus does not cause additional seismic stresses. The final seismic

amplitudes transmitted to the substructure are sensitive to the density and shear wave velocity of the backfill material. For a substructure that penetrates multiple soil layers, the highest amplification in the seismic earth pressure occurs at the depths where the backfill is loose compared to the soil layer. However, when the shear modulus of the backfill approaches that of the soil layer, a critical condition may occur, and seismic waves will encounter further increase in amplitude. The findings of this parametric study imply that these amplified seismic responses are induced by the backfill and the properties of the backfill materials, which was never considered in the literature.

3.10. REFERENCES

Abraham, J. R., Smerzini, C., Paolucci, R., and Lai, C. G. (2016). "Numerical study on basin-edge effects in the seismic response of the Gubbio valley, Central Italy." Bulletin of Earthquake Engineering, 14(6), 1437–1459.

Alam, M. I., and Kim, D. (2014). "Spatially Varying Ground Motion Effects on Seismic Response of Adjacent Structures considering Soil-Structure Interaction." Advances in Structural Engineering, SAGE Publications Ltd STM, 17(1), 131–142.

Álamo, G. M., Padrón, L. A., Aznárez, J. J., and Maeso, O. (2015). "Structure-soil-structure interaction effects on the dynamic response of piled structures under obliquely incident seismic shear waves." Soil Dynamics and Earthquake Engineering, 78, 142–153.

Aldaikh, H., Alexander, N. A., Ibraim, E., and Oddbjornsson, O. (2015). “Two dimensional numerical and experimental models for the study of structure–soil–structure interaction involving three buildings.” Computers & Structures, 150, 79–91.

Alexander, N. A., Ibraim, E., and Aldaikh, H. (2013). “A simple discrete model for interaction of adjacent buildings during earthquakes.” Computers & Structures, 124, 1–10.

Behnamfar, F., and Sugimura, Y. (1999). “Dynamic response of adjacent structures under spatially variable seismic waves.” Probabilistic Engineering Mechanics, 14(1), 33–44.

Bybordiani, M., and Arici, Y. (2019). “Structure-soil-structure interaction of adjacent buildings subjected to seismic loading.” Earthquake Engineering & Structural Dynamics, 48(7), 731–748.

Chapman, C. (2004). Fundamentals of Seismic Wave Propagation. Cambridge University Press, Cambridge.

Hesham, A., A., A. N., Erdin, I., and A., K. J. (2018). “Evaluation of Rocking and Coupling Rotational Linear Stiffness Coefficients of Adjacent Foundations.” International Journal of Geomechanics, American Society of Civil Engineers, 18(1), 4017131.

Karabalis, D. L., and Mohammadi, M. (1998). "3-D dynamic foundation-soil-foundation interaction on layered soil." Soil Dynamics and Earthquake Engineering, 17(3), 139–152.

Kitada, Y., Hirotani, T., and Iguchi, M. (1999). "Models test on dynamic structure–structure interaction of nuclear power plant buildings." Nuclear Engineering and Design, 192(2), 205–216.

Knappett, J. A., Madden, P., and Caucis, K. (2015). "Seismic structure–soil–structure interaction between pairs of adjacent building structures." Géotechnique, 65(5), 429–441.

Kobori, T., Minai, R., and Kusakabe, K. (1973). "Dynamical Characteristics of Soil-Structure Cross-Interaction System - 1." Bulletin of the Disaster Prevention Research Institute, 22(2): 111-151.

Koketsu, K., and Miyake, H. (2008). "A seismological overview of long-period ground motion." Journal of Seismology, 12(2), 133–143.

Komatitsch, D., and Tromp, J. (2014). "SPECFEM2D User Manual Version 7.0." Computational Infrastructure for Geodynamics.

Kramer, S. L. (1996). Geotechnical Earthquake Engineering. Prentice Hall, New Jersey.

Lehmann, L., and Antes, H. (2001). "Dynamic structure - soil - structure interaction applying the symmetric Galerkin boundary element method (SGBEM)." Mechanics Research Communications, 28(3), 297–303.

Li, P., Liu, S., Lu, Z., and Yang, J. (2017). "Numerical analysis of a shaking table test on dynamic structure-soil-structure interaction under earthquake excitations." The Structural Design of Tall and Special Buildings, John Wiley & Sons, Ltd, 26(15), e1382.

Liang, J., Han, B., Todorovska, M. I., and Trifunac, M. D. (2017). "2D dynamic structure-soil-structure interaction for twin buildings in layered half-space I: Incident SH-waves." Soil Dynamics and Earthquake Engineering, 102, 172–194.

Liang, J., Han, B., Todorovska, M. I., and Trifunac, M. D. (2018). "2D dynamic structure-soil-structure interaction for twin buildings in layered half-space II: Incident SV-waves." Soil Dynamics and Earthquake Engineering, 113, 356–390.

Lin, H. -T, Roesset, J. M., and Tassoulas, J. L. (1987). "Dynamic interaction between adjacent foundations." Earthquake Engineering & Structural Dynamics, 15(3), 323–343.

Lou, M., Wang, H., Chen, X., and Zhai, Y. (2011). "Structure–soil–structure interaction: Literature review." Soil Dynamics and Earthquake Engineering, 31(12), 1724–1731.

Lu, Y., Li, B., Xiong, F., Ge, Q., Zhao, P., and Liu, Y. (2020). “Simple discrete models for dynamic structure-soil-structure interaction analysis.” Engineering Structures, 206, 110188.

Luco, J. E., and Contesse, L. (1973). “Dynamic structure-soil-structure interaction.” Bulletin of the Seismological Society of America, 63(4), 1289–1303.

Matthees, W., and Magiera, G. (1982). “A sensitivity study of seismic structure-soil-structure interaction problems for nuclear power plants.” Nuclear Engineering and Design, 73(3), 343–363.

Mccamy, K., Meyer, R.P., and Smith, T. J. (1962). “Generally applicable solutions of Zoeppritz’ amplitude equations.” Bulletin of the Seismological Society of America, 52(4), 923–955.

Mulliken, J. S., and Karabalis, D. L. (1998). “Discrete model for dynamic through-the-soil coupling of 3-D foundations and structures.” Earthquake Engineering and Structural Dynamics.

Murakami, H., and Luco, J. E. (1977). “Seismic Response of a Periodic Array of Structures.” ASCE J Eng Mech Div, 103(5), 965–977.

Ngo, V. L., Kim, J. M., and Lee, C. (2019). “Influence of structure-soil-structure interaction on foundation behavior for two adjacent structures: Geo-centrifuge experiment.” Geomechanics and Engineering, 19(5), 407–420.

Padrón, L. A., Aznárez, J. J., and Maeso, O. (2011). "3-D boundary element-finite element method for the dynamic analysis of piled buildings." Engineering Analysis with Boundary Elements, 35(3), 465–477.

Reese, C. D., and Eidson, J. V. (2006). Handbook of OSHA Construction Safety and Health. Handbook of OSHA Construction Safety and Health.

Roy, C., Bolourchi, S., and Eggers, D. (2015). "Significance of structure–soil–structure interaction for closely spaced structures." Nuclear Engineering and Design, 295(15), 680–687.

Seed, H. B., and Whitman, R. V. (1970). "Design of Earth Retainig Structures for Dynamic Loads." ASCE Specialty Conference on Lateral Stresses in the Ground and Design of Earth-Retaining Structures, Cornell Univ., Ithaca, New York, 103–147.

Stein, S., and Wysession, M. (2003). An Introduction to Seismology, Earthquakes, and Earth Structure. Seismological Research Letters, Blackwell Publishing Ltd., Malden, USA.

Vicencio, F., and Alexander, N. A. (2018). "Higher mode seismic structure-soil-structure interaction between adjacent building during earthquakes." Engineering Structures, 174, 322–337.

Vicencio, F., and Alexander, N. A. (2019). “Dynamic Structure-Soil-Structure Interaction in unsymmetrical plan buildings due to seismic excitation.” Soil Dynamics and Earthquake Engineering, 127, 105817.

W., T. N., H., B. M., C., H. T., D., Z. J., D., B. J., and L., K. B. (2015). “Nonlinear Soil–Foundation–Structure and Structure–Soil–Structure Interaction: Engineering Demands.” Journal of Structural Engineering, American Society of Civil Engineers, 141(7), 4014177.

Wair, B. R., Dejong, J. T., and Shantz, T. (2012). “Guidelines for Estimation of Shear Wave Velocity Profiles.” Pacific Earthquake Engineering.

Wang, H. feng, Lou, M. lin, Chen, X., and Zhai, Y. mei. (2013). “Structure-soil-structure interaction between underground structure and ground structure.” Soil Dynamics and Earthquake Engineering, 54, 31–38.

Warburton, G. B., Richardson, J. D., and Webster, J. J. (1971). “Forced vibrations of two masses on an elastic half space.” Journal of Applied Mechanics, Transactions ASME, 38(1), 148–156.

Whitman RV. (1969). “Current Status of Soil Dynamics.” Applied Mechanics Reviews, 22, 1–8.

Wolf, J. P. (1989). “Soil-structure-interaction analysis in time domain.” Nuclear Engineering and Design.

Wong, H. L., and Luco, J. E. (1986). “Dynamic interaction between rigid foundations in a layered half-space.” Soil Dynamics and Earthquake Engineering, 5(3), 149–158.

Zoeppritz, K. (1919). “Über Erdbebenwellen Part VII b . Über Reflexion und Durchgang seismischer Wellen durch Unstetigkeitsflächen.” Nachrichten von der Gesellschaft der Wissenschaften zu Göttingen, Mathematisch-Physikalische Klasse, 66–84.

3.11. TABLES

Table 3.1. Ratios of the transmitted and reflected amplitudes to the incident amplitude at the boundaries of a soil layer.

	f_{TV}, f_{TI}	f'_{TV}, f'_{TI}	$f_{RV}, \ f_{RI}, \ f_{RU}, f_{RL}$	$f'_{RV}, \ f'_{RI}, \ f'_{RU}, f'_{RL},$
SV-wave	A_T/A	B_T/A	A_R/A	B_R/A
P-wave	B_T/B	A_T/B	B_R/B	A_R/B

Table 3.2. Characteristics of the Layered Soil Profile

Layer #	1	2	3	Backfill 1	Backfill 2	Half-space
Layer Thickness h_f (m)	4	3	5	2.5	Variable	-
Density ρ (kg/m^3)	1500	1700	1900	1600	1600	2500
V_s (m/s)	200	250	350	220	220	600
Poisson's ratio ν	0.25	0.25	0.25	0.25	0.25	0.25

Table 3.3. Ratios of the final wave amplitudes transmitted to Structure 1 at $\theta = 34°$

Layer #	Wavepath	$L = 30\ m$			$L = 25\ m$			$L = 15\ m$		
		A_f/A_n (%)	B_f/A_n (%)	h_f (m)	A_f/A_n (%)	B_f/A_n (%)	h_f (m)	A_f/A_n (%)	B_f/A_n (%)	h_f (m)
Layer (1)	$P0$	$+0.044$	$+1.076$	2.650	-0.047	-1.170	3.480	$+0.666$	$+16.436$	0.595
	$P1$	$+0.106$	$+2.626$	1.070	$+0.106$	$+2.626$	2.850	N/A	N/A	N/A
	$SV0$	-6.479	-0.382	1.750	$+6.479$	$+0.382$	0.202	-6.479	-0.382	3.450
	$SV1$	-0.102	-0.014	1.315	$+1.428$	$+0.191$	1.920	N/A	N/A	N/A
Layer (2)	$P0$	-0.004	-0.086	1.576	$+0.020$	$+0.404$	0.203	-0.023	-0.467	2.237
	$P1$	-0.001	-0.012	2.930	-0.001	-0.012	1.150	$+0.003$	$+0.058$	2.409
	$SV0$	$+2.348$	$+0.147$	0.197	$+2.348$	$+0.147$	2.217	$+6.403$	$+0.400$	0.258
	$SV1$	-0.009	-0.002	1.805	$+0.005$	$+0.001$	1.438	$+0.028$	$+0.005$	1.923
Layer (3)	$P0$	$+0.719$	$+4.770$	1.037	$+0.719$	$+4.770$	2.896	-0.931	-6.175	3.036
	$P1$	-0.043	-0.287	0.858	$+0.185$	$+1.225$	0.394	$+0.185$	$+1.225$	4.866
	$SV0$	-8.529	-1.523	4.356	-8.529	-1.523	2.673	$+18.86$	$+3.367$	1.680
	$SV1$	$+0.030$	$+0.018$	4.642	-0.071	-0.043	2.421	$+0.669$	$+0.403$	4.733

Table 3.4. Ratios of the final wave amplitudes transmitted to Structure 1 at $\theta = 45°$

Layer #	Wave-path #	A_f/A_n (%)	B_f/A_n (%)	h_n (m)
Layer (1)	$SV0$	12.92	N/A	2.0
Layer (2)	$SV0$	14.10	N/A	1.5
Layer (3)	$SV0$	35.68	N/A	2.5

Table 3.5. Ratios of the final wave amplitudes transmitted to Structure 1 at $\theta = 53°$

Layer #	Wave-path #	$L = 30\ m$			$L = 25\ m$			$L = 15\ m$		
		A_f/A_n (%)	B_f/A_n (%)	h_f (m)	A_f/A_n (%)	B_f/A_n (%)	h_f (m)	A_f/A_n (%)	B_f/A_n (%)	h_f (m)
Layer (1)	$SV0$	$+15.30$	$+0.58$	3.20	-15.30	-0.58	3.37	-15.30	-0.58	0.50
Layer (2)	$SV0$	$+3.06$	$+0.13$	0.07	$+7.64$	$+0.33$	1.38	-7.64	-0.33	1.70
Layer (3)	$SV0$	$+21.42$	$+2.70$	4.07	-21.42	-2.70	4.50	-21.42	-2.70	1.63

3.12. FIGURES

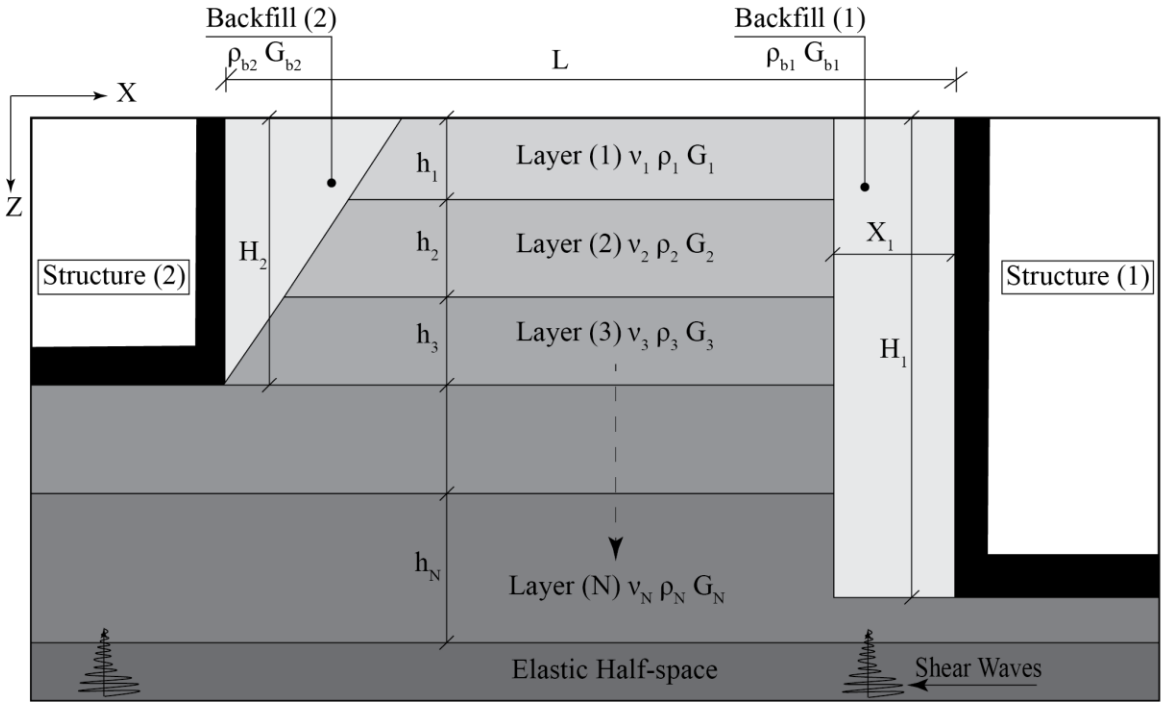

Figure 3.1. Schematic representation of two structure inserted into a layered site at different depths.

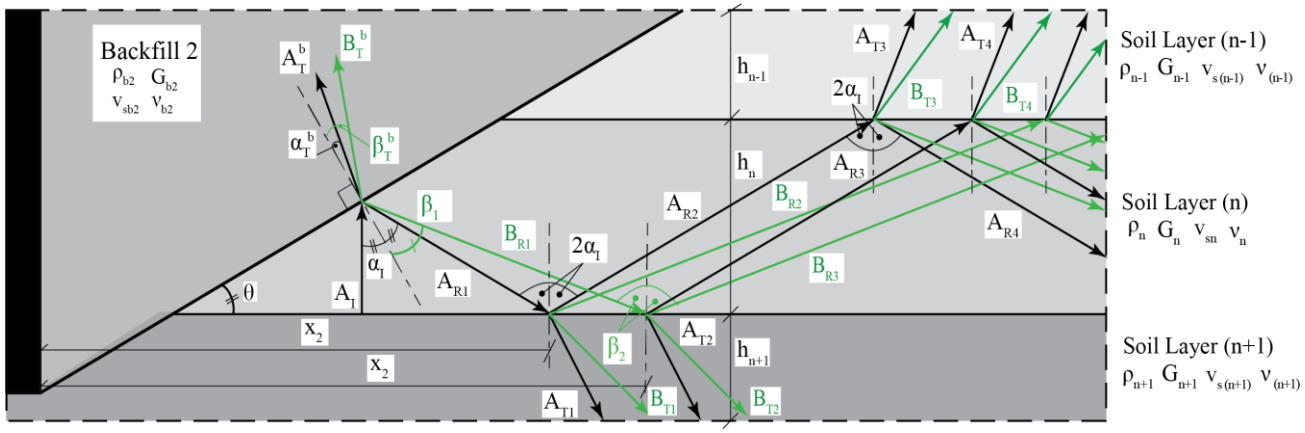

Figure 3.2. Geometry and wave interference of a vertically propagating SV-wave incident on the interface between a soil layer n and Backfill 2.

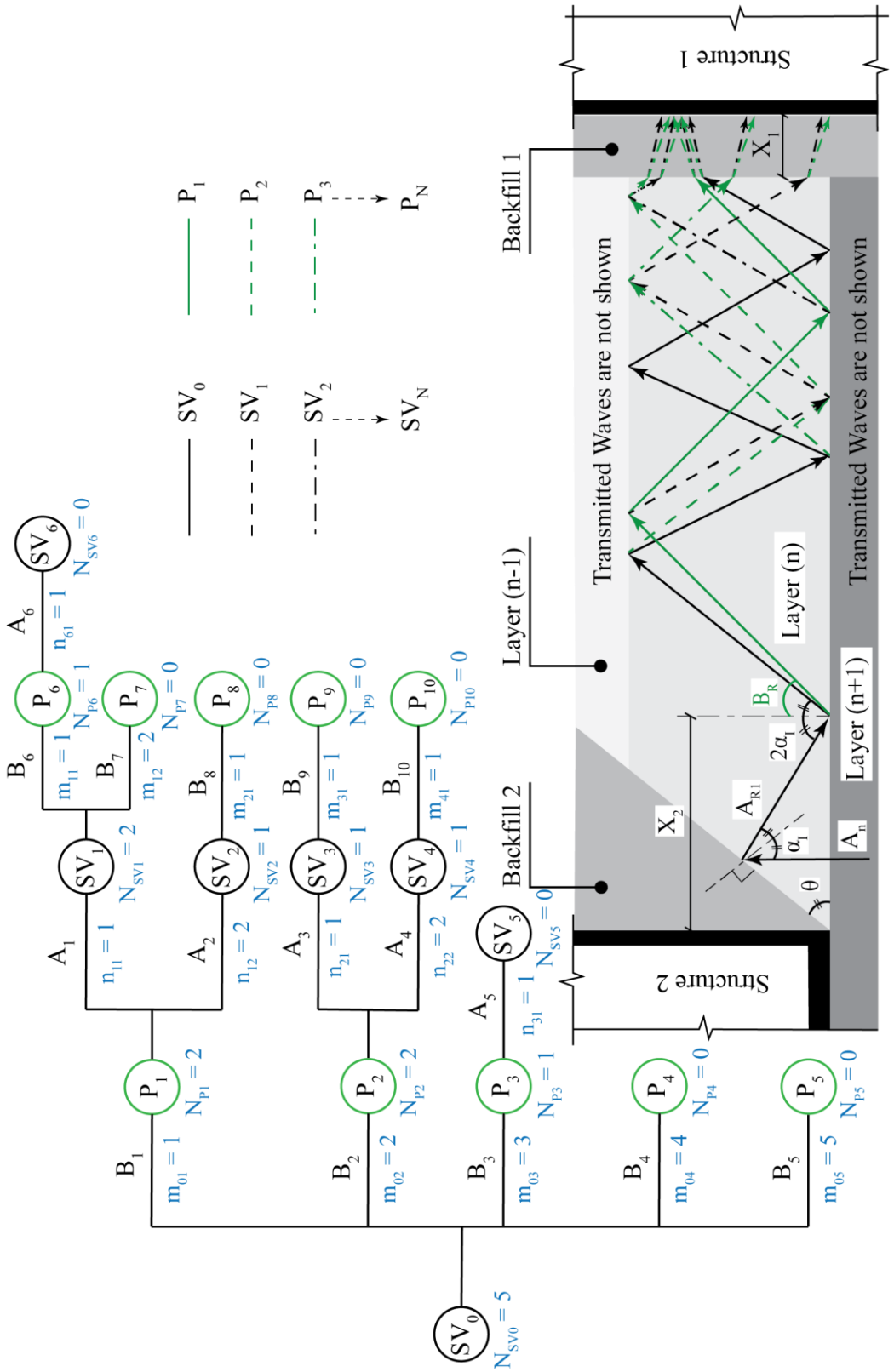

Figure 3.3. Interaction of Seismic Waves with the Layer boundaries and a Guided Flowchart

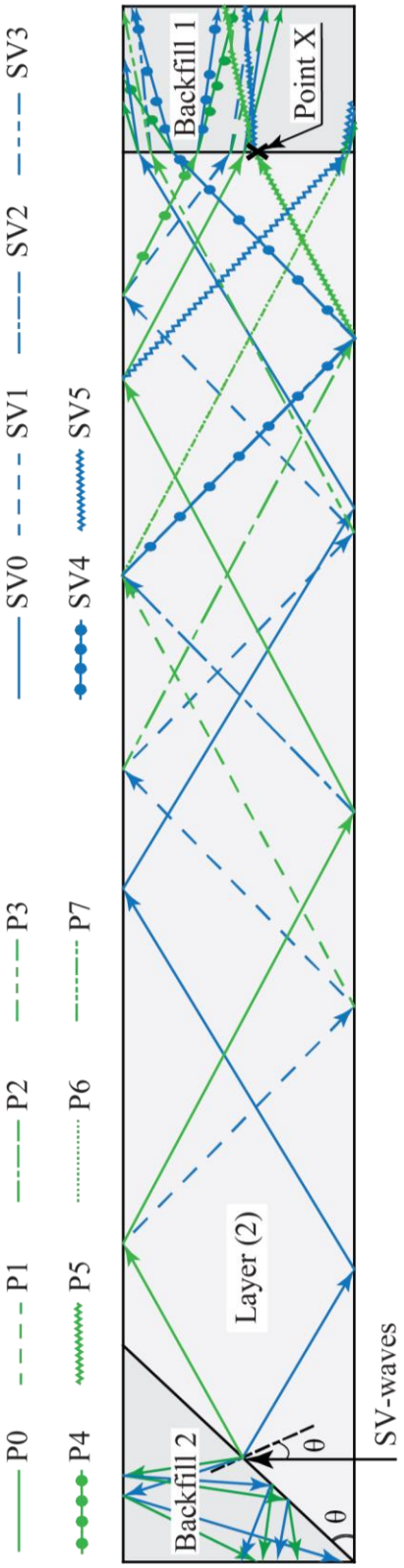

Figure 3.4. Interference of SV- and P-wavepaths in Layer 2 due to Vertical SV-waves impinge the boundary of Backfill 2, given $L = 30m$.

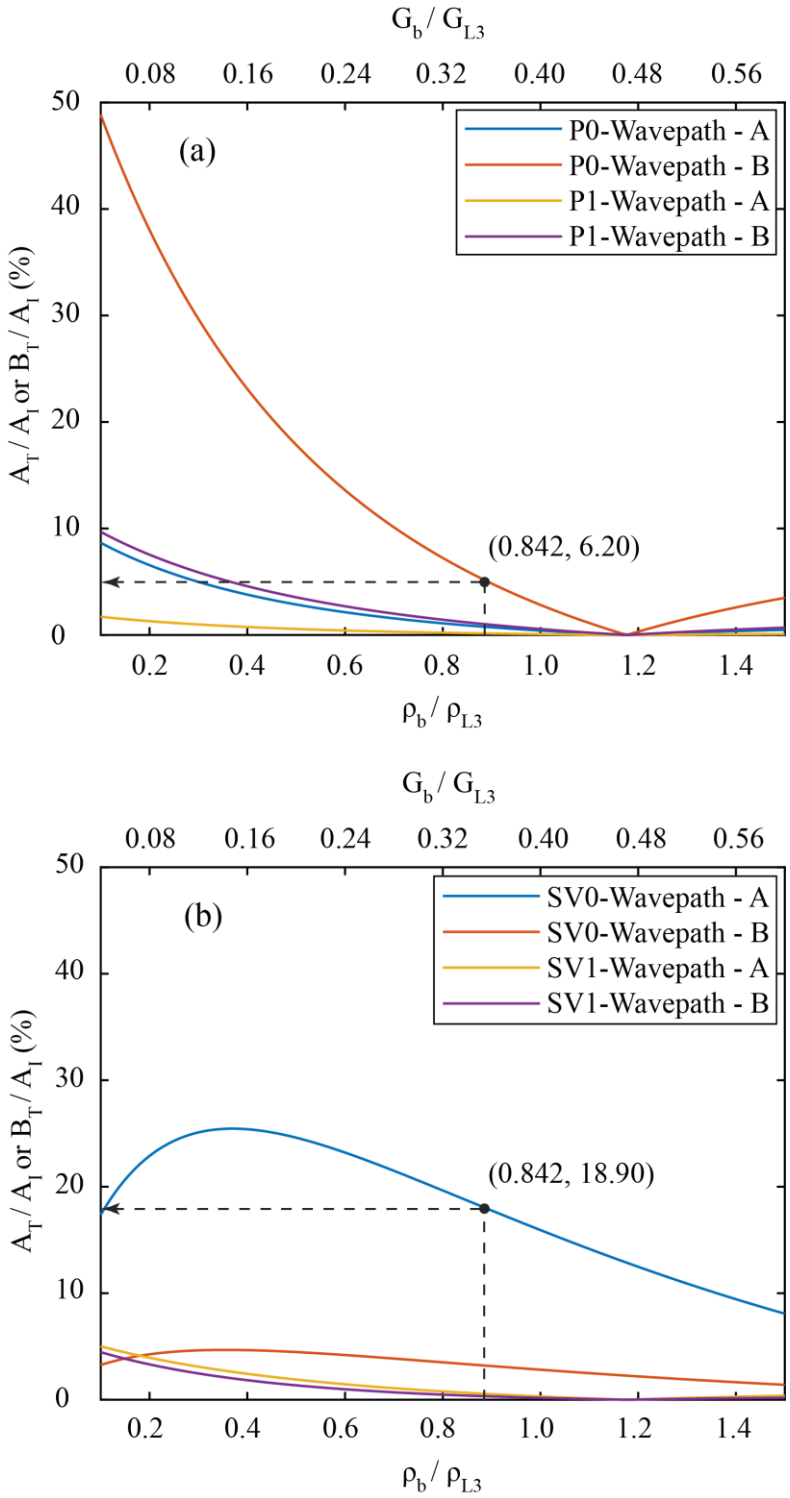

Figure 3.5. Variation of the final transmitted amplitudes due to different backfill densities: a) P-wavepaths; and b) SV-wavepaths.

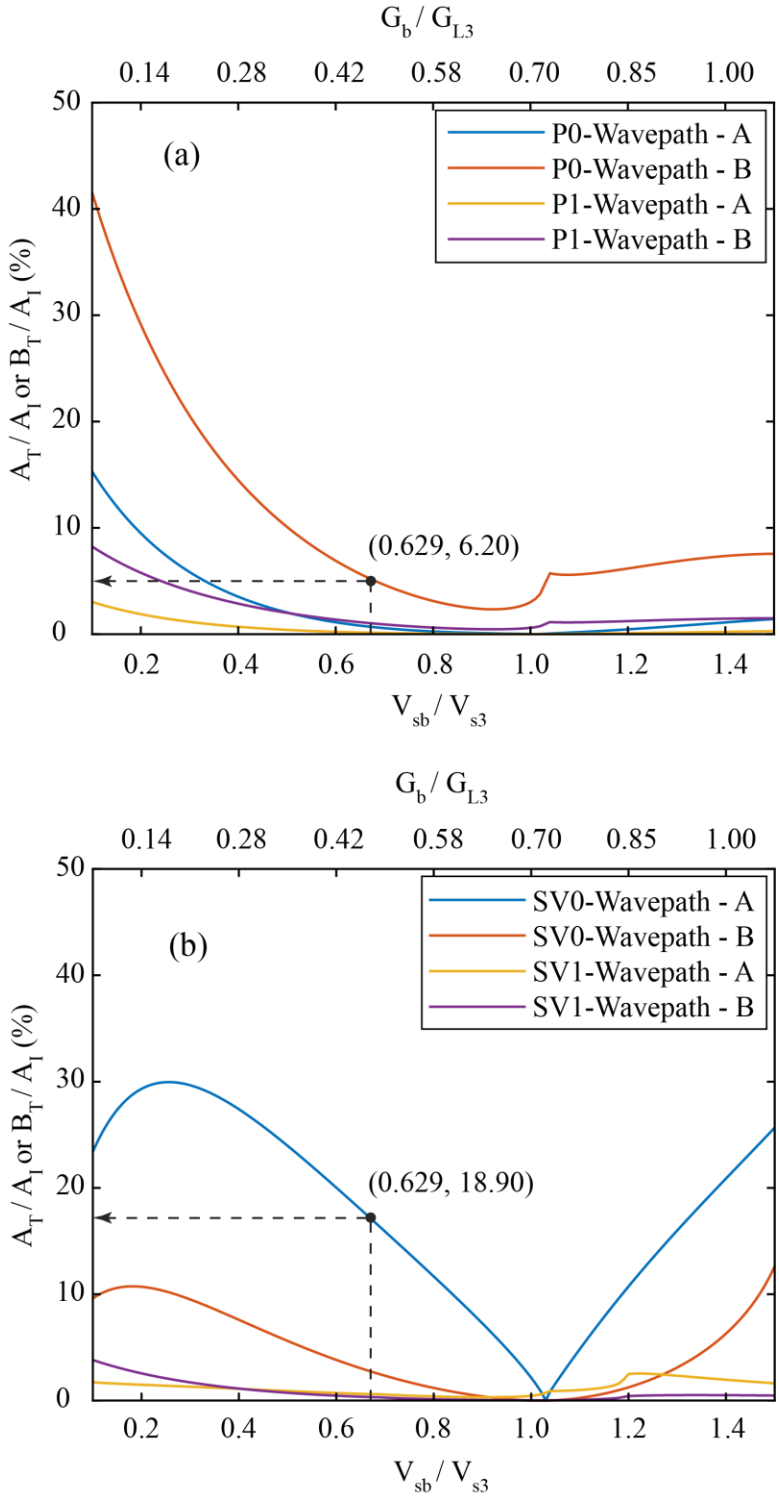

Figure 3.6. Variation of the final transmitted amplitudes due to different shear wave velocities of the backfill: a) P-wavepaths; and b) SV-wavepaths.

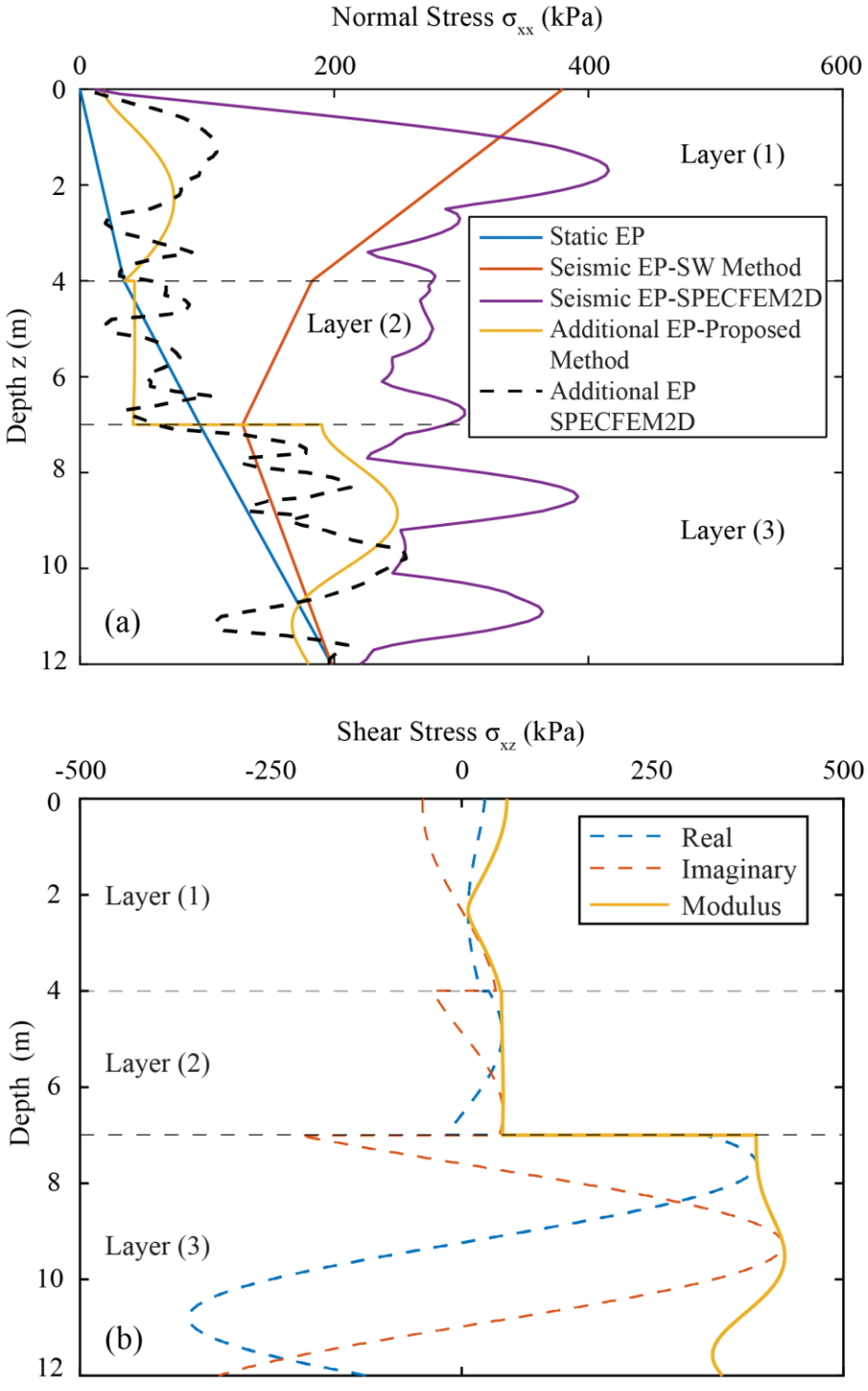

Figure 3.7. Additional seismic earth pressure on Structure 1 at $\theta = 34°$: a) Normal stresses; b) Shear stresses

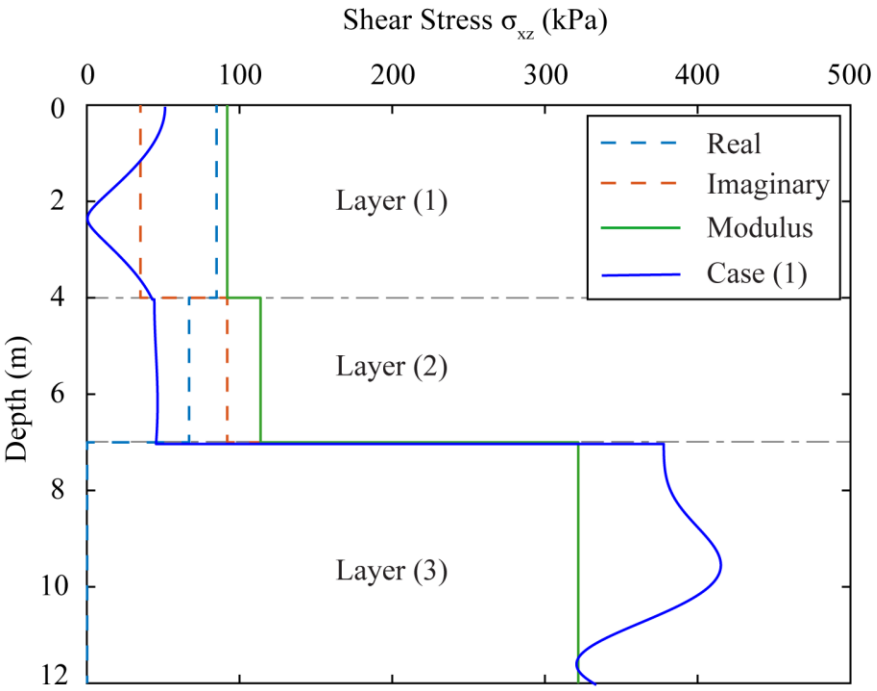

Figure 3.8. Additional shear stresses on Structure 1 at $\theta = 45°$

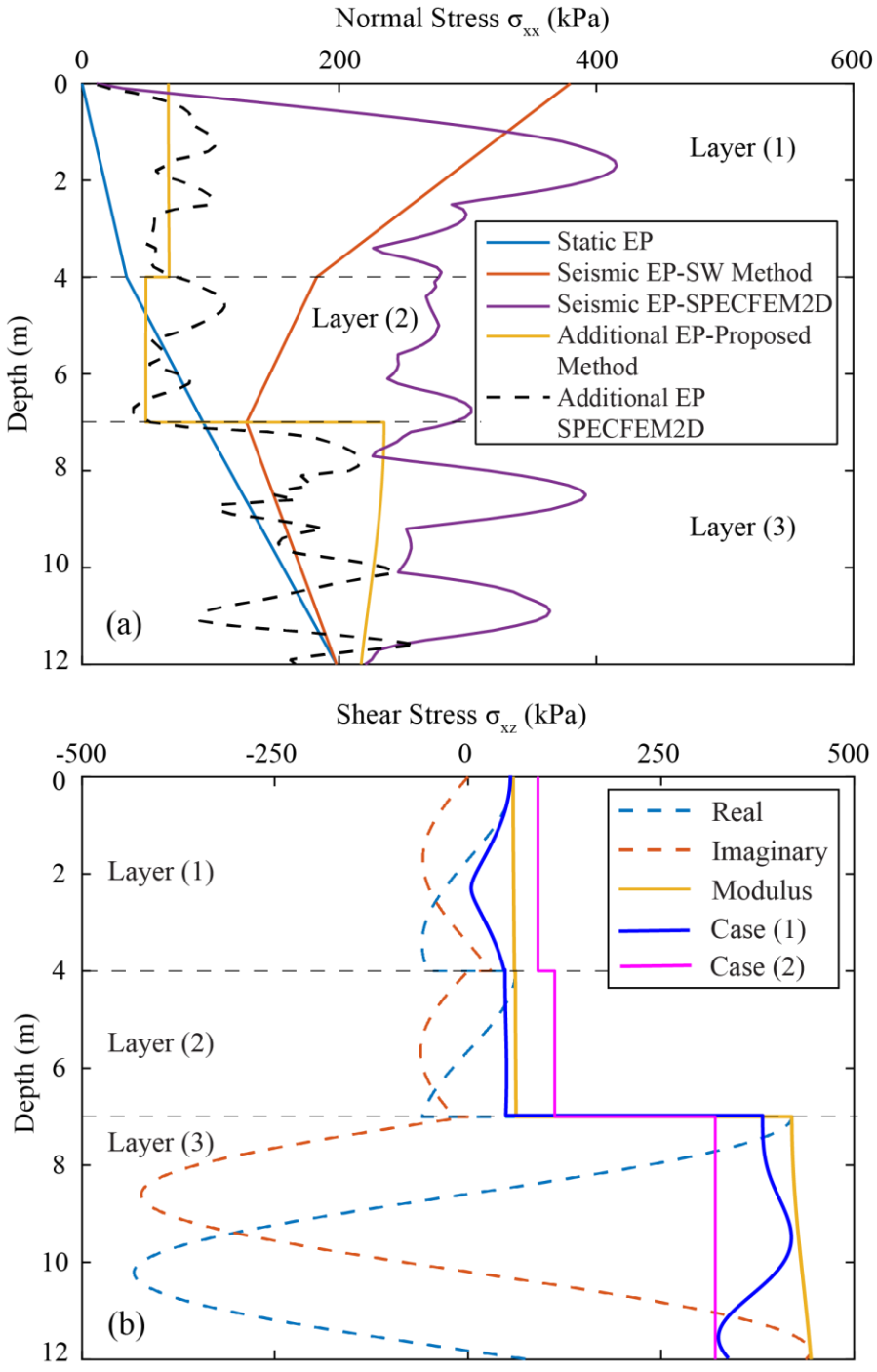

Figure 3.9. Additional seismic earth pressure on Structure 1 at $\theta = 53°$: a) Normal stresses; b) Shear stresses

Chapter 4

SEISMIC INTERACTION BETWEEN DEEPLY EMBEDDED SUBSTRUCTURES AND NEARBY PIPELINES

4.1. ABSTRACT

In the nuclear industry, buried pipelines are usually built to connect structures in proximity. This paper investigates the seismic interaction between substructures and buried pipelines, with the focuses on the seismic earth pressure on the substructures and the pipeline. Two-dimensional numerical simulations were performed using the spectral element method. Three pipeline configurations were analyzed by considering the influences of the clear distance between the substructures, excitation frequency, and material damping.

The results revealed that both the structures and the pipeline experienced cycles of amplified and/or reduced seismic forces within the specified range of interest for each parameter. The seismic pipeline-substructure interaction was negligible when the distance between substructures was relatively large, or the soil profile had high energy absorption capabilities. The variations of earth pressure on the substructures were apparent in the soil close to the pipeline and gradually vanished with an increase in the distance from the pipeline. The seismic stresses on the pipeline perimeter and the resulting deformations were both asymmetric. The seismic earth pressure response spectra indicate that the seismic interaction has a

significant influence on the pipeline, while it has a marginal effect on the substructures when the buildings are relatively far from each other.

Author keywords: Seismic lateral earth pressure; Shear waves; Primary Waves; Wave propagation; Structure-soil-structure interaction.

4.2. INTRODUCTION

In major facilities such as conventional Nuclear Power Plants (NPPs), the potential hazard related to seismic events must be properly mitigated due to the serious consequences. The infrastructure of such facilities, including substructures and pipelines, is the first line of defence against any disaster related to earthquakes. In some situations, pipelines may pass between two or more adjacent structures of different substructure depths, leading to two major concerns in a seismic event. The first is related to the additional forces on the substructures due to the seismic structure-soil-structure interaction (SSSI) and the interaction between the substructures and the pipelines. The second concern is associated with the integrity of the non-structural element (i.e., the pipeline) during and after the earthquake. It is important in NPPs that the major non-structural components required for the operation sequence of the plant maintain its functionality during seismic events in order to keep the plant in a stable condition.

For seismic analysis of most structures, the primary focus is usually placed on vertically propagating shear waves (i.e., S-waves), where the polarization of particle displacements is in the horizontal direction. As a result, the energy of the

seismic waves is fully transferred to the substructures as horizontal stresses, assuming a horizontally stratified soil profile and vertical structures. When designing buried pipelines, however, the primary waves (i.e., P-waves) are more important since they apply direct stresses to the pipeline, leading to non-uniform deformations around the perimeter of the pipeline.

Over the past decades, seismic SSSI and the damage to buried pipelines due to seismic waves have been viewed as separate problems without proper consideration of substructure- pipeline interaction. Pipeline damage induced by an earthquake has been extensively investigated in the Oil and Gas industry. Analytical and numerical models based on various assumptions have been developed to estimate pipeline damage due to wave propagation (Datta et al. 1984; Kouretzis et al. 2006; Newmark and Hall 1975; Takada and Tanabe 1987; Trifonov and Cherniy 2010). In addition, empirical relationships based on experimental and in-situ observations have been proposed, usually as functions of ground motion parameters such as peak ground acceleration (Katayama et al. 1975) and peak ground velocity (O'Rourke and Ayala 1993).

As for SSSI, the pioneering work by Whitman (1969) raised concerns about the dynamic coupling of foundations through the surrounding soil. Due to the complexity of the SSSI problem, analytical solutions are available only for simple cases of shallow foundations on the surface of homogeneous half-space (Warburton et al. 1971; Triantafyllidis and Prange 1988; Rodríguez-Castellanos et al. 2010). Semi-analytical methods allowed the use of different excitation types (Lee and

Wesley 1973), lumped-element models (Wolf 1994), and time-lagging effect due to wave propagation (Mulliken and Karabalis 1995). Various numerical methods, including the Finite Element Method and Boundary Element Method, have been proposed. These methods can address the effect of various parameters, including but not limited to radiation damping, material damping, and frequency effect (Lin et al. 1987; Karabalis and Mohammadi 1998; Padrón et al. 2011).

Analytical methods have been developed in the framework of elasticity to solve wave propagation problems in elastic/viscoelastic media. The most common methods are the three-dimensional wave equation (Kramer 1996), ray theory (Julian and Gubbins 1977), and the integral equation method (Rizzo et al. 1985). Closed-form solutions of these methods are available only at some specific conditions under which the stresses and strains can be determined explicitly. For most practical problems such as pipeline passing between two adjacent buildings, these methods can be applied via integration with various numerical techniques, such as the Finite Difference Method (FDM), Finite Element Method (FEM), Pseudo-Spectral Method (PSM), and Spectral-Element Method (SEM).

Motivated by the above literature review, this paper attempts to investigate the seismic interaction between two deeply buried structures and pipelines passing in between. As seismic waves approach the site, a series of reflections/refractions occur between the substructures and the pipeline, leading to amplified seismic stresses. The focus is placed on the change in the seismic earth pressure on the structural elements (i.e., substructures) caused by the pipeline (i.e., non-structural

element), which may adversely affect the seismic margin of the original design. The integrity of the non-structural element is also examined by taking into account its interaction with nearby substructures.

The seismic substructures- pipeline interaction is affected by the geometrical characteristics of the pipeline and the substructures, as well as the mechanical properties of ground soil and the pipeline. However, the scope of this study focuses only on the effect of the distance between substructures, excitation frequency, and material damping. The spectral-element method is employed due to its high capabilities in solving wave equations in the time domain and combining the advantages of the FEM and PSM in terms of flexibility and accuracy, respectively.

4.3. A BRIEF INTRODUCTION OF SEM AND SPECFEM2D

4.3.1. SPECTRAL ELEMENT METHOD (SEM)

The equation of motion that governs seismic wave propagation can generally be expressed in strong or weak forms, depending on the solution technique. For a homogeneous isotropic linear elastic medium, the strong form of the equation of motion is expressed as (Stein and Wysession 2003):

$$\rho \frac{\partial^2 \mathrm{u}}{\partial t^2} - (\lambda + \mu)\nabla(\nabla \cdot \mathrm{u}) - \mu \nabla^2 \mathrm{u} = \mathrm{F} \qquad (1)$$

where ρ is the mass density of the medium, u is the displacement vector $u = (u_x,\ u_y,\ u_z)$, ∇^2 is Laplace operator, λ and μ are Lamé constants of the material, and F is the body force of the seismic source. However, once the seismic waves

propagate away from the source, the value of F is neglected, and the equation of motion depends only on the stress-displacement relationship (Stein and Wysession 2003). A typical example of an analytical method that solves the strong form of the equation of motion is the Pseudo-Spectral Method. In the weak formulation, the integral form of the equation of motion is used to solve the wave propagation problem. By introducing an arbitrary test function w and then integrating by parts over a domain of volume V of the medium (Komatitsch and Tromp 1999), the weak form expression of Equation (1) can be written as:

$$\int_V \rho w \cdot \ddot{\mathrm{u}}\, d^3\mathrm{u} + \int_V \big((\lambda+\mu)\nabla(\nabla\cdot\mathrm{u}) - \mu\nabla^2\mathrm{u}\big)\mathrm{w}\, d^3\mathrm{u} = \int_V \mathrm{F}\cdot\mathrm{w}\, d^3\mathrm{u} + \int_\Gamma (T\cdot\hat{n})\cdot\mathrm{w}\, d^2\mathrm{u} \tag{2a}$$

where Γ is the absorbing boundaries of the domain, T is the stress tensor, and $\hat{n}$ represents the outward unit vector normal to all boundaries. Equation (2a) is the basis of the finite element method, including the spectral element method. Two observations can be made regarding Equation (2a). Firstly, the last term vanishes at the free surface on which $T\cdot\hat{n}=0$. Secondly, the third term disappears since $\mathrm{F}=0$ at any point away from the seismic source. As a result, Equation (2a) is simplified to the typical equation of motion of plane waves:

$$\int_V \rho w \cdot \ddot{\mathrm{u}}\, d^3\mathrm{u} + \int_V \big((\lambda+\mu)\nabla(\nabla\cdot\mathrm{u}) - \mu\nabla^2\mathrm{u}\big)\mathrm{w}\, d^3\mathrm{u} = \mathbf{0} \tag{2b}$$

In the spectral element method (SEM), the model volume V and the absorbing boundaries Γ are divided into smaller non-overlapping volumes V_e and surface elements Γ_b. Unlike the FEM, the SEM employs only hexahedral elements and quadrilateral surface elements to model the subdivided volumes and absorbing boundaries, respectively. Volume elements and boundary elements are then mapped to a reference square and cube by a series of control nodes and shape functions. Special care must be taken as the Jacobian of the transformation should never vanish for both volume and boundary elements.

The shape functions are typically defined using low-order Lagrange polynomials, and the control points are represented by Gauss-Lobatto-Legendre points. The wavefield is then discretized by means of high-order Lagrange interpolating polynomials and integrated over the surface elements Γ_b and volume elements V_e using Gauss-Lobatto-Legendre integration rules. The benefit of such discretization and integration process is the diagonal global mass matrix of the analytical model, which definitely reduces analysis time. Overall, the SEM has proven that it combines the accuracy of the PSD and the flexibility of the FEM. More details about the shape functions and the mathematical relationship between the hexahedral/quadrilateral elements and the reference cube/square elements can be found in Komatitsch and Tromp (1999).

4.3.2. SPECFEM2D SOFTWARE

SPECFEM2D is an open-source software suite for spectral element analysis and computer-aided engineering modelling. It specializes in seismic analysis and waves propagation modelling at various scales. It allows the use of advanced discretization and integration techniques (i.e., Lagrange Polynomials and GLL points), leading to faster convergence and higher accuracy. SPECFEM2D possesses several capabilities that set it apart from other software packages. Among these capabilities are precisely handling distorted mesh elements, automatically satisfying free surface boundary conditions, generating diagonal mass matrices, and calculating sensitivity kernels based on adjoint modelling. Furthermore, different absorbing boundaries are implemented to account for radiation damping and eliminate any spurious wave reflections, such as convolution Perfectly Matched Layer (PML), Stacey boundaries, and periodic boundaries. Moreover, SPECFEM2D has the ability to simulate multiple sources of a seismic event in the same medium.

The spectral element method and SPECFEM2D software have been well validated against analytical solutions of two-dimensional wave propagation problems such as Lamb's problem, Garvin's problem (Komatitsch and Vilotte 1998), and the two-layered elastic model (Peter et al. 2011).

4.4. MODEL DESCRIPTION

4.4.1. GEOMETRICAL PROPERTIES

In this study, we investigate the SSSI of two substructures of different burial depths with a pipeline passing in between. All the elements are buried in a layered ground, as shown in Figure 4.1. The burial depths of the two substructures are $H_1 = 30$ m and $H_2 = 15\ m$, respectively. The soil profile consists of four horizontally stratified layers of homogeneous isotropic materials laid above an elastic half-space, with a total thickness of $100\ m$. The pipeline diameter D_p is $3\ m$, while the thickness and material properties of each soil layer are listed in Table 4.1.

Since both P- and S-waves are essential in the current analysis, a moment tensor that can generate both types of waves is placed at the base of the model, where the assigned magnitude is $M_w = 100\ kN.m$. Other characteristics, including the distance L between the substructures, soil damping ζ, and excitation frequency f , are assigned to various values in the simulation. The two-dimensional analysis approach is employed in this paper since the primary focus is placed on seismic earth pressure on the substructures. However, the three-dimensional analysis would be required for a complete evaluation of the pipeline integrity as joints between pipeline segments are the weakest point in a pipeline system.

4.4.2. DISCRETIZATION

The domain to be analyzed (as shown in Figure 4.1) is discretized by a family of mesh generated using the Gmsh package (Geuzaine and Remacle 2009). The mesh was generated by Delaunay 2D algorithm using four-noded quad elements, and all elements produced a positive Jacobian ratio. In particular, the domain was discretized to $10\,165$ spectral elements, with the maximum and minimum grid sizes of $1.56\,m$ and $0.21\,m$, respectively. Regarding the GLL points, the minimum distance between the points was $0.036\,m$, with an average of $0.052\,m$. Given the wave velocities of different soil layers in Table 4.1 and the mesh size, the maximum frequency that could be resolved was $106.8\,Hz$. Figure 4.2 shows the variation of two parameters characterizing the features of the discretized mesh for the material properties given in Table 4.1.

The Newmark time-stepping scheme was utilized in the analysis. To meet the CFL stability conditions using the GLL basis function, a time step of $2x10^{-5}$ seconds was specified for a total of $50\,000$ steps. The previously described analytical parameters produced a CFL condition of 0.4832, which achieved the CFL limits stipulated in De Basabe and Sen (2010) and the SPECFEM2D manual (Komatitsch and Tromp 2014).

In general, the attenuation of seismic waves is induced by two mechanisms: geometrical damping (radiation damping) and material damping. As a mechanical property of a material, the material damping can be described by a constitutive

model. Radiation damping occurs as a result of the spread of seismic waves over an unbounded soil medium which reduces the intensity of seismic energy even though there is no energy dissipation. For a bounded medium such as the model illustrated in Fig. 1, artificial absorbing boundaries were used on the left, bottom, and right edges of the model. Several techniques have been developed to eliminate spurious wave reflections at the artificial boundaries, such as Stacey boundary conditions (Stacey 1988). Nevertheless, Perfectly Matched Layer (PML) absorbing boundaries were used in the current analysis due to their high absorption efficiency for all types of seismic waves regardless of frequency or angle of incidence.

In SPECFEM2D, receivers (i.e., point for output of numerical simulation) should be defined at desired locations in order to record the analysis output. Therefore, receivers were placed every $100\,mm$ along the depth of each of the substructures and every 2.5 degrees along the perimeter of the pipeline, as shown in Figure 1.

4.5. FINDINGS AND DISCUSSION

As pointed out previously, this study investigated the effect of three parameters on the seismic substructure-pipeline interaction. These parameters are the clear distance L between the substructures, material damping ζ, and excitation frequency f. In particular, the clear distance between substructures varied from $20\,m$ to $60\,m$. The pipelines with three configurations (single, dual and triple) were located at the midway between the two substructures, as illustrated in Figure 4.3.

The seismic earth pressure was measured along the pipeline perimeter and the depth of substructures 1 and 2. The material damping was assumed at four levels with ζ=0 (elastic), 0.5%, 2%, and 5%, respectively. Low to high excitation frequencies were considered by investigating three excitation frequencies of $f = 10\,Hz,\ 25\,Hz,$ and $50\,Hz$. For simplicity, the terms S1 and S2 will be used to denote substructures 1 and 2, respectively, in the rest of the paper.

4.5.1. STRUCTURE-SOIL-STRUCTURE INTERACTION (SSSI)

Before proceeding with the effect of each parameter, the seismic SSSI and the substructure- pipeline interaction was evaluated at $L = 60\,m.$, which was chosen as a reference case. Figure 4.4 shows the seismic lateral earth pressures on S1 and S2 at $t = 0.20\,sec$. Cases (1) represents the soil-structure system illustrated in Figure 4.1, but the pipeline is removed from the model in case (2). The soil-structure system in Case (3) involves only S1 or S2 buried in the layered ground. Figure 4.4 presents the earth pressure distribution on the substructure for the three cases at t=0.2 sec. It is observed that neglecting the seismic SSSI (Case 3) tends to significantly underestimate the seismic demand of both substructures. Comparing with the results for a single structure in Case (2), the existence of the pipeline or the other substructure not only amplified the earth pressure but also altered the earth pressure distribution with shifted peaks. This was attributed to the series of wave reflections/refractions between the substructures and the pipeline through the soil. When examining the results of Case (1) and Case (2), one observes that the pipeline

does not seem to cause a remarkable variation in the earth pressure distribution. The influence of the pipeline on the seismic earth pressure will be further discussed in the upcoming sections.

It should be noted that Figure 4.4 only showed the earth pressure distribution at a specific time of excitation ($t = 0.2\ sec$) for easy reading. To elaborate the variation of earth pressure with time, Figure 4.5 presents the data from receivers 51 and 201, both at a depth of $10\ m$ from the ground surface, on S1 and S2 respectively. The time histories of the seismic pressures at Receiver 51 presented in Figure 4.5(a) show two distinct aspects regarding the effect of SSSI and pipeline. The first is associated with the amplified peaks starting from the excitation onset down to $0.3\ sec$. The second one is another peak earth pressure that appears at longer durations (i.e., $> 0.3\ sec$). Since the earth pressure on the single substructure in Case (3) vanished after $t = 0.3\ sec$, we conclude that the second peak of earth pressure in Cases (1) and (2) was caused by the wave reflections/refractions between the substructures.

The earth pressure amplitude on S2 is higher than that on S1, specifically up to $t = 0.2\ sec$. This can be attributed to the different burial depths of the two substructures. Due to the shallow depth of S2, it is anticipated that part of the seismic waves will be firstly incident upon S1, which causes reflected wave propagating towards S2. Therefore, the total forces on S2 consist of seismic waves propagating directly from the seismic source and seismic waves reflected from S1.

The increased seismic earth pressure at S1 is attributed to the reflected wave from S2.

4.5.2. SEISMIC INTERACTION WITH A SINGLE PIPELINE

4.5.2.1 Seismic Earth Pressure Distribution

Since the seismic earth pressure at the location of each "receiver" was recorded, similar to that presented in Figure 4.5, we can examine the distinction of instantaneous maximum seismic earth pressure with the effect of the seismic interaction between the substructures and the pipeline. Figure 4.6 plotted the instantaneous maximum earth pressures on S1 at all receivers corresponding to different distance L between the substructures, the damping ratio ζ, and the excitation frequency f. For the sake of clarity, the maximum earth pressure is plotted up to a depth of $15\ m$ from the ground surface. Different from the earth pressure distribution presented in Figure 4.6, the instantaneous maximum earth pressures at different depths in Figure 4.6 did not appear at the same time.

In general, with the variation of the three factors examined, the impact of the pipeline on the earth pressure was neither consistent nor uniform across the depth of the substructure. The presence of the pipeline may amplify the earth pressure or appear as normal seismic isolation resulting in reduced forces on the infrastructure. At large depths, the pipeline had a negligible effect on the amplitudes of earth pressure. On the other hand, discrepancies were observed at shallow depths (typically $< 10\ m$) where the pipeline was located. For all cases, the impact of the

pipeline is clearly visible at smaller distances L between the substructures but decays as the distance increases. The reason behind this is the soil damping as well as the interaction between the seismic waves reflected from the pipeline with the upper and lower soil layers before impinging the substructures. The waves are more likely to undergo several interactions at longer distances, leading to a successive decrease in the amplitude due to geometrical and material damping.

The instantaneous maximum earth pressure distribution in Figure 4.6 also shows the influence of material damping. For a selected excitation frequency, noticeable differences were observed between the earth pressure with and without a pipeline for elastic soil (e.g., Figure 6a, d, g). As the material damping increases to $\zeta = 5\%$, the difference almost vanished; as shown in Figure 4.6(c, f, i). In other words, the effect of the pipeline can be neglected if the soil layers have high energy absorption capabilities and the distance between the substructures is relatively large. Otherwise, the seismic interaction with the pipeline should be considered when determining the seismic earth pressure on the substructures, especially at depths near the pipeline. Regarding the excitation frequency, the variation of the earth pressure with depth was generally jagged at high frequencies but approached smooth curves at low frequencies. The discrepancies are high at low excitation frequency with $L < 60\ m$, but they vanish at high excitation frequency in soil of higher damping ratio.

Since any change in the seismic earth pressure distribution on the substructures inevitably affects the forces on the pipeline, the seismic earth pressure

distribution on the pipeline was also extracted, and the results were plotted in Figure 4.7. The values in Figure 4.7 represent the time history of the maximum of the earth pressure at each receiver along the pipeline perimeter. In addition, a reference case of a pipeline buried in a free-filed was analyzed and included in Figure 4.7 (i.e., PL Only).

Figure 4.7 generally indicates that neglecting the seismic interaction between the substructures and the pipeline tends to underestimate the seismic earth pressures on the pipeline, especially when the soil damping is low. The impact of such seismic interaction was practically negligible when a pipeline in soil of high damping ratio subjected to high frequency excitation, as shown in Figure 4.7(i). Furthermore, the seismic earth pressure on the pipeline was asymmetric, which caused asymmetric deformations. The asymmetric stress distribution was closely related to the phase shift of the seismic waves reflected from S1 and S2 in the vicinity of the pipeline. The upper half of the pipeline is more likely to experience higher stresses than the lower half. This difference is associated with the seismic waves that were reflected from the free ground surface and incident upon the pipeline, leading to amplified earth pressure on the upper half of the pipeline.

The influence of the distance L between the substructures on the instantaneous earth pressure distribution on the pipeline was also examined. No consistent results were obtained for the five inter-substructure distances investigated. For instance, in Figure 4.7(d), the maximum seismic earth pressure on the pipeline at $L = 30\,m$ was observed at the top of the pipeline, while the

maximum occurred at an angle of 45° when $L = 40\,m$. The dependence of the stress distribution shown in Figure 4.7 on the distance L was not monotonic, but it depends on the seismic wave propagation along the distance between the pipeline and the substructure. A slight change in the distance L can affect the number of reflections that seismic waves undergo at the upper and lower boundaries of a soil layer, thus affecting the amplitude of earth pressure acting on the pipeline. The results indicate that the seismic design of pipelines without accounting for the interaction with the surrounding structural elements may not be reliable and may lead to unfavourable results as a seismic event usually contains all the frequency components.

It should be noted that the instantaneous maximum earth pressure at different points did not appear at the same time, which is similar to the instantaneous maximum seismic earth pressure on the substructure presented in Figure 4.6. This is why the rose diagrams in Figure 7 have many spikes that appeared at different times and corresponded to different reflected waves from different objects (e.g., S1, S2 or the ground surface).

4.5.2.2 Seismic Earth Pressure Response Spectrum

In order to obtain deep insights into the seismic interaction between the pipeline and substructures, we next analyze the spectra of seismic earth pressure responses on the substructures and the pipeline. Figure 4.8 presents the envelope response spectra developed for S1 for the earth pressure within soil layers (1) and (2), with and without a pipeline, for different soil damping ratios when $L = 20\,m$ and $40\,m$,

respectively. The effect of the single pipeline is negligible in the low-frequency range (typically < 9 Hz). However, the presence of the pipeline tends to amplify the earth pressure on S2 when $f > 9$Hz. With an increase of the distance L between S1 and S2 and damping ratio of the soil layer, the amplification factor decreases. This is also observed for the earth pressure in layer (2) where the pipeline does not cause any additional pressure on the substructure at $L = 40\,m$ (see Figure 4.8b), comparing with that when $L = 20\,m$ (see Figure 4.8a). Given the natural frequency of the substructure, the seismic earth pressure in the presence of the pipeline can be determined conservatively from the response spectra given in Figure 4.8. Furthermore, the difference between the response spectra with and without a pipeline could be of great importance in the marginal seismic assessment of the substructures.

The response spectra of the earth pressure on the pipeline were also generated using the data at receivers distributed along the perimeter of the pipeline. Figure 4.9 shows the envelope response spectra for the pipeline at different damping ratios and distances between the substructures. It is clearly shown that neglecting the interaction with neighbouring substructures significantly underestimated the seismic earth pressure for the pipeline in soil layers of low damping ratios and short distance L. However, this effect decreased with an increase in the damping ratio of soil or the distance L between the substructures or both. Consequently, designing the pipeline without considering its seismic interaction with the nearby structural

elements using free-field ground responses underestimates the stress on the pipeline.

4.5.3. SEISMIC INTERACTION WITH DUAL AND TRIPLE PIPELINE CONFIGURATIONS

Various pipeline configurations can be found in engineering practice other than the single pipeline shown in Figure 4.1. Figure 4.3 shows two additional configurations that can alter the wave propagation pattern between the substructures, and thus influence of the seismic earth pressure distribution and total forces on both the substructure and the pipeline. Configurations (2) and (3) have been incorporated in the numerical model described earlier and compared with the reference configuration (1), as will be discussed in the following sections. The pipelines act as a barrier preventing the seismic energy from instantly propagating between the substructures. Instead, part of the seismic energy is absorbed by the pipelines and the remainder is reflected towards the substructure. However, the pipelines of Configurations (2) and (3) in Figure 4.3 did not experience the same seismic earth pressure or the earth pressure distribution.

4.5.3.1 Seismic Earth Pressure Distribution

The distribution of the instantaneous maximum seismic earth pressure on S1 was obtained for different damping ratios, excitation frequencies, and distance *L*, considering the pipeline configurations depicted in Figure 4.3. Figure 4.10 and Figure 4.11 show the instantaneous maximum earth pressure distribution on S1 up

to the depth of $15\,m$ at $L = 20\,m$ and $40\,m$, respectively. Differences observed between the three configurations are prominent in the elastic case (ζ=0); however, the differences practically vanished at ζ= 5%. The dual and triple pipeline configurations tend to amplify the earth pressure at a higher rate than the single pipeline. Comparing with the case without pipelines, the highest differences appeared in soil layers (1) and (2) in the elastic case, where pipelines amplify the seismic earth pressure. Otherwise, the seismic interaction between substructures can be evaluated without considering any pipeline in the analysis, regardless of the pipeline configuration. However, the integrity of the pipelines may be compromised since they absorb part of the seismic energy reflected from both substructures.

Figure 4.12 and Figure 4.13 show the instantaneous maximum earth pressure distribution on the pipeline perimeter corresponding to the different pipeline configurations described in Figure 4.3. It is observed that the pipelines near the ground surface (i.e., P3 and P6) generally had the lowest earth pressure compared to the other pipelines located in layer (2). This can be traced back to the location of P3 and P6, which are bounded by the free surface at the top and P2, and P4&P5, respectively, at the bottom. Most of the seismic energy propagating upward is absorbed by P2, P4, and P5, and the remainder travelled towards P3 and P6. The earth pressure distributions on P1 and P2 were almost identical for most cases except when soils are elastic. Discrepancies appeared at some local peak earth pressures in the upper half of P2 due to the presence of P3, which prevented the

waves reflected at the free surface from reaching P2 directly. Regardless of the distance L, pipelines P1, P2, P4, and P5 experienced similar earth pressure distributions, especially at high excitation frequencies and when the soils had high damping ratios. It is also observed that the earth pressure on P5, which is next to S1, increased at a higher rate than the other pipelines as the damping ratio and excitation frequency increased. This is obvious in Figure 4.12(f) and Figure 4.13(f), where P5 enclosed the other pipelines at $L = 20\ m$ and $40\ m$, respectively, except at some local peaks. It should be emphasized that the instantaneous maximum earth pressure shown in Figure 4.10 to Figure 4.13 at different points did not appear at the same time.

4.5.3.2 Seismic Earth Pressure Response Spectrum

Figure 4.14 presents the seismic earth pressure response spectra obtained for S1 for the different pipeline configurations. The response spectra in Figure 4.14 represent the envelope spectra at all receivers located in soil layers (1) and (2). The overall trend of the response spectra at distances $L = 20\ m$ and $40\ m$ is similar with small discrepancies. However, as an exception, the elastic response spectrum at layer (1) for configuration (2) approached the response spectrum in the same layer for configuration (3) at $L = 40\ m$. Both response spectra corresponded to a similar geometry where a pipeline is located in layer (1), as shown in Figure 4.3. As the damping ratio increases, it is apparent that the discrepancies between the response spectra at layers (1) and (2) gradually vanish. This is obvious in L1-configuration (2) and L1-configuration (3) at the 5% damping ratio in Figure 4.14(b).

By comparing Figure 4.14(a) and Figure 4.8(a), it is observed that the elastic response spectrum in layer (1) due to the triple pipeline configuration (i.e., case 3) corresponds roughly to the same peak of the response spectrum with no pipeline considered. However, the three pipeline configurations produce higher peaks in layer (2) than the case with no pipeline considered. Figure 4.14(b) and Figure 4.8(b) reveal that when the distance L becomes relatively large, the response spectra that correspond to the cases with no pipeline envelope the response spectra due to all pipeline configurations.

The envelope response spectra were developed for all pipelines shown in Figure 4.3 for the elastic case and at 5% damping ratio and plotted in Figure 4.15. At $L = 20\ m$, pipelines P1, P2, and P4 produce response spectra with approximately similar peaks. However, there is a slight shift in the natural frequency corresponding to each peak. Although P4 and P5 are located in the same layer and elevation, P4 produces a higher response spectrum than P5. This can be attributed to the different burial depths of substructures 1 and 2, where S2 is expected to attract more seismic energy, as discussed in an earlier section related to Figure 4.5. However, as distance L and damping ratio increase the seismic waves are subjected to more attenuation, and thus the discrepancies in the P4 and P5 response spectra decrease, as shown in Figure 4.15(b). It can also be noticed that the response spectra at $L = 40\ m$ became more broadened than their conterparts at $L = 20\ m$. By closely examining Figure 4.15 and Figure 4.14, it is obvious that the pipelines absorb more seismic energy when distance L is short, while the opposite

occurs in the substructure. Accordingly, the integrity of the pipeline is compromised when the substructures are located in relatively close proximity.

4.6. CONCLUSIONS

In nuclear power plants, buried pipelines may be located in close proximity to a substructure or passing between two or more substructures. One of the intrinsic problems that could adversely affect risk mitigation associated with earthquakes is the seismic interaction between substructures and pipelines through the soil. To investigate this concern, the soil-structure system shown in Figure 4.1 has been analyzed in the two-dimensional space, and the potential issues have been identified. The primary focus was the impact of the pipeline on the seismic earth pressures on the substructures, with a secondary focus on the pipeline. Different pipeline configurations have been considered (see Figure 4.3), and three variables have been examined in the analysis, namely the clear distance between the substructures, excitation frequency, and damping ratio.

The effect of the pipeline is not uniform across the depth of the substructures and fluctuates frequently depending on the pipeline location and the combination of the three parameters L, ζ, and f. The earth pressure distribution on substructures is most affected at depth within the immediate vicinity of the pipeline configuration, which is layers (1) and (2) in this analysis. Since the pipeline has minimal impact on the wave propagation at great depths of the substructures, the effect of the pipeline can be neglected. Furthermore, as the damping ratio and distance between

substructures increase, seismic waves reflected from the pipelines experience a successive reduction in amplitude, and thus the original earth pressure on substructures is marginally affected. Regarding the different pipeline configurations, it is observed that the double and triple pipeline configurations generally tend to amplify the earth pressure at a higher rate than the single pipeline. The results also showed that neglecting the interaction with nearby substructures would jeopardize the integrity of the pipeline due to the significant increase in the seismic earth pressure on the pipeline as a result of this interaction.

Seismic earth pressure response spectra were also developed for the substructures and pipeline to examine the amplified/reduced envelope earth pressure at different natural frequencies. It was found that the interaction with the pipelines amplifies the original response spectra of the substructures at all frequencies greater than 9Hz when the distance L is relatively short. When the distance L increases, the amplification factor decreases and the original response spectra envelopes their counterparts with the interaction with pipelines considered. However, for the response spectra of the pipelines, the interaction with nearby substructures is crucial, where it generally amplifies the original response spectra regardless of the damping ratio or the distance L.

The findings of this study are of great interest in the seismic design of new elements and the assessment of existing elements. Furthermore, it gives insight into the selection of backfill materials with appropriate energy absorption capabilities

in order to reduce seismic forces on the structural and non-structural (i.e., pipeline) elements.

4.7. ACKNOWLEDGEMENT

The financial support for the study was provided through the Canadian Nuclear Energy Infrastructure Resilience under Systemic Risk (CaNRisk) – Collaborative Research and Training Experience (CREATE) program of the Natural Science and Engineering Research Council (NSERC) of Canada.

4.8. REFERENCES

ACI Committee 349. (2010). "ACI 349-06. Code Requirements for Nuclear Safety-Related Concrete Structures and Commentary." *American Concrete Institute (ACI)*.

ASCE/SEI 4-16. (2017). *Seismic analysis of safety-related nuclear structures*. *Seismic Analysis of Safety-Related Nuclear Structures*, American Society of Civil Engineers.

ASME. (2019). *BPVC Section III-Rules for Constructions of Nuclear Facility Components-Subsection NCA-General Requirements for Division 1 and Division 2*.

De Basabe, J. D., and Sen, M. K. (2010). "Stability of the high-order finite elements for acoustic or elastic wave propagation with high-order time stepping." *Geophysical Journal International*, 181(1), 577–590.

Budnitz, R. J., Konstandinidis, D., and Zhou, Z. (2015). *Evaluations of NRC Seismic-Structural Regulations and Regulatory Guidance, and Simulation-Evaluation Tools for Applicability to Small Modular Reactors (SMRs)*.

Canadian Nuclear Safety Commission (CNSC). (2016). *Small Modular Reactors : Regulatory Strategy, Approaches and Challenges*. *Discussion Paper DIS-16-04*.

Canadian Standards Association (CSA). (2008). *CSA N291-Requirements for safety-related structures for CANDU nuclear power plants*.

Canadian Standards Association (CSA). (2014). *CSA N287.3-Design requirements for concrete containment structures for nuclear power plants*.

Chapman, C. (2004). *Fundamentals of Seismic Wave Propagation*. Cambridge University Press, Cambridge.

Chavda, J. T., and Dodagoudar, G. R. (n.d.). "Experimental studies on a circular open caisson." *International Journal of Physical Modelling in Geotechnics*, 0(0), 1–18.

Cheng, Z., Law, H., and Jiang, Y. (2010). *Soil-Structure Interaction Analysis For Bridge Caisson Foundation*.

CSA N289.3-10. (2015). *Design procedures for seismic qualification of nuclear power plants*. Canadian Standards Association.

Datta, S. K., Shah, A. H., and Wong, K. C. (1984). "Dynamic stresses and

displacements in buried pipe." *Journal of Engineering Mechanics*, 110(10), 1451–1466.

Gaudio, D., and Rampello, S. (2016). "Dynamic Soil-structure Interaction of Bridge-pier Caisson Foundations." *Procedia Engineering*, 158, 146–151.

Gerolymos, N., and Gazetas, G. (2006). "Static and dynamic response of massive caisson foundations with soil and interface nonlinearities—validation and results." *Soil Dynamics and Earthquake Engineering*, 26(5), 377–394.

Geuzaine, C., and Remacle, J. F. (2009). "Gmsh: A 3-D finite element mesh generator with built-in pre- and post-processing facilities." *International Journal for Numerical Methods in Engineering*, 79(11), 1309–1331.

Haskell, N. A. (1953). "The dispersion of surface waves on multilayered media." *Bulletin of the Seismological Society of America*, 43(1), 17–34.

Hubert, L., Po, L. I., and Patrick, W. (2014). "Soil-Structure Interaction for Gravity Caissons in Bridge Seismic Design." *Structures Congress 2014*, Proceedings.

IAEA. (2020). *Operating Experience with Nuclear Power Stations in Member States*. Operating Experience with Nuclear Power Stations in Member States (CD-ROM), INTERNATIONAL ATOMIC ENERGY AGENCY, Vienna.

Jalbi, S., Shadlou, M., and Bhattacharya, S. (2018). "Impedance functions for rigid skirted caissons supporting offshore wind turbines." *Ocean*

Engineering, 150, 21–35.

John P.wolf. (1994). *Foundation vibrational analysis using simple physical models*. *Prentice Hall*, Englewood Cliffs, New Jersey.

Julian, B. R., and Gubbins, D. (1977). "Three-dimensional seismic ray tracing." *Journal of Geophysics*.

Karabalis, D. L., and Mohammadi, M. (1998). "3-D dynamic foundation-soil-foundation interaction on layered soil." *Soil Dynamics and Earthquake Engineering*, 17(3), 139–152.

Katayama, T., Kubo, K., and Sato, N. (1975). "Earthquake Damage To Water and Gas Distribution Systems." *Proceedings of the US National Conference on Earthquake Engineering, EERI*, Ann Arbor, 396–405.

Kloukinas, P., Langousis, M., and Mylonakis, G. (2012). "Simple wave solution for seismic earth pressures on nonyielding walls." *Journal of Geotechnical and Geoenvironmental Engineering*, 138(12), 1514–1519.

Komatitsch, D., and Tromp, J. (1999). "Introduction to the spectral element method for three-dimensional seismic wave propagation." *Geophysical Journal International*.

Komatitsch, D., and Tromp, J. (2014). "SPECFEM2D User Manual Version 7.0." *Computational Infrastructure for Geodynamics*.

Komatitsch, D., and Vilotte, J.-P. (1998). "The spectral element method: An

efficient tool to simulate the seismic response of 2D and 3D geological structures." *Bulletin of the Seismological Society of America*, 88(2), 368–392.

Kouretzis, G. P., Bouckovalas, G. D., and Gantes, C. J. (2006). "3-D shell analysis of cylindrical underground structures under seismic shear (S) wave action." *Soil Dynamics and Earthquake Engineering*, 26(10), 909–921.

Kramer, S. L. (1996). *Geotechnical Earthquake Engineering*. Prentice Hall, New Jersey.

Lee, M. K. W., and Finn, L. W. D. (1978). "{DESRA}-2: Dynamic effective stress response analysis of soil deposits with energy transmitting boundary including assessment of liquefaction potential." *Soil Mechanics*, 38(38).

Lee, T. H., and Wesley, D. A. (1973). "Soil-structure interaction of nuclear reactor structures considering through-soil coupling between adjacent structures." *Nuclear Engineering and Design*, 24(3), 374–387.

Lei, W., Weiming, G., Yonggao, Y., and Xiaodong, T. (2021). "Field Experimental Study on Vertical Bearing Capacity of Root-Caisson Foundation." *Advances in Soil Dynamics and Foundation Engineering*, Proceedings.

Lin, H. -T, Roesset, J. M., and Tassoulas, J. L. (1987). "Dynamic interaction between adjacent foundations." *Earthquake Engineering & Structural*

Dynamics, 15(3), 323–343.

Longuet-Higgins, M. S. (1950). "A theory of the origin of microseisms." *Philosophical Transactions of the Royal Society of London. Series A, Mathematical and Physical Sciences*, 243(857), 1–35.

Lowrie, W. (2007). *Fundamentals of Geophysics*. Cambridge University Press, New York, NY, USA.

Mccamy, K., Meyer, R.P., and Smith, T. J. (1962). "Generally applicable solutions of Zoeppritz' amplitude equations." *Bulletin of the Seismological Society of America*, 52(4), 923–955.

Mononobe, N., and Matsuo, H. (1929). "On the Determination of Earth Pressures During Earthquakes." *Proceedings of World Engineering Congress*, Tokyo, Japan, 274–280.

Mulliken, J. S., and Karabalis, D. L. (1995). "Discrete Model For Foundation-soil-foundation Interaction." *Soil Dynamics and Earthquake Engineering*, 8, 1–3.

Mylonakis, G., and Gazetas, G. (2000). "Seismic soil-structure interaction: Beneficial or detrimental?" *Journal of Earthquake Engineering*, 4(3), 277–301.

Newmark, N. M., and Hall, W. J. (1975). "Pipeline Design To Resist Large Fault Displacement." 416–425.

NP-T-3.20. (2018). *Buried and Underground Piping and Tank Ageing Management for Nuclear Power Plants*. Vienna.

NuScalePower. (2020). "NuScale Final Safety Analysis Report." <https://www.nrc.gov/docs/ML2022/ML20224A491.pdf>.

O'Rourke, M., and Ayala, G. (1993). "Pipelinpipeline damage due to wave propagatione." *Journal of Geotechnical Engineering*, 119(9), 1490–1498.

Okabe, S. (1926). "General theory of earth pressure." *Journal of the Japanese Society of Civil Engineers*, 12(1), 1277–1323.

P., D. J., T., H. G., and J., D. A. (2005). "Stiffness of Flexible Caisson Foundations Embedded in Nonhomogeneous Elastic Soil." *Journal of Geotechnical and Geoenvironmental Engineering*, American Society of Civil Engineers, 131(12), 1498–1508.

Padrón, L. A., Aznárez, J. J., and Maeso, O. (2011). "3-D boundary element-finite element method for the dynamic analysis of piled buildings." *Engineering Analysis with Boundary Elements*, 35(3), 465–477.

Peter, D., Komatitsch, D., Luo, Y., Martin, R., Le Goff, N., Casarotti, E., Le Loher, P., Magnoni, F., Liu, Q., Blitz, C., Nissen-Meyer, T., Basini, P., and Tromp, J. (2011). "Forward and adjoint simulations of seismic wave propagation on fully unstructured hexahedral meshes." *Geophysical Journal International*, 186(2), 721–739.

Reese, C. D., and Eidson, J. V. (2006). *Handbook of OSHA Construction Safety and Health*. *Handbook of OSHA Construction Safety and Health*.

Rizzo, F. J., Shippy, D. J., and Rezayat, M. (1985). "A boundary integral equation method for radiation and scattering of elastic waves in three dimensions." *International Journal for Numerical Methods in Engineering*.

Rodríguez-Castellanos, A., Rodríguez-Sánchez, J. E., and Carbajal-Romero, M. (2010). "Coupled response for rigid foundations." *Journal of Geotechnical and Geoenvironmental Engineering*, 135(12), 1971–1975.

Scott, R. F. (1973). "Walls, Earthquake-Induces Earth pressures by Retaining." *5thWorld Conference on Earthquake Engineering*, Tokyo, Japan, 1611–1620.

Seed, H. B., and Whitman, R. V. (1970). "Design of Earth Retainig Structures for Dynamic Loads." *ASCE Specialty Conference on Lateral Stresses in the Ground and Design of Earth-Retaining Structures*, Cornell Univ., Ithaca, New York, 103–147.

Skau, K. S., Jostad, H. P., Eiksund, G., and Sturm, H. (2019). "Modelling of soil-structure-interaction for flexible caissons for offshore wind turbines." *Ocean Engineering*, 171, 273–285.

Stacey, R. (1988). "Improved transparent boundary formulations for the elastic-wave equation." *Bulletin of the Seismological Society of America*, 78(6),

2089–2097.

Steedman, R. S., and Zeng, X. (1990). “The influence of phase on the calculation of pseudo-static earth pressure on a retaining wall.” *Geotechnique*, 40(1), 103–112.

Stein, S., and Wysession, M. (2003). *An Introduction to Seismology, Earthquakes, and Earth Structure*. *Seismological Research Letters*, Blackwell Publishing Ltd., Malden, USA.

Takada, S., and Tanabe, K. (1987). “Three-dimensional seismic response analysis of buried continuous or jointed pipelines.” *Journal of Pressure Vessel Technology, Transactions of the ASME*, 109(1), 80–87.

Telford, W. M., Geldart, L. P., and Sheriff, R. E. (1990). *Applied Geophysics*. *Cambridge University Press.*

Teng, T.-L. (1987). *Geophysics - Field Measurements*. *Methods in Experimental Physics*.

Thomson, W. T. (1950). “Transmission of elastic waves through a stratified solid medium.” *Journal of Applied Physics*, 21, 89–93.

Triantafyllidis, T., and Prange, B. (1988). “Rigid circular foundation: Dynamic effects of coupling to the half-space.” *Soil Dynamics and Earthquake Engineering*, 7(1), 40–52.

Trifonov, O. V., and Cherniy, V. P. (2010). “A semi-analytical approach to a

nonlinear stress-strain analysis of buried steel pipelines crossing active faults." *Soil Dynamics and Earthquake Engineering*, 30(11), 1298–1308.

U.S. NRC. (2013). *Standard Review Plan for the Review of Safety Analysis Reports for Nuclear Power Plants: LWR Edition. Section 3.7.3 Seismic Subsystem Analysis Review Responsibilities*. *NUREG 0800*.

USGS. (2009). "Determining the Depth of an Earthquake." *Earthquake Information Bulletin (USGS)*, 9(4), 16.

Veletsos, A. S., and Younan, A. H. (1994). "Dynamic soil pressures on rigid vertical walls." *Earthquake Engineering & Structural Dynamics*, 23(3), 275–301.

W., G., and J., C. (2021). "Experimental Study of Installation of Concrete Suction Caisson in Clay." *IFCEE 2015*, Proceedings.

Warburton, G. B., Richardson, J. D., and Webster, J. J. (1971). "Forced vibrations of two masses on an elastic half space." *Journal of Applied Mechanics, Transactions ASME*, 38(1), 148–156.

Whitman RV. (1969). "Current Status of Soil Dynamics." *Applied Mechanics Reviews*, 22, 1–8.

Wolf, J. P. (1989). "Soil-structure-interaction analysis in time domain." *Nuclear Engineering and Design*.

Wood, J. H. (1973). *Earthquake-induced soil pressures on structures*. *PhD*

Thesis, Pasadena, CA.

Yao, W. A., and Mao, L. (2010). "Symplectic system based analytical solution for bending of rectangular plates on Winkler foundation." *The IES Journal Part A: Civil & Structural Engineering*, Taylor & Francis, 3(1), 28–37.

Zoeppritz, K. (1919). "Über Erdbebenwellen Part VII b . Über Reflexion und Durchgang seismischer Wellen durch Unstetigkeitsflächen." *Nachrichten von der Gesellschaft der Wissenschaften zu Göttingen, Mathematisch-Physikalische Klasse*, 66–84.

4.9. TABLES

Table 4.1. Characteristics of the layered soil profile

	Thickness $h_f(m)$	Density (kg/m^3)	Poisson's ratio (ν)	$V_s\ (m/s)$
Layer (1)	5	1500	0.3	200
Layer (2)	7	1700	0.3	300
Layer (3)	9	1900	0.3	400
Layer (4)	11	2100	0.3	500
Layer (5) Elastic Half-space	68	2300	0.3	700

4.10. FIGURES

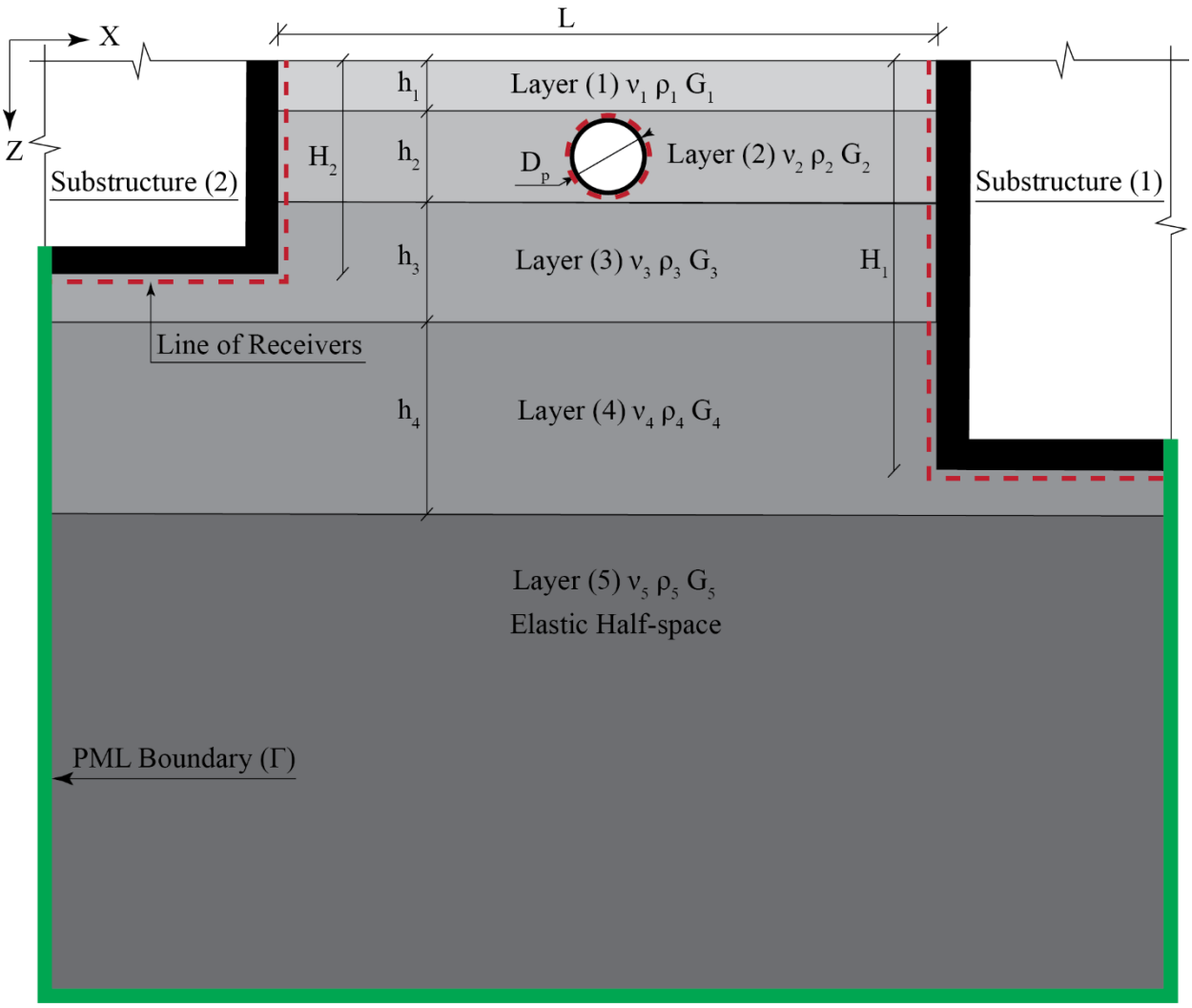

Figure 4.1. Schematic representation of the model considered in the analysis

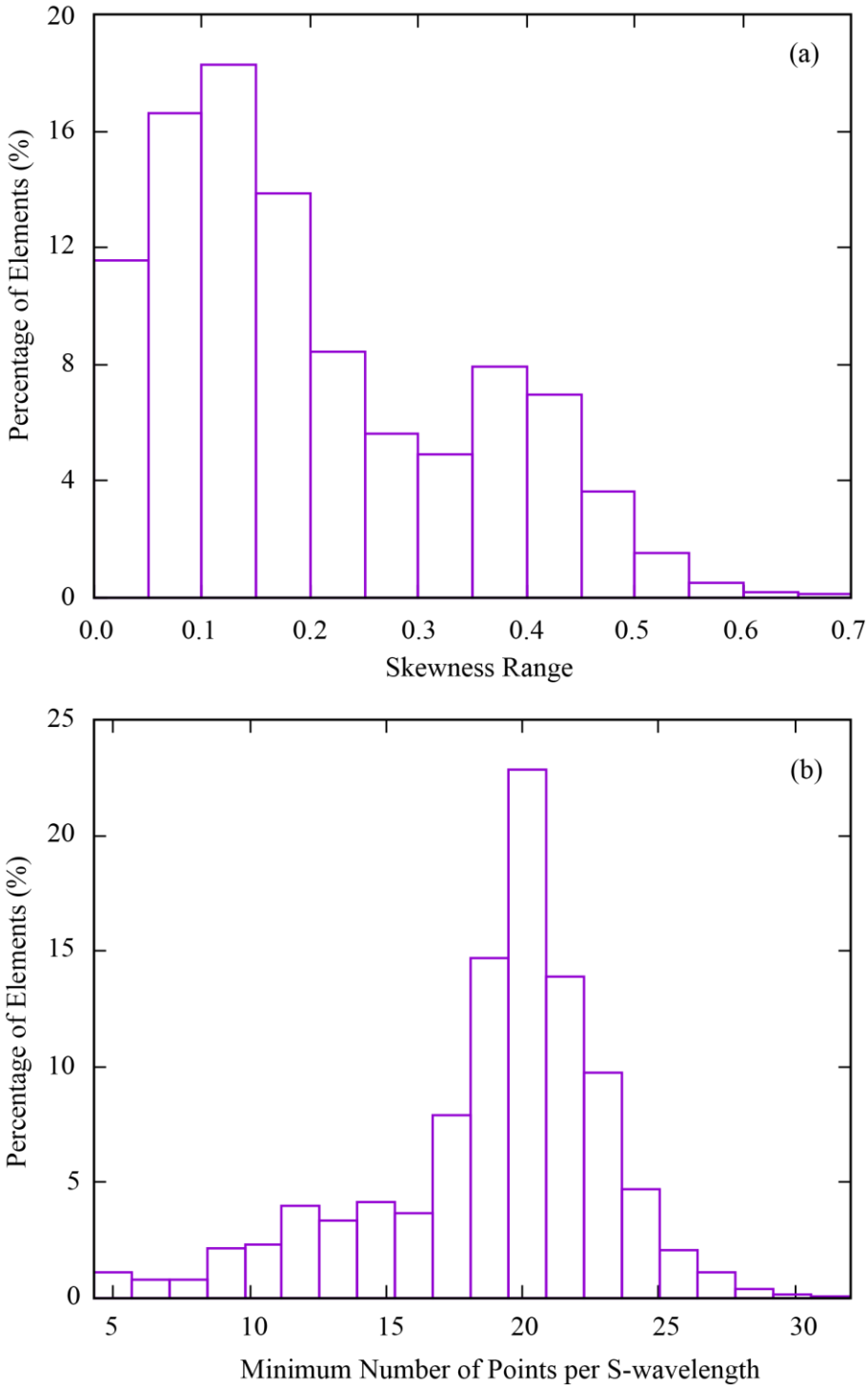

Figure 4.2. Simulation parameters calculated by SPECFEM2D include: A) Mesh quality histogram; and B) Number of elements per S-wavelength.

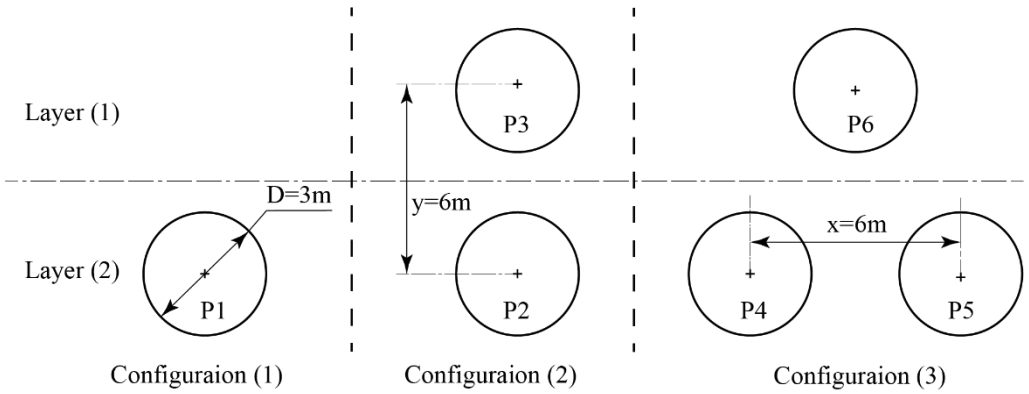

Figure 4.3. Schematic of the pipeline configurations considered in the analysis.

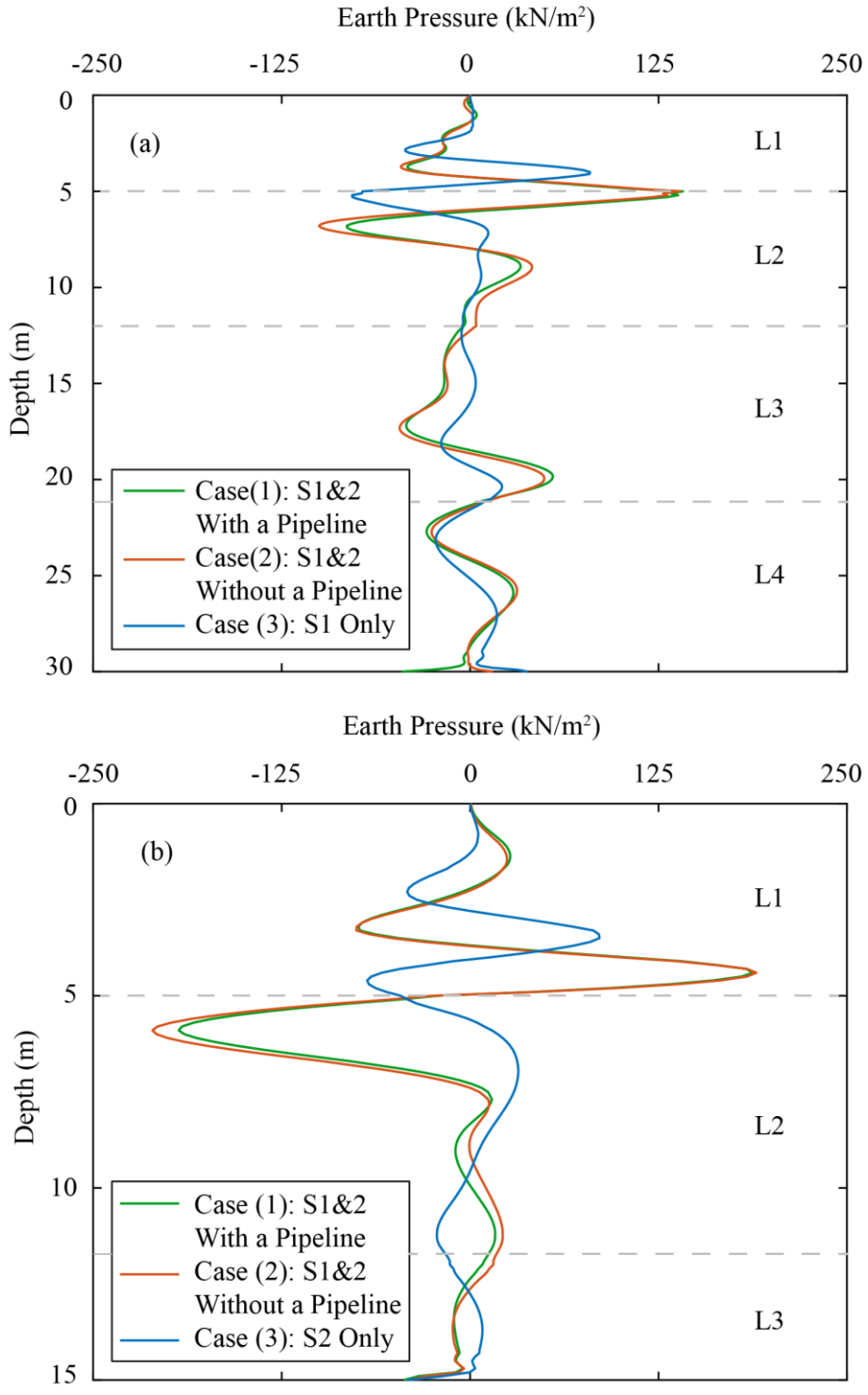

Figure 4.4. Seismic lateral earth pressure distribution on (A) Substructure 1; and (B) Substructure 2 at $t = 0.20\ sec\ L = 60\ m$.

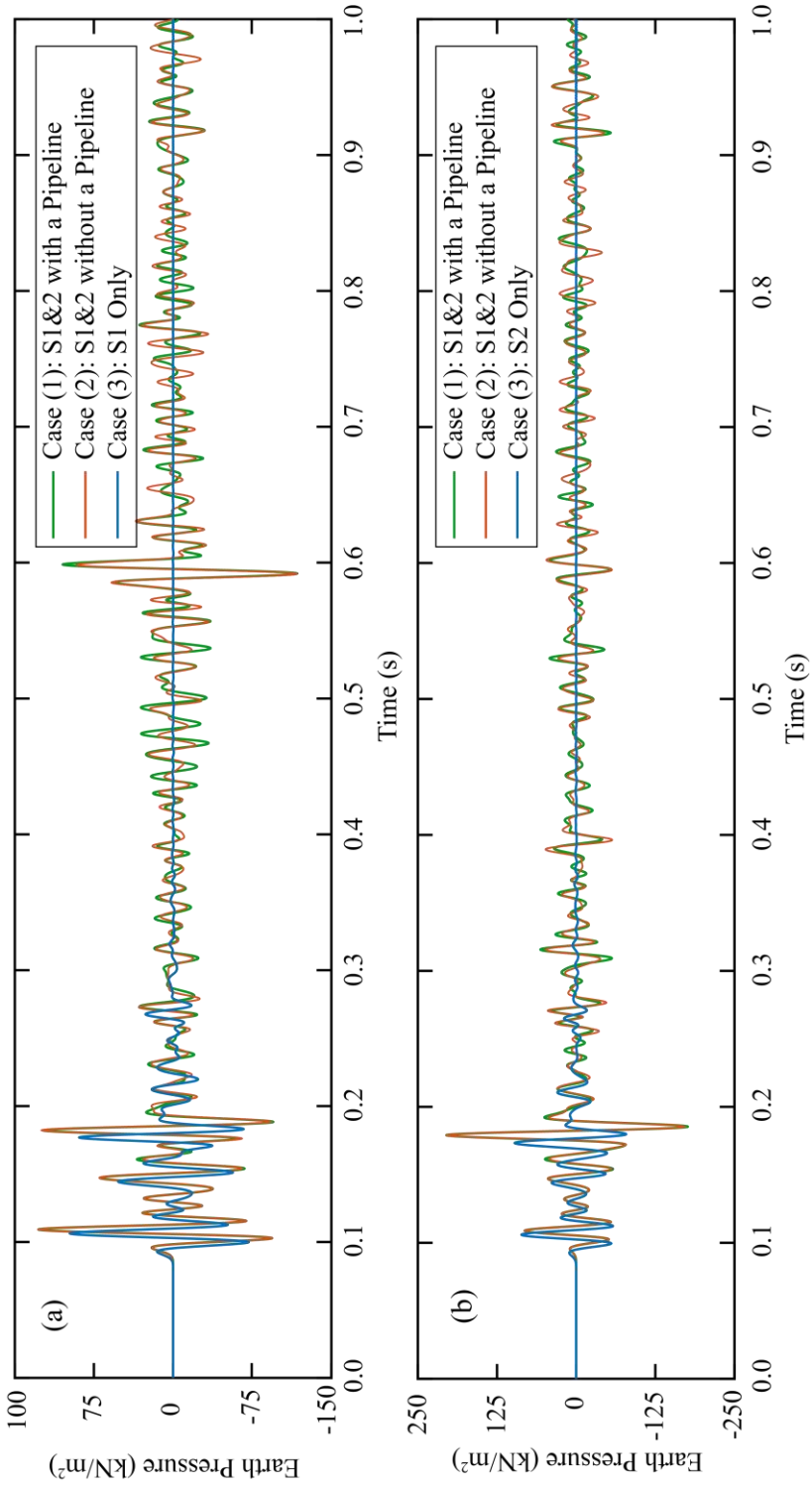

Figure 4.5. Seismic earth pressure time history at (a) Receiver 51 on Substructure 1; and (b) Receiver 201 on Substructure 2, where $L = 60\ m$

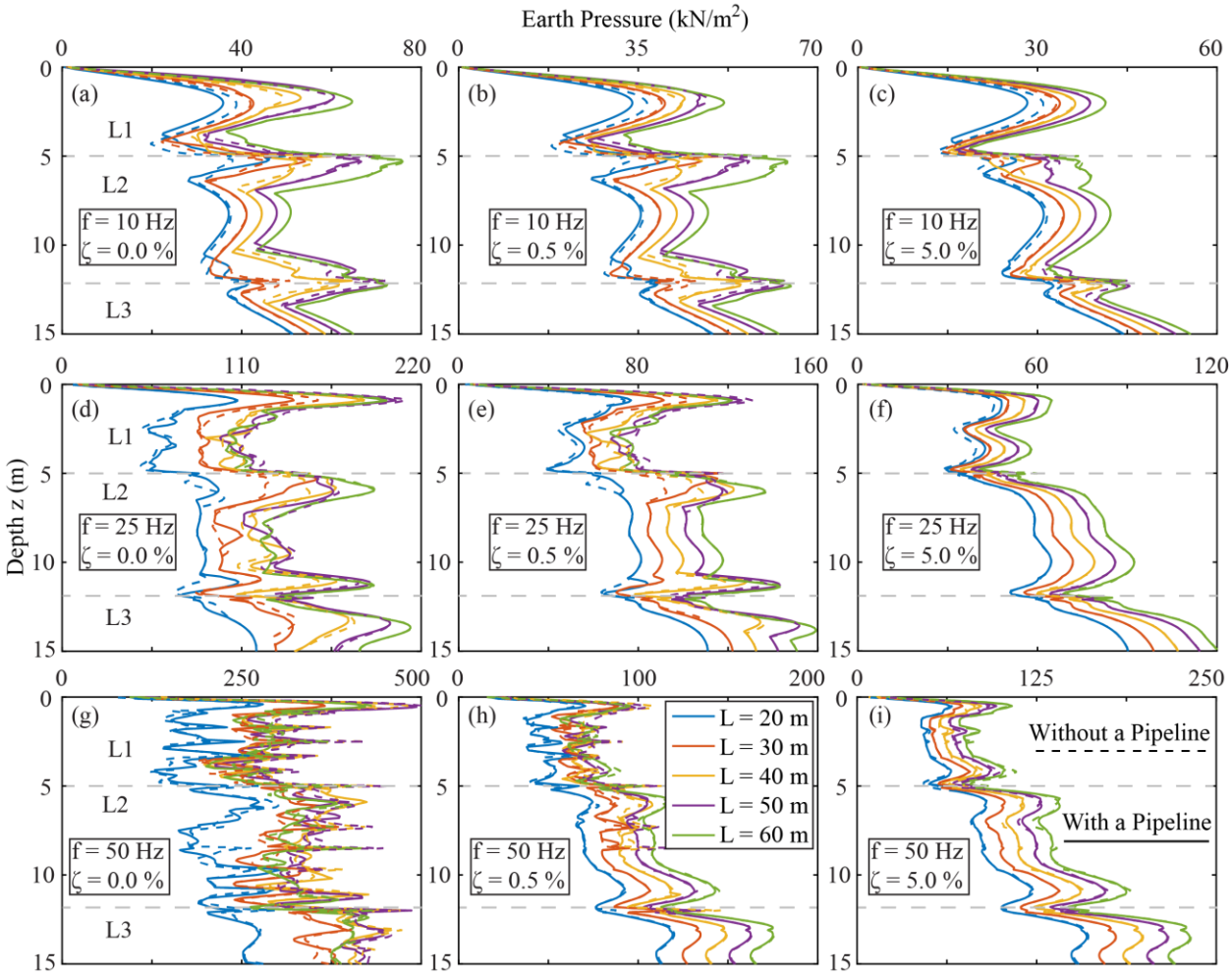

Figure 4.6. Distribution of the instantaneous maximum seismic earth pressure on Substructure 1 due to different distance L, damping ratio ζ, and excitation frequency f. (Note: The instantaneous maximum earth pressures at different depth are not at the same time)

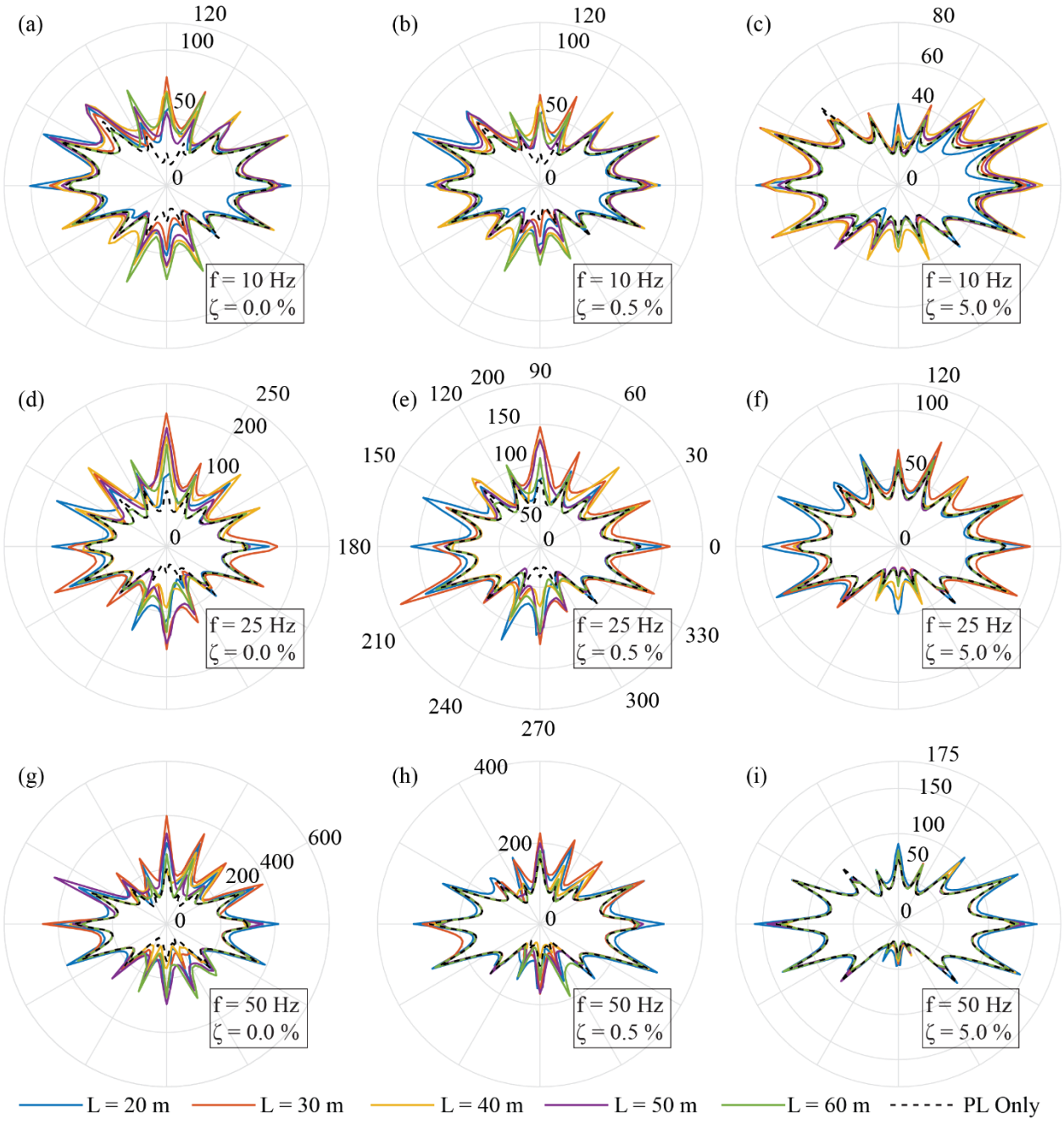

Figure 4.7. Distribution of instantaneous maximum seismic earth pressure on the pipeline at different distances between S1 and S2

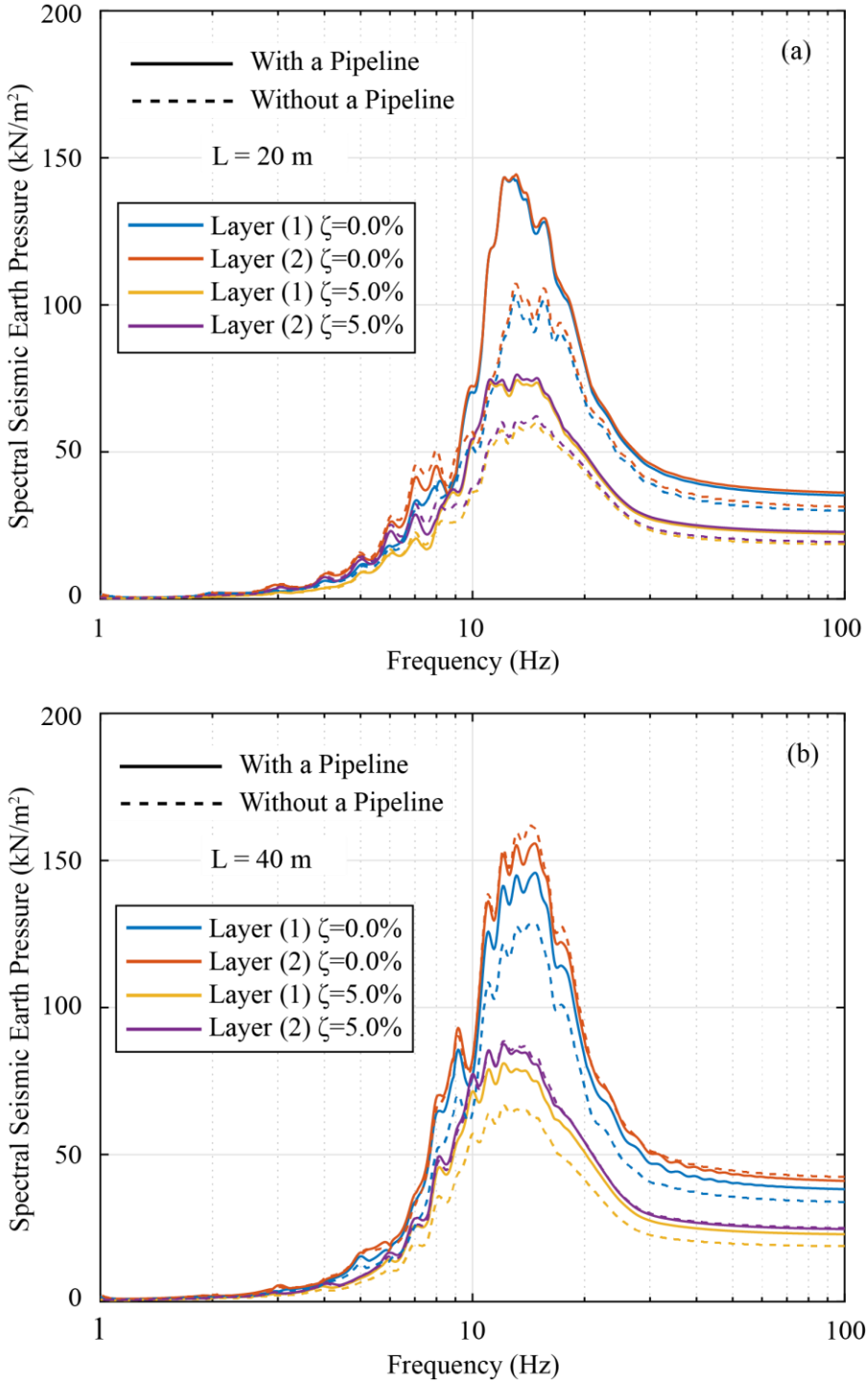

Figure 4.8. Envelope seismic earth pressure response spectrum for S1 at layers (1) and (2)

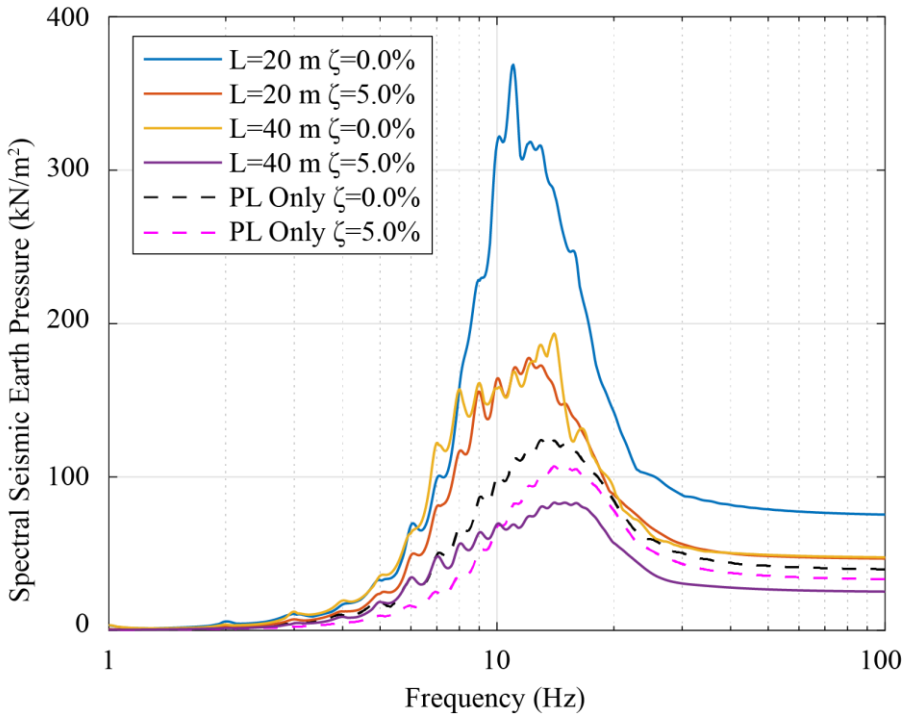

Figure 4.9. Envelope Earth Pressure Response Spectra for the pipeline.

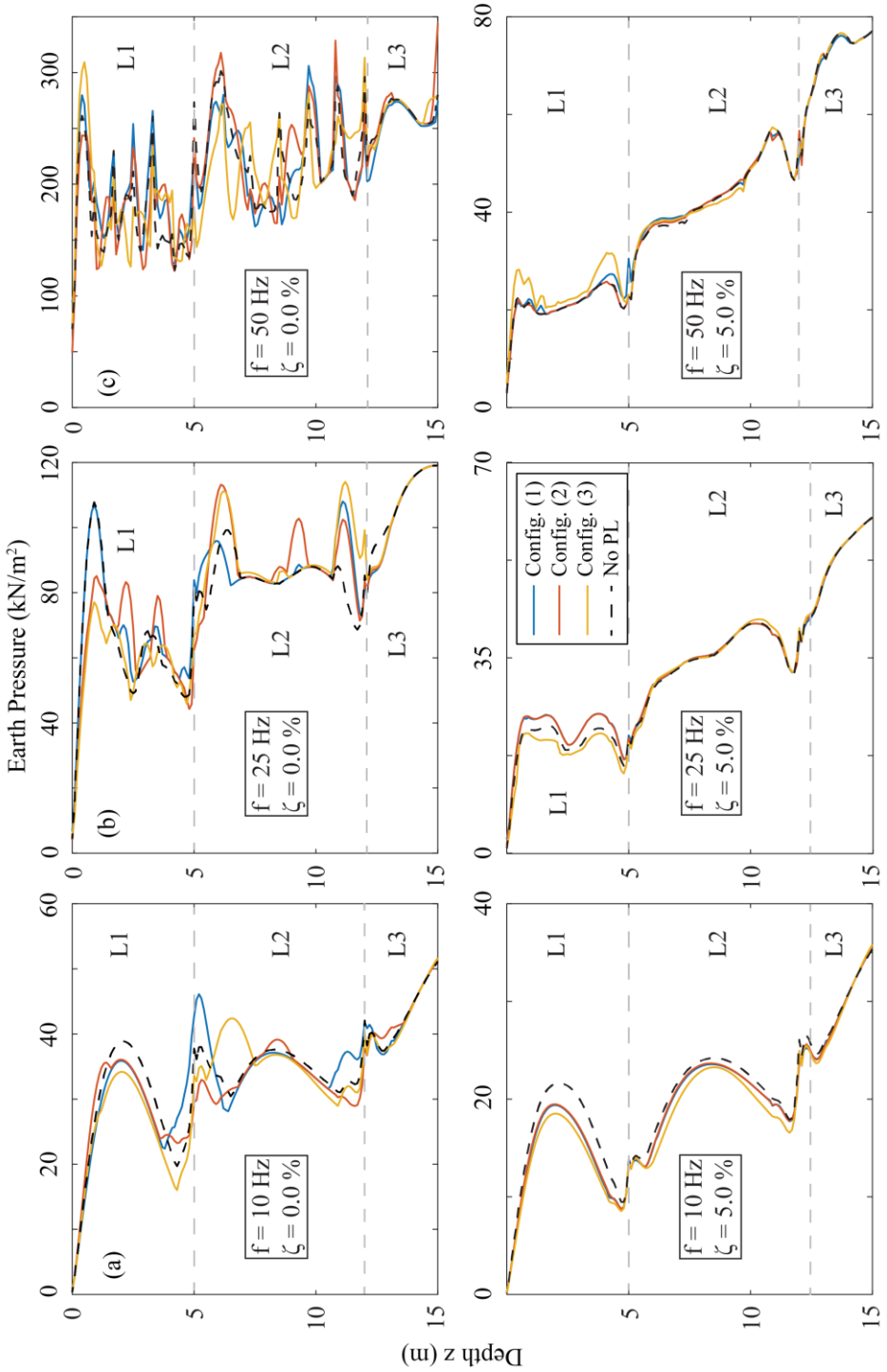

Figure 4.10. Instantaneous maximum seismic earth pressure on S1 due to the pipeline configurations shown in Figure 4.3 at $L = 20\ m$.

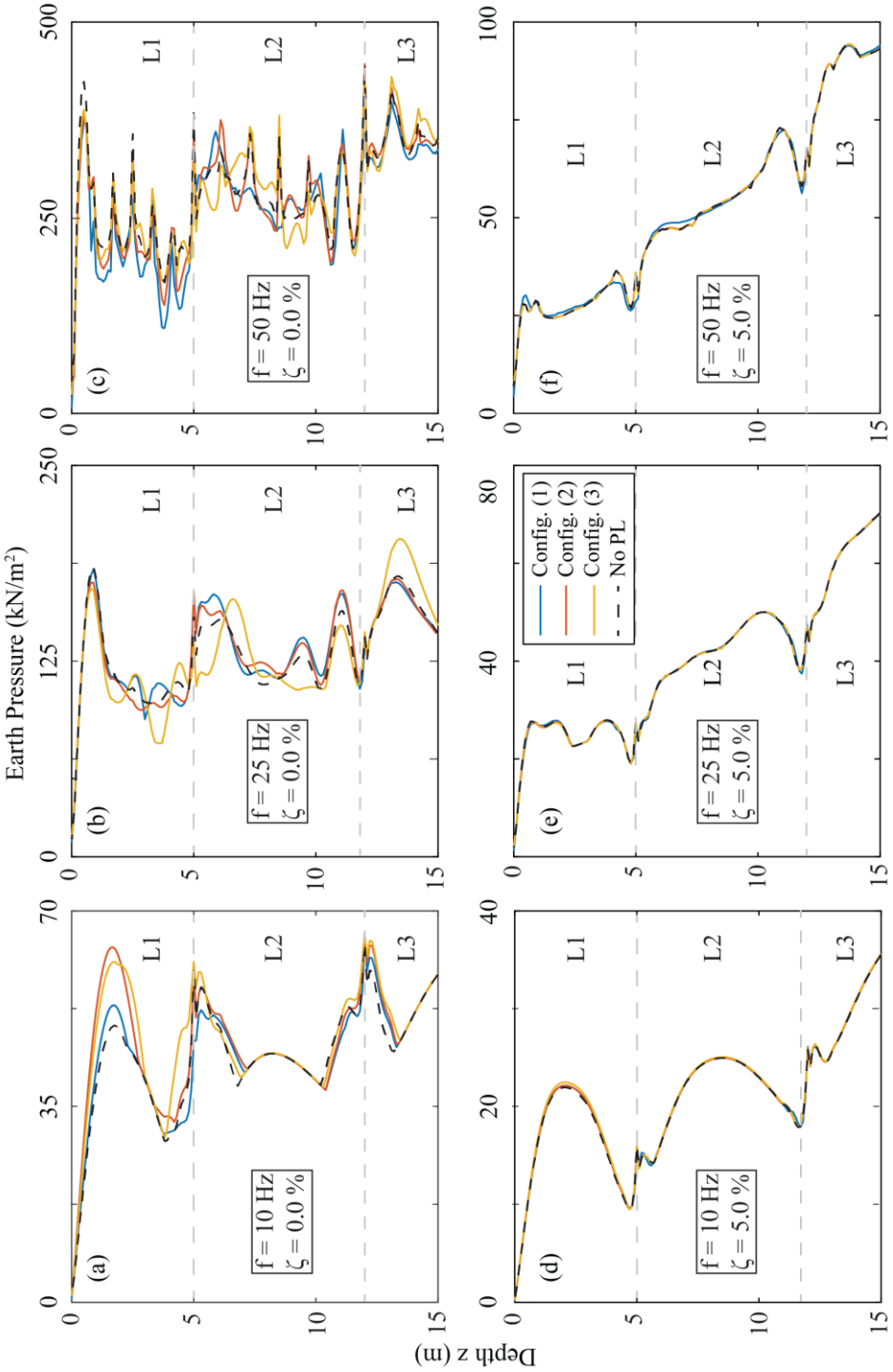

Figure 4.11. Instantaneous maximum seismic earth pressure on S1 due to the pipeline configurations shown in Figure 4.3 at $L = 40\ m$.

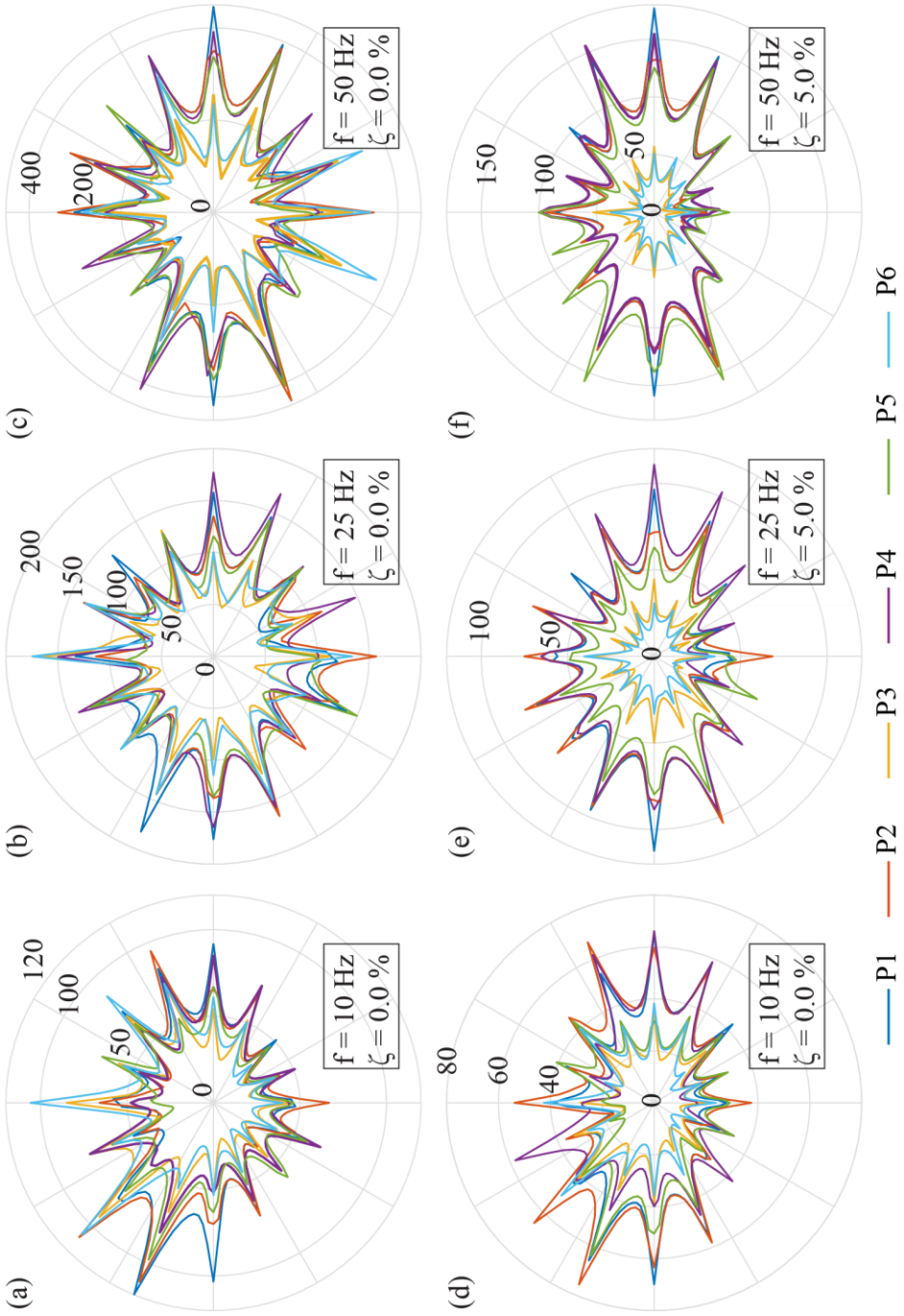

Figure 4.12. Instantaneous maximum seismic earth pressure (kN/m2) on the pipeline configurations shown in Figure 4.3 at $L = 20\ m$

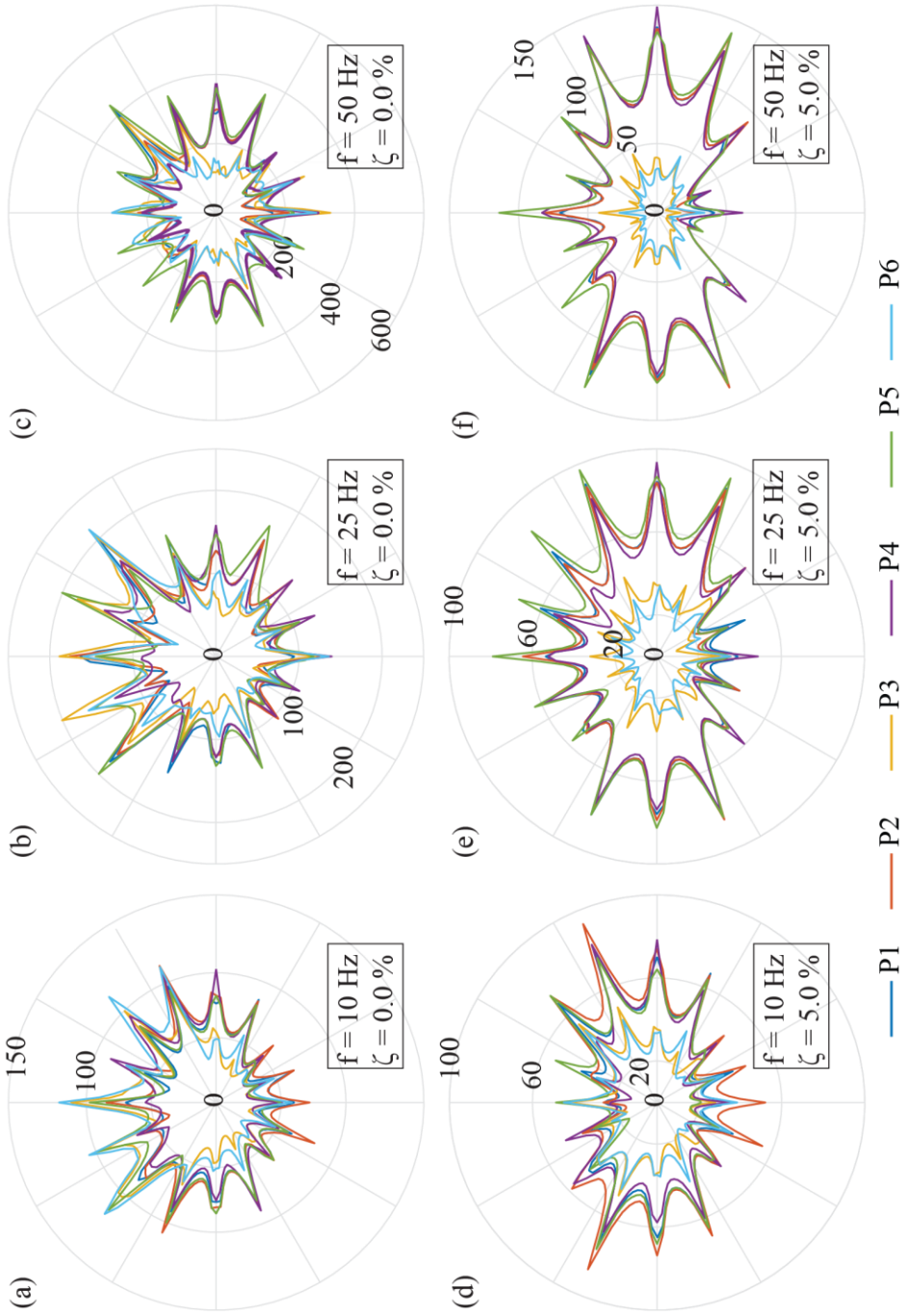

Figure 4.13. Instantaneous maximum seismic earth pressure (kN/m2) on the pipeline configurations shown in Figure 4.3 at $L = 40\ m$

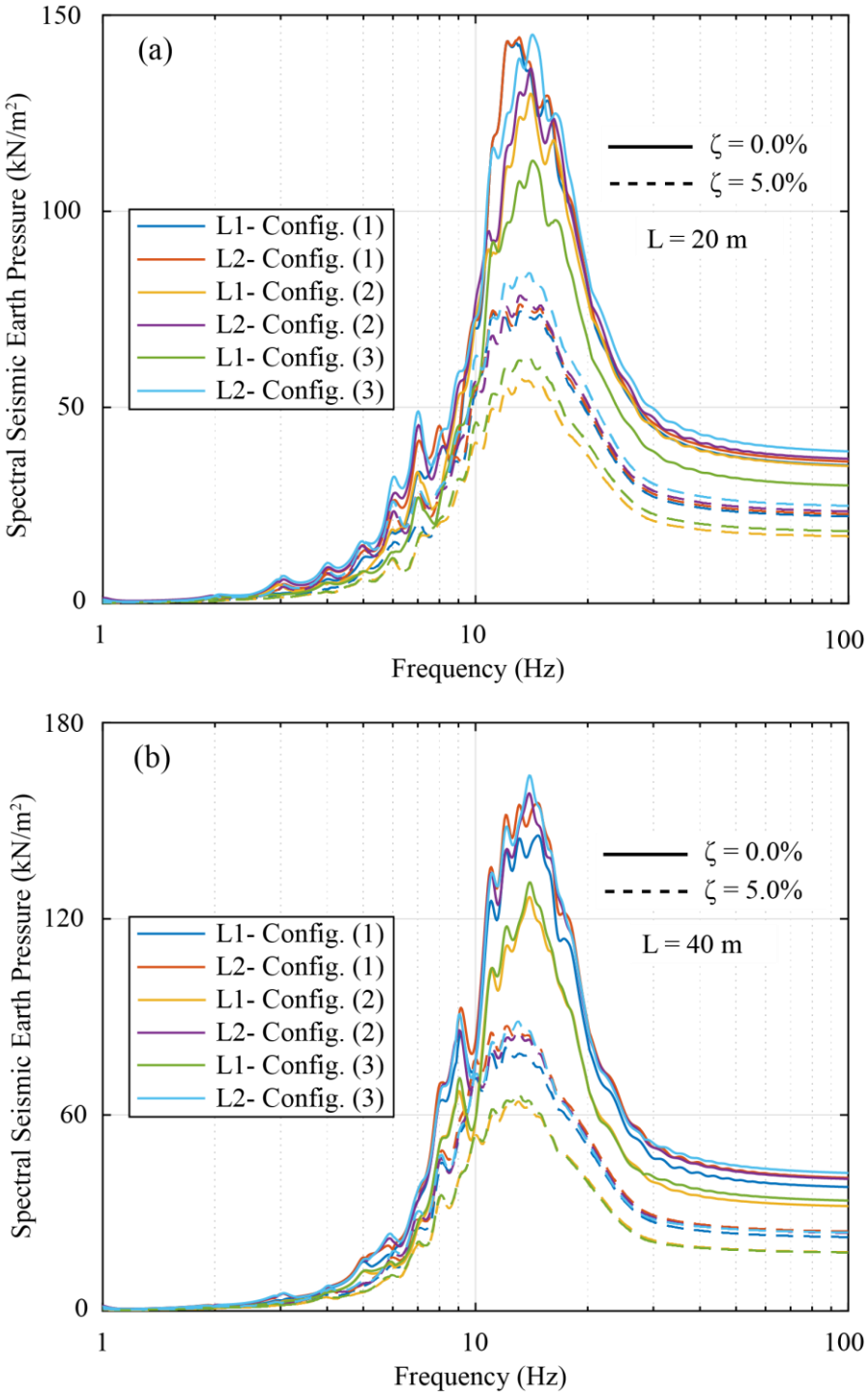

Figure 4.14. Envelope Seismic earth pressure response spectra for S1 at layers (1) and (2) due to the pipeline configurations shown in Figure 4.3

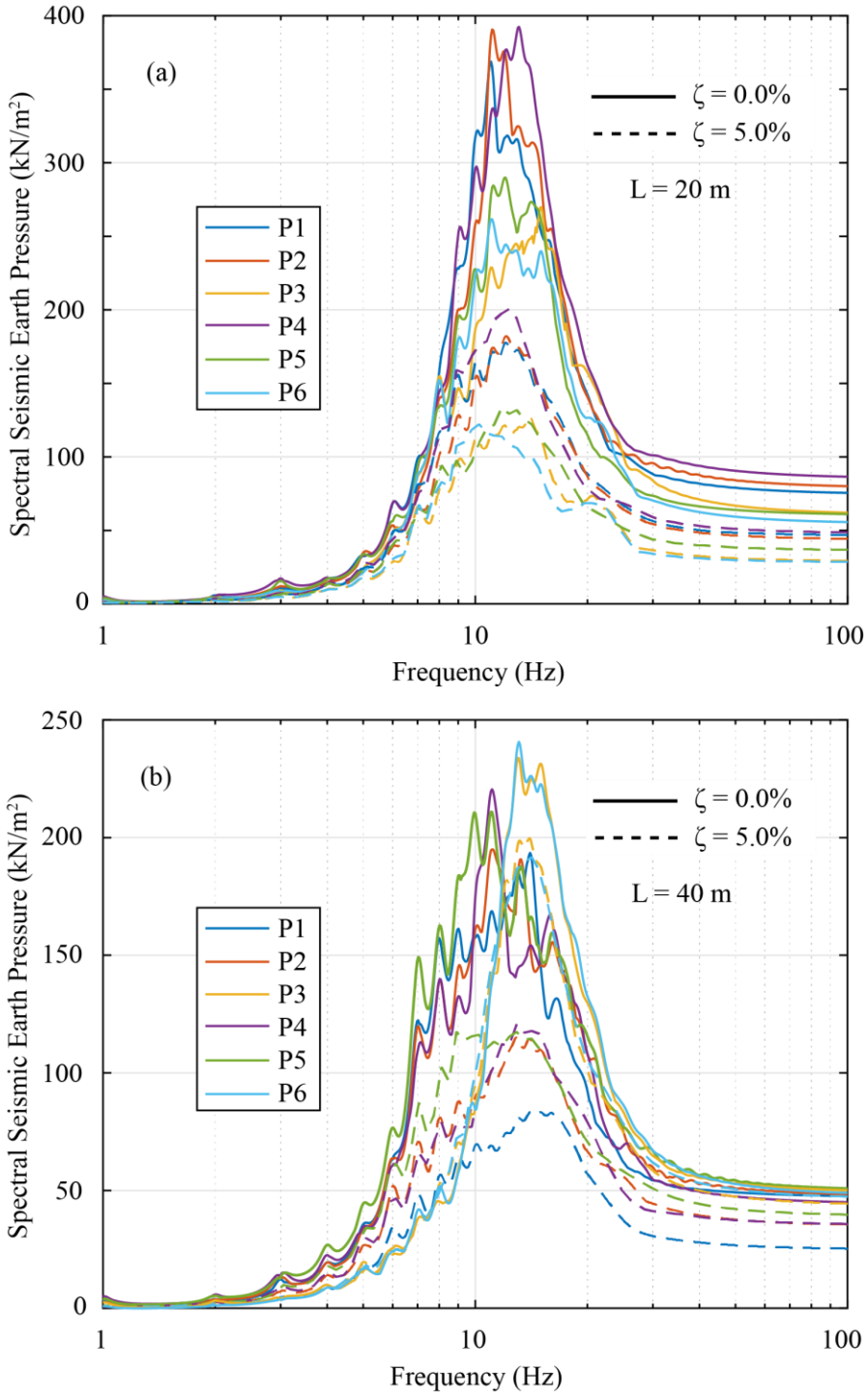

Figure 4.15. Envelope Seismic earth pressure response spectra for the pipeline configurations shown in Figure 4.3

Chapter 5

SUMMARY, CONCLUSIONS, AND RECOMMENDATIONS

5.1. SUMMARY

The transition from conventional NPPs to more affordable and manageable alternatives has put small modular reactors (SMRs) in the priority of various research areas to mitigate risks that could jeopardize the reliability of the new technology. From a civil engineering perspective, some of the challenges are attributed to the deep embedment of the SMR containment structure, which has reached 30 m in the design proposed by NuScale Power (NuScale Power 2020). The design of substructures with such large depths has not yet been established in the current international codes and standards in the nuclear industry. One of the concerns that have been raised by the CNSC in the discussion paper (DIS-16-04, 2016) is the seismic soil-structure interaction (i.e., SSI). This dissertation addresses three issues associated with the seismic SSI of the SMR containment structure and develop effective to perform SSSI analysis for industrial use. The first issue is related to the seismic earth pressure induced by Rayleigh waves in stratified media. The three-dimensional wave propagation theory was employed to calculate the seismic earth pressure due to Rayleigh waves on a rigid substructure inserted into layered soils. The results were compared with their counterparts for a substructure surrounded by homogeneous soil. The second issue is associated with how the seismic interaction between the SMR structure and neighbouring structures through

the soil affecting the earth pressure on the SMR substructure. An analytical method is developed using the three-dimensional wave propagation theory. A simplified procedure is provided to track seismic wave interference in the soil layer, taking into account the back-and-forth wave propagation phases between substructures. In addition, a mathematical expression is proposed to calculate the optimal distance between two adjacent structures that produces minimal SSSI, which can be used in new designs or evaluating existing plants. The third issue is pertinent to the seismic interaction between the SMR substructure and buried pipelines, which represents an interaction between structural and non-structural components. A numerical model is constructed using the spectral element method, in which the three-dimensional wave propagation theory is successfully implemented, to solve the wave propagation problem for the soil-structure-pipeline system of concern. Effective conclusions are drawn to trigger alarms on the adverse impact of such an interaction on the seismic integrity of substructures and buried pipelines. Three variables were extensively investigated in the analysis, namely pipeline location, excitation frequency, and material damping.

5.2. CONCLUSIONS AND CONTRIBUTIONS

The dissertation intensively investigated the previously outlined objectives of the research and provided practical tools for industrial use and guidance for inclusion in the seismic design of SMR containment structures in the codes and standards of

nuclear facilities. The following conclusions highlight the main findings and contributions of the research presented in the previous chapters:

5.2.1. SEISMIC EARTH PRESSURE DUE TO RAYLEIGH WAVES IN VISCOELASTIC MEDIA

- Using the three-dimensional wave propagation theory, an analytical solution for lateral seismic earth pressure induced by Rayleigh waves has been developed for a rigid substructure surrounded by homogeneous viscoelastic soils and rested on a bedrock. Closed-form solutions for the earth pressure distribution, total forces at the base level, and point of application of the dynamic thrust are given as functions of the depth of substructure, Poisson's ratio, damping ratio, and modulus of elasticity.
- Due to the deep embedment depth of the SMR containment structure, the substructures are anticipated to penetrate different soil layers. A semi-analytical method for lateral seismic earth pressure induced by Rayleigh waves was developed for a rigid substructure buried in horizontally stratified multilayer viscoelastic soils and laid above a rigid bedrock. The characteristic equation for the soil-structure system was derived and the corresponding dispersion curves were obtained.
- A combination of increase and decrease of the normal stresses is exerted on the substructure, where the depth "X" at which the direction of incremental normal stress is reversed depends on the soil properties and the number of natural mode

shapes produced by the characteristic equation. This behaviour is in line with the general nature of Rayleigh wave particle motion, which takes the form of a retrograde elliptical motion near the ground surface (up to a depth "X") and prograde elliptical motion for the remainder of the depth,

- The effect of Poisson's ratio and damping ratio of soil is prominent near the ground surface and dwindles with depth. The total earth pressure, which include contributions of the normal and shear stresses, increases as Poisson's ratio of the soil layer increases. However, the effect of the damping ratio is neither uniform nor consistent for normal and shear stresses across the depth of the substructure. Some portions of the substructure are subjected to increased normal/shear stresses as the damping ratio increases, while the opposite occurs at other depths,
- The force of total earth pressure, the total moment at the base, and the location of the dynamic thrust induced by Rayleigh waves are strongly dependant on the number of natural mode shapes corresponding to the excitation frequency. The number of mode shapes resulting from solving the characteristic equation increases at higher excitation frequencies.
- The solutions of homogeneous soils was compared to the results of a soil-structure system inserted into multilayered soils. It was found that treating a multilayered soil profile as a homogeneous medium using the corresponding average mechanical properties drastically underestimates the seismic lateral earth pressure on the substructure. Furthermore, the point of application of the

dynamic thrust is always located at a higher level from the base compared to the accurate analysis using the layered soils. However, the total moment at the base is still underestimated by a large margin. The reason behind this variation is relevant to the number of natural mode shapes produced from the propagation of Rayleigh waves in homogeneous and layered soils. As discussed earlier, Rayleigh waves produce only a single fundamental mode shape in homogeneous soil, unlike layered soils that produce several mode shapes depending on the excitation frequency,

- The Stiff and soft thin layers cannot be neglected in the SSSI analysis. The stiff thin layers generally absorb most of the seismic energy, leading to lower seismic earth pressures on the substructure except at locations corresponding to the thin layers. The opposite occurs in the case of soft thin layers, in which seismic earth pressures are generally amplified.

5.2.2. STRUCTURE-SOIL-STRUCTURE INTERACTION ANALYSIS FOR LATERAL SEISMIC EARTH PRESSURE OF A DEEPLY BURIED STRUCTURE IN LAYERED GROUND

- A closed-form solution was developed based on the three-dimensional wave propagation theory to calculate additional seismic earth pressure on substructures due to structure-soil-structure interaction and engineering backfill. The proposed solution accounts for multi phases of wave propagation back and forth between substructures. The proposed expressions were

accompanied by a guided flowchart to simplify the analysis by tracing the interference of seismic waves in a soil layer,

- An expression has been provided to calculate the optimal distance between two structures that corresponds to minimal seismic SSSI, in the presence of the backfill,
- The assumption of vertically propagating horizontally polarized shear waves is not conservative in the presence of adjacent structures and engineering backfill with an inclined interface with soil layers,
- Regarding the effect of excavation slope (i.e., the inclined interface between the backfill soil layers), it was found that steep slopes amplify the earth pressure on substructures at a higher rate than gentle slopes. At an angle of inclination of 45°, the seismic waves reflected from the backfill do not interact with the upper and lower boundaries of the soil layer but travel directly towards the adjacent substructure. Since the reflected waves are vertically polarized, no additional seismic earth pressure is exerted on the adjacent substructure.
- Regarding the mechanical properties of the backfill soil, higher additional earth pressures are produced when the backfill is relatively loose compared to the adjacent soil layer. Furthermore, material properties should be selected carefully to avoid the development of surface waves in the backfill.
- The total seismic amplitudes transmitted to substructures due to SSSI and backfill soils decrease as the distance between adjacent structures increases. The accumulated additional earth pressures are closely related to the number of

reflections/refractions the seismic waves undergo at the upper and lower boundaries of the soil layer along the distance between adjacent structures.

5.2.3. SEISMIC INTERACTION BETWEEN DEEPLY EMBEDDED SUBSTRUCTURES AND NEARBY PIPELINES

- The effect of the pipeline is not uniform across the depth of the substructures and fluctuates frequently depending on the pipeline layout in the soil profile.
- The impact of buried pipelines on the seismic earth pressure on substructures is most prominent in the immediate vicinity of the pipeline and gradually vanish from the pipeline.
- As the damping ratio ζ of the soil and the distance between substructures L increase, seismic waves reflected from the pipelines experience a successive reduction in amplitude, and thus the original earth pressure on substructures is marginally affected.
- At a relatively short distance L, seismic interaction with pipelines tend to reduce the seismic earth pressure on substructures at low excitation frequency but amplify the earth pressure at high excitation frequency. However, the opposite occurs when the distance L increases. Since a seismic event may include a broad range of frequencies ranging from low to high, all frequency ranges should be considered in the analysis.

- Phase shifts were observed in the recorded earth pressure time histories at the same location due to different excitation frequencies, where higher frequencies produce earlier peaks and the phase shift decreases as the frequency increases.
- At relatively short distance L, the pipelines amplifies the original response spectra of the substructures at all frequencies greater than a certain natural frequency depending on the geometrical and mechanical properties of the soil-structure system. When the distance L increases, the amplification factor decreases and the original response spectra envelopes their counterparts with the interaction with pipelines considered.
- For the response spectra of the pipelines, the interaction with nearby substructures is crucial, where it generally amplifies the original response spectra regardless of the damping ratio or the distance L.
- Regarding the different pipeline configurations, the double and triple pipeline configurations generally tend to amplify the earth pressure at a higher rate than the single pipeline as they block more seismic energy from propagating between the substructures.
- The pipeline is anticipated to be subjected to non-uniform stresses along its perimeter, resulting in non-uniform deformations.
- The seismic interaction with the adjacent substructure is very critical to the design of the pipeline and must be considered in the analysis. The risk of such seismic interactions is accumulated at low damping ratios, high excitation

frequencies, and when the distance to the adjacent substructure allows new wavepaths to be developed.

Collectively, the finding from of this research can help improve the understanding of seismic behaviour of deeply embedded structures and add more layers of safety to the overall integrity of small modular reactors.

5.3. RECOMMENDATIONS FOR FUTURE RESEARCH

The main objective of this research was to develop theoretical and numerical methods/tools that can be used to mitigate the hazards related to the seismic response of deeply embedded structures (i.e., SMRs) due to soil-structure interactions. Three major issues have been thoroughly studied in Chapters 2 to 4: lateral seismic earth pressure due to surface waves, seismic structure-soil-structure interaction, and seismic interaction between substructures and buried pipelines. The assumptions and limitations of each issue were clearly discussed and integrated into the corresponding chapter. The following recommendations are building upon the findings of this research and can be used to extend the proposed solutions or obtain better accuracy in some cases; however, they will not affect the main conclusions of this research:

- Soil-structure interaction can be divided into two phenomena: kinematic interaction and inertial interaction. The proposed methods discussed in Chapters 2 and 3 considered only the kinematic interaction. It is trongly recommended to extend the proposed solution to include the contribution of the

inertial interaction. Two sources of inertial interaction should be considered: the mass of the backfill/original soil and the mass of the substructure. The mass of the substructure depends on the mass distriction inside the structure.

- In the installation of buried pipelines, layers of primary initial backfill and bedding foundation are always placed at the bottom and around the pipelines to prevent vertical deformations. Therefore, backfilling should be provided around the pipelines in the seismic structure-pipeline interaction discussed in Chapter 4.
- Three-dimensional modelling is essential for seismic interaction with nearby pipelines as the joints connecting pipeline segments are the weakest point in pipeline analysis. In the three dimensional analysis, it should be noted that the soil medium surrounding the substructure consists of two layers: the backfill material and the native soil. Therefore, the seismic waves considered in the analysis will have to propagate through the two layers before impinging the substructure.
- For substructures with such a deep embedment, the compaction level of the backfill and construction criteria are key parameters and should be taken into account in the seismic analysis of deeply embedded structures.
- The seismic wave interference inside the backfill surrounding the substructure and its adverse impact if the mechanical properties of the soil profile allow surface waves to be developed,

- The walls of the substructures in this research are assumed rigid and fixed to the base. Future research is needed to account for the deformations in the walls,
- The seismic interaction between two adjacent buildings in the presence of an underground tunnel connecting the substructures,
- Although the ground level is considered as a free surface in this research, large equipment and components may be located in NPPs near a building or across the distance between two buildings. In such cases, the boundary conditions of the problem of interest are changed, and further investigation is required to address the pertaining issues, and
- It will be important that future research investigate the effect of oblique seismic waves on the interaction with adjacent substructures.